SECURITY INFORMATION

Copy 246

RM A52L04a

NACA RM A52L04a

TECH LIBRARY KAFB, NM
014527

6339

RESEARCH MEMORANDUM

DAMPING IN PITCH OF LOW-ASPECT-RATIO WINGS AT SUBSONIC AND SUPERSONIC SPEEDS

By Murray Tobak

Ames Aeronautical Laboratory
Moffett Field, Calif.

Classification cancelled (or changed to UNCLASSIFIED)
By Authority of NASA Tech Pub Announcement #36
(OFFICER AUTHORIZED TO CHANGE)
By ..... 2 May 58
NAME AND
GRADE OF OFFICER MAKING CHANGE)
27 Mar 61
DATE

NATIONAL ADVISORY COMMITTEE
FOR AERONAUTICS

WASHINGTON
April 8, 1953

I 19.98/13

TECH LIBRARY KAFB, NM

0143527

TABLE OF CONTENTS

	Page
SUMMARY	1
INTRODUCTION	1
NOTATION	3
THEORY	5
Application of Indicial Functions to the Aerodynamic Theory of Unsteady Flows	5
Definition of coordinate system	5
Concept of indicial functions	7
Application of indicial functions to harmonic pitching oscillations	9
Application of indicial functions to harmonic plunging oscillations	12
Application of indicial functions to harmonic rotary oscillations	13
Correspondence between indicial lift and moment analysis and other methods	18
Physical concepts relating to the indicial loading	22
Damping in Pitch of Low-Aspect-Ratio Wings	28
Effect of static margin	28
Effect of Mach number	31
Effect of aspect ratio	33
Effect of plan-form shape	35
Effect of frequency	38
Effect of thickness	41

TABLE OF CONTENTS - Concluded

	Page
EXPERIMENT	49
Wind Tunnel	49
Models	49
Model Support System	50
Scope of Tests	51
Reduction of Data	51
Corrections to Data	52
RESULTS	53
Damping Coefficients	53
Reynolds Number Effects	54
Aeroelastic Effects	54
Transfer of Axes	55
DISCUSSION	55
Effect of Aspect Ratio	55
Effect of Plan Form Shape	56
Effect of Thickness	57
Effect of Nonlinearities	58
CONCLUSIONS	62
APPENDIX A - Transfer of Axes	63
REFERENCES	65
FIGURES	69

NATIONAL ADVISORY COMMITTEE FOR AERONAUTICS

RESEARCH MEMORANDUM

DAMPING IN PITCH OF LOW-ASPECT-RATIO WINGS AT SUBSONIC AND SUPERSONIC SPEEDS

By Murray Tobak

SUMMARY

The concept of indicial functions is applied to the analysis of the aerodynamic phenomena associated with the short-period pitching mode of wings in subsonic and supersonic flight. Simple physical relationships are pointed out and are used to study the effect on the rotary-damping-moment coefficient of changes in center-of-gravity position, Mach number, aspect ratio, plan form, frequency, and thickness. Qualitative conclusions are drawn from the results of this investigation and are compared with the results of experiments for a series of low-aspect-ratio wing-body combinations having triangular, swept, and unswept wing plan forms.

Results of the experimental investigation, which were obtained by a single-degree-of-freedom free-oscillation technique over the Mach number ranges 0.6 to 0.9 and 1.2 to 1.9, were in good agreement with the results of theoretical computations. The predictions of ranges of supersonic Mach number and center-of-gravity positions over which dynamic instability may be expected, of the beneficial effect on the damping moment of a reduction in aspect ratio, and of only a small effect of thickness on the damping moment were confirmed by the experimental results.

The occurrence at high subsonic Mach numbers of small-amplitude self-sustained pitching oscillations is noted, and a hypothesis is advanced for its explanation.

INTRODUCTION

In the classical study of the longitudinal motion of an aircraft, it is usually found that the motion resulting from a small equilibrium-destroying disturbance consists of two modes: one, a lightly damped, low-frequency motion at essentially constant attitude, called the phugoid

[redacted]

oscillation; the other, a rotary-pitching and plunging oscillation of high frequency (relative to the phugoid frequency) called the short-period oscillation. The phugoid oscillation has generally been described as resulting from a slow interchange of potential and kinetic energy as the aircraft experiences periodic variations in airspeed and altitude. The character of the phugoid motion as influenced by airspeed, altitude, and aircraft geometry has been well understood for some time (see, e.g., ref. 1). The short-period motion, on the other hand, having in the past been found to be highly damped and of short duration, has been the cause of no concern. Its characteristics therefore have not been as fully investigated as those of the phugoid oscillation. With the advent of flight at speeds approaching and exceeding the speed of sound, however, the loss of rotary damping occurring in practically all aircraft at speeds near the sonic speed has caused renewed interest in the short-period pitching mode. Unlike the easily controlled phugoid oscillation, the deterioration of damping in the short-period mode is of serious concern to the pilot, since the period of the oscillation can be of the same order of magnitude as the pilot's reaction time. The oscillation may therefore be difficult or even impossible for the pilot to control manually. Furthermore, the additional load imposed upon the airframe due to a rapid growth of the amplitude of a negatively damped oscillation makes possible the occurrence of structural failure. It is therefore of considerable interest to obtain an understanding of the nature of the short-period mode, parallel to that which has been gained of the phugoid mode.

One means of viewing the aerodynamic phenomena occurring during the short-period oscillation from a fundamental standpoint is through application of the concept of indicial functions. In this approach, the variations with time of the aircraft angle of attack and angular velocity during the oscillation are replaced by a large number of small instantaneous or step changes. The transient aerodynamic reactions to these step changes are termed "indicial functions," and have been calculated theoretically for several classes of wings (refs. 2 to 6). By suitable superposition of these results (refs. 7 to 9), the aerodynamic forces and moments caused by the given maneuver can be studied. It will be the purpose of this report to make such a study for the simplified case of an aircraft performing single-degree-of-freedom rotary oscillations. For this maneuver, which corresponds to the short-period oscillation when the plunging velocity of the aircraft is zero, the use of simple physical relationships associated with the indicial function concept enables qualitative studies to be made of the separate effects on the aerodynamic forces and moments of changes in Mach number, aspect ratio, plan form, frequency, and thickness. Results of this investigation are then compared with the results of experiments with a group of low-aspect-ratio wing-body combinations. The tests were conducted in the Ames 6- by 6-foot supersonic wind tunnel and were similar in technique to those reported in reference 10.

NOTATION

A	aspect ratio, b^2/S
C_L	lift coefficient, lift/$q_o S$
C_m	pitching-moment coefficient, pitching moment/$q_o S\bar{c}$
C_p	pressure coefficient, $\frac{p-p_o}{q_o}$
I	moment of inertia, slug-ft^2
M_o	free-stream Mach number, V_o/a_o
R	Reynolds number, based on wing mean aerodynamic chord
S	wing area, including portion enclosed by body, sq ft
V_o	flight speed, ft/sec
a_o	speed of sound in free stream, ft/sec
b	wing span, ft
c_o	wing root chord, ft
$\bar{c}$	wing mean aerodynamic chord, $\frac{2}{S}\int_o^{b/2}(\text{local chord})^2 dy$
e	base of natural logarithms
i	$\sqrt{-1}$
k	reduced frequency parameter, $\omega\bar{c}/2V_o$
Δp	local loading at plan-form surface, $\frac{\text{pressure lower surface - pressure upper surface}}{q_o}$
q	angular velocity due to pitching, radians/sec
q_o	free-stream dynamic pressure, $\frac{1}{2}\rho_o V_o^2$, lb/sq ft
t	time, sec
t_a	time required following an instantaneous change in angle of attack or angular velocity for the transient lift or moment to attain steady state, sec

[redacted]

x,y,z rectangular coordinates

$x_{a.c.}$ distance from leading edge of M.A.C. to aerodynamic center, ft

x_o distance from leading edge of M.A.C. to axis of rotation, ft

Δx_o $x_{a.c.} - x_o$

α angle of attack of wing center line with respect to free-stream direction (sketch a)

β $\sqrt{|M_o^2-1|}$

γ ratio of specific heat at constant pressure to that at constant volume

δ airfoil-thickness ratio, maximum thickness/chord

θ angle of wing center line with respect to horizontal axis (sketch a)

ν acute angle between wing plane of symmetry and trailing edge (sketch p)

ρ_o free-stream density, slugs/cu ft

ω angular frequency of oscillation, radians/sec

σ_a distance traveled, measured in half M.A.C. lengths, in the time interval t_a, $2V_o t_a/\bar{c}$

When α, $\dot{\alpha}$, and q are used as subscripts, a nondimensional derivative is indicated, and this derivative is evaluated as the independent variable (α,$\dot{\alpha}$, or q) approaches zero. For example,

$$C_{m_\alpha} = \left[\frac{\partial C_m}{\partial \alpha}\right]_{\alpha \to 0} \qquad C_{m_{\dot{\alpha}}} = \left[\frac{\partial C_m}{\partial \frac{\dot{\alpha}\bar{c}}{2V_o}}\right]_{\dot{\alpha} \to 0}$$

$$C_{m_q} = \left[\frac{\partial C_m}{\partial \frac{q\bar{c}}{2V_o}}\right]_{q \to 0}$$

THEORY

Application of Indicial Functions to the Aerodynamic Theory of Unsteady Flows

One of the most useful tools in the study of unsteady flows is the concept of indicial aerodynamic functions which may be defined briefly as the aerodynamic response of the airfoil as a function of time to an instantaneous change in one of the conditions determining the aerodynamic properties of the airfoil in a steady flow. Theoretical aerodynamic indicial functions were first derived by Wagner (ref. 2) for the two-dimensional wing in incompressible flow. More recently, these results have been extended by Heaslet and Lomax to cover the compressible case for both subsonic and supersonic speeds (ref. 4). In addition, theoretical indicial functions have now been obtained for both wide and slender triangular wings and rectangular wings, all for supersonic speeds (refs. 4 to 6).

The indicial function derives its usefulness primarily through the ease with which it lends itself to the powerful and well-established methods of the operational calculus (refs. 7 to 9). With the use of these methods, the aerodynamic forces and moments caused by arbitrary motions of the airframe can be studied from a fundamental standpoint. Because of the wide range of applicability of this means of approach in unsteady flow analyses, a considerable portion of the succeeding discussion is devoted to the fundamentals involved.

Definition of coordinate system.- In the succeeding analysis the stability system of axes is used. The origin of the coordinate system is placed in the airfoil so that the y axis which is perpendicular to the vertical plane of symmetry is coincident with the axis of rotation of the airfoil; the positive branch of the x axis is pointed in the direction of flight; and the z axis lies in the vertical plane of symmetry, positive downward. The angle of attack α is measured as the angle between the chord plane of the airfoil and the xy plane, and is shown as positive in sketch (a). The angle of pitch θ is the angle between the chord plane of the airfoil and the horizontal plane (an arbitrary reference) and is also shown positive in sketch (a). Forces are measured as positive upward, whereas pitching moments are positive when tending to increase the angle of pitch in the positive direction. When the airspeed V_o is constant which corresponds to the

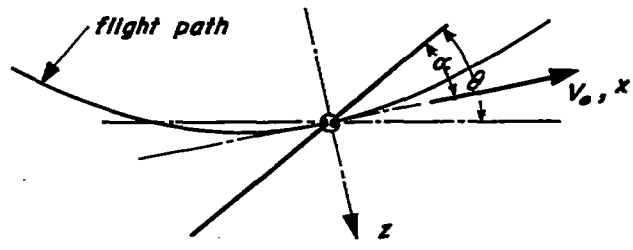

Sketch (a)

[redacted]

condition under study, the translatory and angular motions of the airfoil with respect to any system of coordinates are defined if the time histories of the angle of attack α and the angle of pitch θ and their derivatives are known. For purposes of clarity, two different harmonic motions of the aircraft are shown, illustrating the difference between a flight path which involves a constant angle of attack and a varying angle of pitch (sketch (b)) and one which involves a constant angle of pitch and a varying angle of attack (sketch (c)).

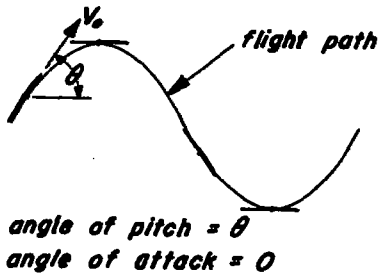

Sketch (b)

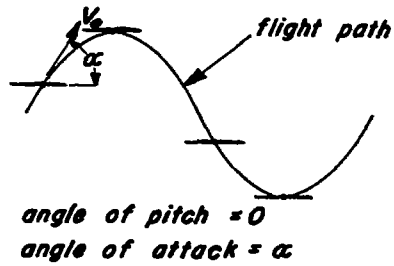

Sketch (c)

Now consider the case of a wing executing harmonic rotary oscillations about the y axis while the origin of the coordinate system traverses a level path at constant velocity V_o. This case corresponds to that of a wind-tunnel model mounted to permit single-degree-of-freedom rotary oscillations, or to the short-period mode of an aircraft in flight when the plunging velocity of the center of gravity is zero. Here α and θ are equal, so that the maneuver is defined by one variable, the time history of either α or θ. Let the angle of attack be α and the angular velocity be q ($q \equiv d\theta/dt = d\alpha/dt$). At any instant, the normal velocity at any point on the airfoil surface is composed of two parts, one due to the instantaneous angle of attack αV_o, the other due to the angular velocity at the same instant $-qx$ (see sketch (d)). These are two of the instantaneous boundary conditions of the unsteady flow.

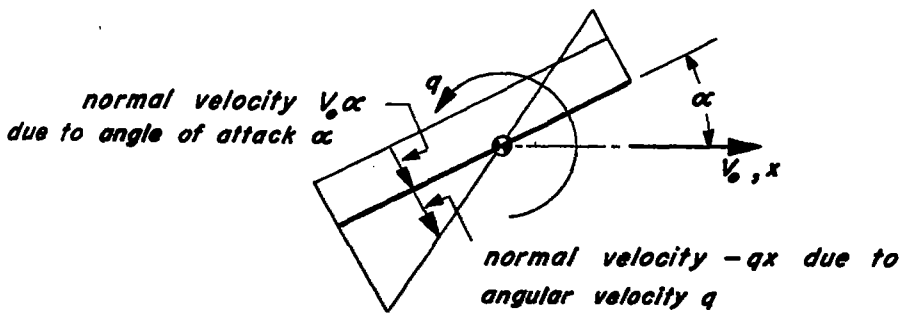

Sketch (d)

Solutions for the aerodynamic forces and moments which correspond to these boundary conditions may be derived by a number of methods involving various degrees of approximation. In succeeding sections, the use of the concept of indicial functions and the principle of superposition for this purpose will be illustrated and compared with other current widely used methods.

Concept of indicial functions.- In order to illustrate this concept, assume that the airfoil under consideration has been flying a level path at zero angle of attack. At some time, which is designated time zero, the wing is caused to attain simultaneously a constant angle of attack α and angular velocity q. The normal velocity of the flow next to the surface of the airfoil therefore changes discontinuously from zero to a pattern that is constant with time and identical in shape to the pattern shown previously in sketch (d). The lift and pitching moment that result are of a transient character and attain their steady-state values corresponding to these new boundary conditions only after a significant interval of time has passed. It should be noted there exists an essential difference between the length of this time interval at subsonic and supersonic speeds. At supersonic speeds, the vorticity shed into the airfoil wake cannot influence the flow about the airfoil but at subsonic speeds this influence exists for all time. The result is that the lift and moment reach steady-state values in a finite time at supersonic speeds but approach these values asymptotically at subsonic speeds. In either case, however, the time responses in lift and moment to the step changes in α and q are termed indicial functions. Sketch (e) illustrates typical subsonic and supersonic indicial lift responses to a step change in the angle of attack.

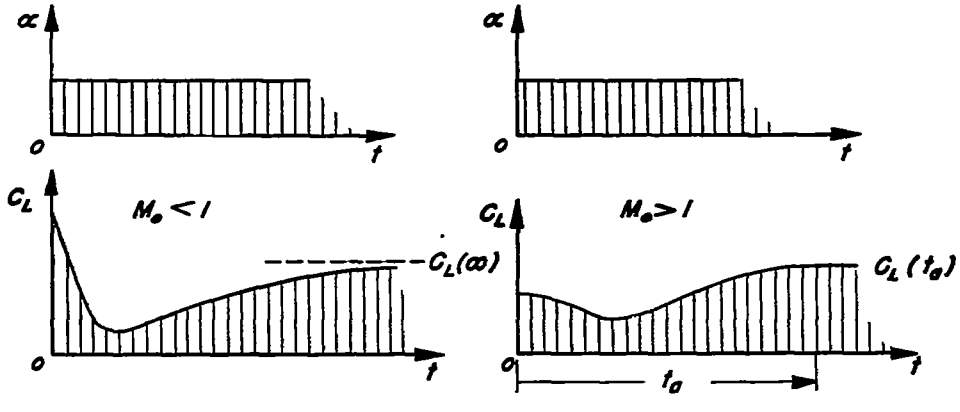

Sketch (e)

[redacted]

It is obvious that the time history of the wing motion during a short-period oscillation may be broken down into an infinite number of infinitesimally small step changes in the angle of attack and step changes in the angular velocity. The summation of the indicial lift and moment for these steps then yields the total lift and moment at any prescribed time. In sketch (f), the mechanics of the procedure are illustrated for an arbitrary angle-of-attack variation. Here, the given angle-of-attack variation is replaced by a number of small step changes. Within each step the corresponding response in lift is shown plotted for convenience. It is then apparent that the total lift at time t is equal to the sum of the increments of lift in each step at time t. As indicated by the leaders, however, it is clear that the increments of lift for the various steps at time t are equivalent to increments in the first step at time $t - t_1$. Alternatively, then, the total lift at time t can be written as[1]

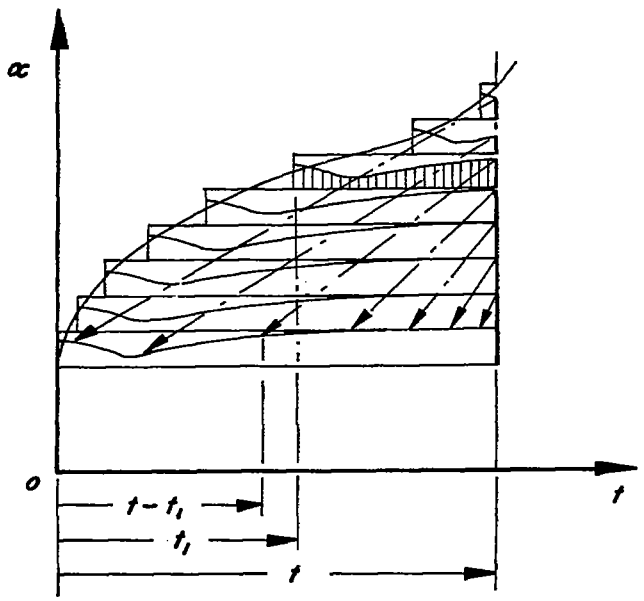

Sketch (f)

$$C_L(t) = C_{L_\alpha}(t)\alpha(0) + \sum_0^t C_{L_\alpha}(t-t_1)\,\frac{\Delta\alpha}{\Delta t}(t_1)\Delta t_1 \qquad (1)$$

After a transformation of variables, $t - t_1 = \tau$, and letting the increment of time approach zero, equation (1) can be rewritten in a form of Duhamel's integral (see, e.g., ref. 9)

$$C_L(t) = \frac{d}{dt}\int_0^t C_{L_\alpha}(\tau)\alpha(t-\tau)\,d\tau \qquad (2)$$

[1]Here, and in the remainder of this report, the use of parentheses is reserved solely for the indication of functional dependence. Thus, for example, in equation (1) the term $C_{L_\alpha}(t-t_1)$ is interpreted as the value of C_{L_α} at time $t - t_1$, whereas $\frac{\Delta\alpha}{\Delta t}(t_1)$ is the value of $\Delta\alpha/\Delta t$ at time t_1. All other enclosures indicate algebraic expressions in the usual sense.

A similar procedure is carried out for the angular velocity variation, whereupon the total lift coefficient at the prescribed time t becomes

$$C_L(t) = \frac{d}{dt}\int_o^t C_{L_\alpha}(\tau)\alpha(t-\tau)d\tau + \frac{d}{dt}\int_o^t C_{L_q}(\tau)\frac{\bar{c}}{2V_o}q(t-\tau)d\tau \qquad (3)$$

It should be pointed out that in this form equation (3) is applicable to the analysis of arbitrary motions, the only restriction being that the flight speed is constant. In the following sections, however, the application of equation (3) is restricted to harmonic motions having a single degree of freedom. The reasons for this restriction are twofold: first, the motions of a statically stable aircraft in response to a disturbance are most generally of a harmonic nature; and second, such a restriction permits an assessment of the influence of the time rate of the airfoil motions on the aerodynamic forces and moments.

Application of indicial functions to harmonic pitching oscillations.- Consider first a pure sinusoidal pitching oscillation, the angle of attack being zero throughout the motion. The flight path for such a motion has been illustrated in sketch (b). In this case, the angle of pitch is given by

$$\theta(t) = \theta_o e^{i\omega t}$$

where θ_o is the maximum amplitude of oscillation and ω is the angular frequency. The angular velocity is, of course, $q(t) = \dot{\theta} = i\omega\theta_o e^{i\omega t} = i\omega\theta(t)$. Inserting the value for $q(t)$ in equation (3) and performing the indicated operations, there results

$$C_L(t) = -\frac{\omega^2\bar{c}}{2V_o}\theta(t)\int_o^t C_{L_q}(\tau)e^{-i\omega\tau}d\tau + \frac{i\omega\bar{c}}{2V_o}\theta_o C_{L_q}(t) \qquad (4)$$

[redacted]

Note in sketch (g) that $C_{L_q}(\tau)$ is equal to $C_{L_q}(t)-F_2(\tau)$, and that for subsonic speeds $F_2(\tau)$ approaches zero as τ approaches t.

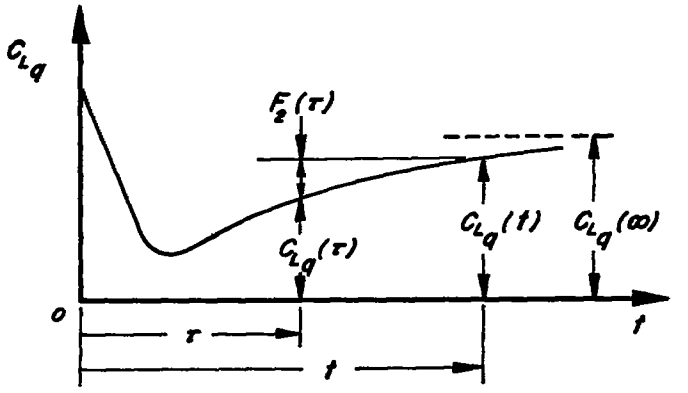

Sketch (g)

Replacing $C_{L_q}(\tau)$ in equation (4) by this equality,

$$\frac{C_L(t)}{\theta(t)} = \frac{i\omega\bar{c}}{2V_o} C_{L_q}(t) + \frac{\omega^2\bar{c}}{2V_o} \int_o^t F_2(\tau)e^{-i\omega\tau}d\tau \tag{5}$$

For subsonic speeds, let t approach infinity. With this substitution, equation (5) thereby represents the lift coefficient due to the harmonic pitching motion after the transient loading subsequent to the start of the motion has reached steady state. Then separating equation (5) into components in-phase (real part) and out-of-phase (imaginary part) with θ, there is obtained

$$\left.\begin{aligned} \frac{C_L}{\theta} &= \frac{\omega^2\bar{c}}{2V_o} \int_o^\infty F_2(\tau) \cos \omega\tau d\tau \\ \frac{C_L}{i\omega\bar{c}\theta/2V_o} &= C_{L_q}(\infty) - \omega \int_o^\infty F_2(\tau) \sin \omega\tau d\tau \end{aligned}\right\} \tag{6}$$

Introduce the nondimensional parameters,

$\varphi = \frac{2V_o}{\bar{c}}\tau$ number of half M.A.C. lengths traveled in time τ

$k = \frac{\omega\bar{c}}{2V_o}$ reduced frequency

In terms of these parameters, equation (6) becomes, for $M_o < 1$,

$$\left.\begin{aligned} \frac{C_L}{\theta} &= k^2 \int_o^\infty F_2(\varphi) \cos k\varphi d\varphi \\ \frac{C_L}{q\bar{c}/2V_o} &= C_{L_q}(\infty) - k \int_o^\infty F_2(\varphi) \sin k\varphi d\varphi \end{aligned}\right\} \tag{7}$$

At supersonic speeds, equations (7) may be simplified somewhat since the build-up in lift is completed in a finite number of half M.A.C. lengths of travel σ_a. In equations (7), therefore, the upper limits of the integrals may be replaced by σ_a, since beyond that point $F_2(\varphi)$ is zero.

$$\left.\begin{aligned} \frac{C_L}{\theta} &= k^2 \int_o^{\sigma_a} F_2(\varphi) \cos k\varphi d\varphi \\ \frac{C_L}{q\bar{c}/2V_o} &= C_{L_q}(\sigma_a) - k \int_o^{\sigma_a} F_2(\varphi) \sin k\varphi d\varphi \end{aligned}\right\} \quad \begin{matrix} \varphi \geq \sigma_a \\ M_o > 1 \end{matrix} \tag{8}$$

Thus, it appears from equations (7) and (8) that there are both in-phase and out-of-phase lift forces associated with the harmonic pitching oscillation. Notice, however, in equations (8) that if the trigonometric terms are expanded and the reduced frequency is required to be small compared to unity (corresponding to the frequencies encountered in dynamic stability work) terms containing second and higher powers of k will be very small compared to first-order terms. Thus, for slow frequencies, the only force of consequence during the pitching oscillation is the first order in frequency out-of-phase lift force, $q\bar{c}/2V_o\ C_{L_q}(\sigma_a)$.[2]

[2] This quantity is, of course, the same lift force in phase with the pitching velocity which would occur alone had the wing been executing a steady turn (q constant). One of the chief advantages of the indicial response method, at least for supersonic speeds, is the ease with which the relative importance of the various terms contributing to the total lift and moment can be assessed and the sources of the important contributions identified.

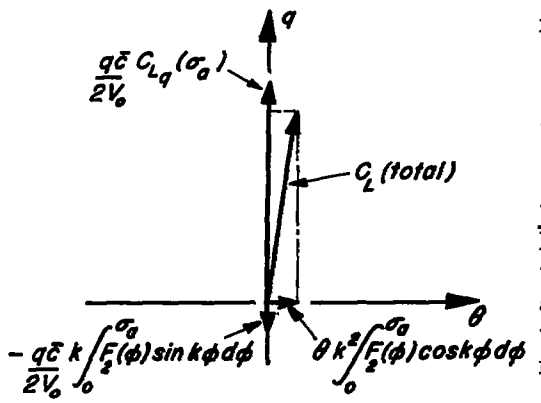

Sketch (h)

The phase relationships for the harmonic pitching oscillation are indicated in sketch (h). It is evident from sketch (h) that the total lift leads the angle of pitch by nearly 90°.

Application of indicial functions to harmonic plunging oscillations.- Next, consider a purely sinusoidal variation of the angle of attack, the angle of pitch being zero throughout the motion. The flight path for this motion has been illustrated in sketch (c). Here, α equals $\alpha_o e^{i\omega t}$, where, as previously, α_o and ω are the maximum amplitude and angular frequency, respectively. Applying equation (3) again,

$$C_L(t) = \alpha_o \frac{d}{dt} \int_o^t C_{L_\alpha}(\tau) e^{i\omega[t-\tau]} d\tau$$

$$= i\omega\alpha(t) \int_o^t C_{L_\alpha}(\tau) e^{-i\omega\tau} d\tau + \alpha_o C_{L_\alpha}(t) \qquad (9)$$

Now, as in the previous example, let $C_{L_\alpha}(\tau) = C_{L_\alpha}(t) - F_1(\tau)$ so that equation (9) becomes

$$C_L(t) = \alpha(t) C_{L_\alpha}(t) - i\omega\alpha(t) \int_o^t F_1(\tau) e^{-i\omega\tau} d\tau \qquad (10)$$

Again, introduce the nondimensional parameters φ and k, separate equation (10) into its real and imaginary parts, and let φ approach infinity for subsonic speeds and σ_a for supersonic speeds. There results

$$\left.\begin{aligned} \frac{C_L}{\alpha} &= C_{L_\alpha}(\lambda) - k \int_o^\lambda F_1(\varphi) \sin k\varphi \, d\varphi \\ \frac{C_L}{\dot{\alpha}\bar{c}/2V_o} &= - \int_o^\lambda F_1(\varphi) \cos k\varphi \, d\varphi \end{aligned}\right\} \quad \begin{aligned} \lambda &= \infty, \quad M_o < 1 \\ \lambda &= \sigma_a, \quad M_o > 1 \end{aligned} \qquad (11)$$

Notice in equations (11) for supersonic speeds that when the trigonometric terms are expanded for the slow frequency case, as was done in the previous example, there appears an in-phase term of zero order in k, $\alpha C_{L_\alpha}(\sigma_a)$, and an out-of-phase term of first order in k, $-\frac{\dot{\alpha}\bar{c}}{2V_o}\int_o^{\sigma_a} F_1(\varphi)d\varphi$. These, then, are the principal contributions to the lift forces for the slow-frequency angle-of-attack variation. The phase relationships for this motion are shown graphically in sketch (i). For this case, it is evident that the total-lift force can lag behind the angle of attack because of the negative out-of-phase contribution,

$$-\frac{\dot{\alpha}\bar{c}}{2V_o}\int_o^{\sigma_a} F_1(\varphi)\cos k\varphi d\varphi$$

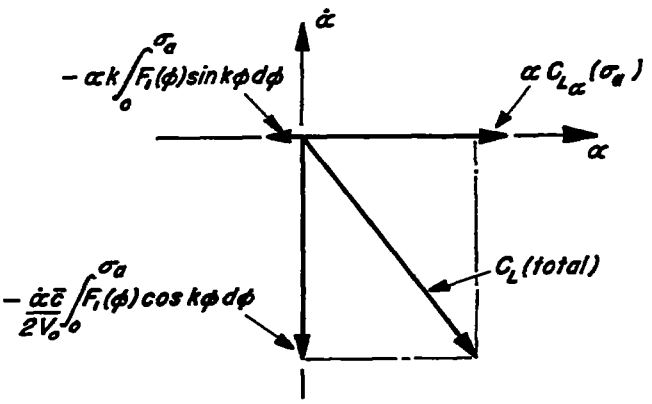

Sketch (i)

Application of indicial functions to harmonic rotary oscillations.- Finally, consider the case of harmonic rotary oscillations. Here, as previously mentioned, the normal velocity over the wing surface is composed of contributions from both the angular velocity and the instantaneous angle of attack, so that the complete expression in equation (3) must be employed to obtain the total lift. However, for single-degree-of-freedom rotary oscillations, α equals θ and $\dot{\alpha}$ equals q, so that in this case the separate expressions given for the harmonically pitching wing (eqs. (7) and (8)) and the harmonically plunging wing (eq. (11)) can be combined to give the total lift for a wing executing harmonic rotary oscillations. Then, adding the results of equations (7), (8), and (11), the in-phase and out-of-phase components of the total lift become

$$\frac{C_L}{\alpha} = C_{L_\alpha}(\lambda) - k\int_o^{\lambda} F_1(\varphi)\sin k\varphi d\varphi + k^2\int_o^{\lambda} F_2(\varphi)\cos k\varphi d\varphi \qquad (12a)$$

$\lambda=\infty,\ M_o<1$

$\lambda=\sigma_a,\ M_o>1$

$$\frac{C_L}{q\bar{c}/2V_o} = C_{L_q}(\lambda) - k\int_o^{\lambda} F_2(\varphi)\sin k\varphi d\varphi - \int_o^{\lambda} F_1(\varphi)\cos k\varphi d\varphi \qquad (12b)$$

The phase relationships for the rotary oscillation may, of course, also be obtained by directly adding the results given in sketches (h) and (i). The result of this addition is shown in sketch (j).

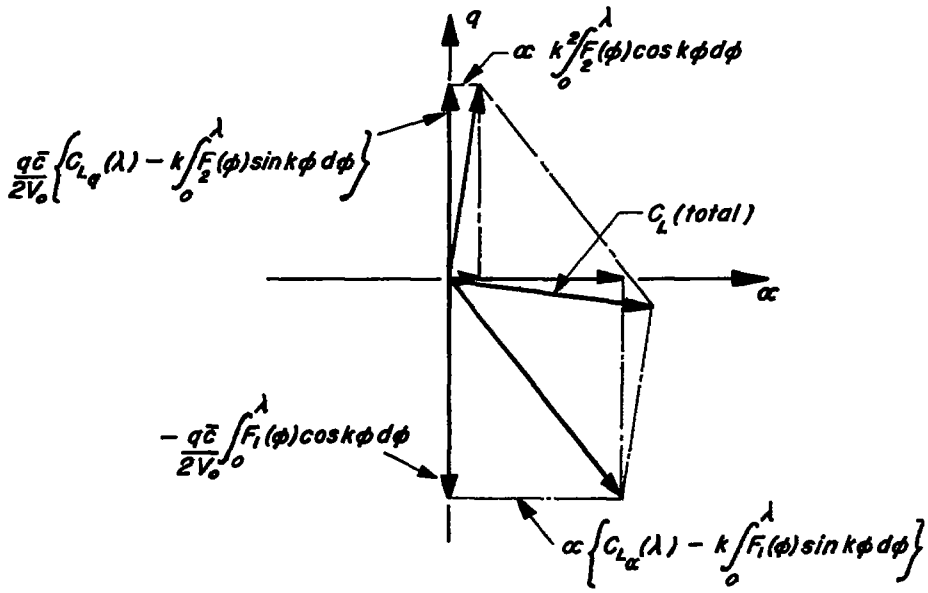

Sketch (j)

It will be noted in sketch (j) that the total-lift force can either lag behind or lead the angle of attack, depending on the relative magnitudes of the three terms comprising the out-of-phase lift. The total lift is shown lagging behind the angle of attack in sketch (j), which situation, for axis positions ahead of the point of concentration of the total lift, gives rise to the possibility of the development of negatively damped rotary oscillations.

Again, the complete frequency-dependent equations for the total lift of a wing in supersonic flow due to the rotary oscillation (eqs. (12), $\lambda = \sigma_a$) may be reduced to first order in k for the slow-frequency case in the same manner as was described in the two previous examples to give

$$\left.\begin{aligned} \frac{C_L}{\alpha} &= C_{L_\alpha}(\sigma_a) \\ \frac{C_L}{q\bar{c}/2V_o} &= C_{L_q}(\sigma_a) - \int_o^{\sigma_a} F_1(\varphi)\, d\varphi \end{aligned}\right\} \qquad (13)$$

For all three examples, the same procedure may, of course, be used to obtain the pitching-moment coefficient. Only the pitching-moment equations for the rotary oscillation are presented below, since the correspondence between the lift and moment equations is obvious. For the rotary oscillation case, then,

$$\left.\begin{aligned} \frac{C_m}{\alpha} &= C_{m_\alpha}(\lambda) - k\int_0^\lambda F_3(\varphi)\sin k\varphi d\varphi + k^2\int_0^\lambda F_4(\varphi)\cos k\varphi d\varphi \\ \frac{C_m}{q\bar{c}/2V_0} &= C_{m_q}(\lambda) - k\int_0^\lambda F_4(\varphi)\sin k\varphi d\varphi - \int_0^\lambda F_3(\varphi)\cos k\varphi d\varphi \end{aligned}\right\} \begin{matrix} \lambda=\infty, \quad M_0<1 \\ \lambda=\sigma_a, \quad M_0>1 \end{matrix} \qquad (14)$$

where, as previously,

$$F_3(\varphi) = C_{m_\alpha}(\lambda) - C_{m_\alpha}(\varphi)$$

and

$$F_4(\varphi) = C_{m_q}(\lambda) - C_{m_q}(\varphi)$$

Again, reducing equations (14) for supersonic speeds ($\lambda=\sigma_a$) to first order in frequency, there results

$$\left.\begin{aligned} \frac{C_m}{\alpha} &= C_{m_\alpha}(\sigma_a) \\ \frac{C_m}{q\bar{c}/2V_0} &= C_{m_q}(\sigma_a) - \int_0^{\sigma_a} F_3(\varphi)\, d\varphi \end{aligned}\right\} \qquad (15)$$

The complete frequency-dependent equations for the lift and pitching-moment coefficients for the rotary-oscillation case (eqs. (12) and (14)) describe completely the aerodynamic forces and moments resulting from the single-degree-of-freedom pitching mode. For the purposes of the present discussion, however, it is sufficient to limit consideration to the simpler first order in frequency results of equations (13) and (15). The significance of the effect of the higher-order terms on the out-of-phase pitching-moment will be examined in a later section of this report.

With regard to the first-order results for the supersonic lift and pitching-moment coefficients, it is instructive to note that the

quantities $\int_0^{\sigma_a} F_1(\varphi)d\varphi$ and $\int_0^{\sigma_a} F_3(\varphi)d\varphi$ in equations (13) and (15) are represented geometrically by the areas of the shaded portions of sketch (k).

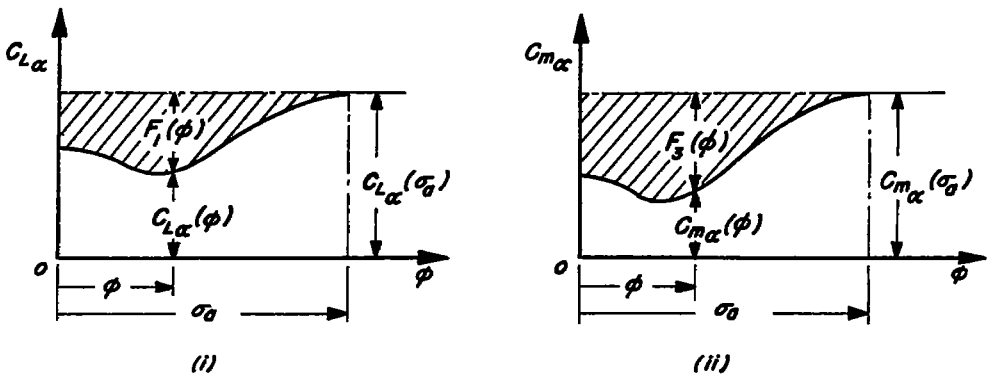

Sketch (k)

The manner in which these areas are affected by variations in Mach number, aspect ratio, plan-form shape, and thickness will be used as a guide in later sections of this report to determine the significance of these parameters.

In the foregoing discussion, no mention has been made of reducing the complete equations for the lift and moment coefficients at subsonic speed (eqs. (12) and (14), $\lambda=\infty$) to first order in frequency as was done for the equations noted as applying at supersonic speed. It is evident that if the same procedure had been applied for subsonic speeds, the area corresponding to the term $\int_0^{\infty} F_1(\varphi)d\varphi$ can either be finite or can become infinitely large, depending on the manner in which the indicial lift function $C_{L_\alpha}(\varphi)$ approaches its steady-state asymptote as $\varphi \to \infty$. In the latter case, there exists the interesting anamoly of an infinite out-of-phase lift force as the frequency approaches zero. As can be seen from the results of reference 4, such will be the case for the two-dimensional wing. This result as the frequency approaches zero is not peculiar to the indicial analysis alone, but has been pointed out by a number of authors using different approaches. As indicated by Miles in reference 11, however, the anamolous result can be considered to be a consequence of assuming a two-dimensional flow, and there is reason to believe that the difficulty as the frequency approaches zero will not exist for finite-span wings.

As has been mentioned previously, the use of the characteristic areas $\int_0^{\sigma_a} F_1(\varphi)d\varphi$ and $\int_0^{\sigma_a} F_3(\varphi)d\varphi$ will be shown to be of considerable value in estimating the damping-in-pitch characteristics of wings at supersonic speeds. For the two-dimensional wing at subsonic speeds, the singularity as $k \to 0$ prevents the use of such a simplified approach

without further study. However, rather than return to the use of the full frequency-dependent equations ((12) and (14)), the reduction of the equations for the out-of-phase lift and moment to first order in frequency will be made in such a manner as to preserve the significance of these areas. To accomplish this end, equation (12b) is reconsidered. It is evident that the first integral in equation (12b) may be discarded, since its contribution to the out-of-phase lift is at least of second order in frequency. The second integral is divided into two parts:

$$\int_0^{\infty} F_1(\varphi)\cos k\varphi d\varphi = \int_0^{\varphi_1} F_1(\varphi)\cos k\varphi d\varphi + \int_{\varphi_1}^{\infty} F_1(\varphi)\cos k\varphi d\varphi \qquad (16)$$

where φ_1 is chosen such that $F_1(\varphi_1)$ is close to zero. The first integral in equation (16), being bounded, then causes no difficulty. Expanding the trigonometric term and retaining only the first term in the expansion, there results $\int_0^{\varphi_1} F_1(\varphi)d\varphi$, which is the characteristic area out to the point φ_1. Now for large values of φ, $F_1(\varphi)$ is approximated in reference 4 by

$$F_1(\varphi) = \mu\left\{\frac{1}{a+\varphi} + \frac{b}{[a+\varphi]^2}\right\}$$

where the values of μ, a, and b are dependent on Mach number, and are given for $M_o = 0$, 0.5, and 0.8 in reference 4. Inserting this quantity in the second integral in equation (16), we have

$$\int_{\varphi_1}^{\infty} F_1(\varphi)\cos k\varphi d\varphi = \mu\int_{\varphi_1}^{\infty}\frac{\cos k\varphi}{a+\varphi}\,d\varphi + \mu b\int_{\varphi_1}^{\infty}\frac{\cos k\varphi}{[a+\varphi]^2}\,d\varphi \qquad (17)$$

Performing the indicated integrations in equation (17), there is obtained a term, $\mu b/a+\varphi_1$, from the second integral, and a term, $-\mu Ci\{k[a+\varphi_1]\}$ from the first integral. For small values of the argument, the cosine integral is approximated by (see ref. 12),

$$Ci\{k[a+\varphi_1]\} \approx \ln\{\gamma k[a+\varphi_1]\}$$
$$k[a+\varphi_1] \to 0$$

where γ is Euler's constant, 1.78107.

Then, through the first order in frequency,

$$\frac{C_L}{q\bar{c}/2V_o} = C_{L_q}(\infty) - \int_0^{\varphi_1} F_1(\varphi)d\varphi + G(\varphi_1,k) \qquad (18a)$$

[redacted]

where

$$G(\varphi_1,k) = \left[\mu \ln\left\{\gamma k[a+\varphi_1]\right\} - \frac{\mu b}{a+\varphi_1}\right]$$

The out-of-phase moment for pitching about the leading edge follows from the above development, with the added result of reference 4 that for large values of φ,

$$F_3(\varphi) \approx -\frac{F_1(\varphi)}{4}$$

Then, through the first order,

$$\frac{C_m}{q\bar{c}/2V_o} = C_{m_q}(\infty) - \int_o^{\varphi_1} F_3(\varphi)d\varphi - \frac{1}{4}G(\varphi_1,k) \qquad (18b)$$

Thus, after fixing φ_1, choosing a (small) value of k, and computing $G(\varphi_1,k)$, the finite areas corresponding to the terms $-\int_o^{\varphi_1} F_1(\varphi)d\varphi$ and $-\int_o^{\varphi_1} F_3(\varphi)d\varphi$ can be assessed in the same manner as will be done for the supersonic case. The advantages of such a procedure will be evident later.

Correspondence between indicial lift and moment analysis and other methods.- Before proceeding further with applications of the indicial response method, it is appropriate to discuss the relationship of this approach to other widely used methods.

Following the fundamental papers of Bryan and Routh, which introduced the basic differential equations of motion of rigid bodies and their stability criteria, the historical development of the theory of longitudinal motions of an aircraft evolved separately in two fields of research: dynamic stability and flutter. Workers in the dynamic stability field soon found that the longitudinal oscillations of a rigid aircraft in flight were generally of small reduced frequency. On this basis, the constants due to the aerodynamic properties of the airframe which appear in the differential equations of motion were considered to be independent of frequency. As a first approach to the problem of obtaining the necessary aerodynamic coefficients analytically, the instantaneous normal velocity distribution at the surface of the airfoil was assumed to be constant with time. The aerodynamic forces and moments arising from the fixed boundary conditions were then calculated using steady-flow theory. Later, this assumption was realized to be an oversimplification for the case of wing-tail combinations and an additional term correct to the first order in frequency was added which accounted for the lag in the tail pitching moment caused by the time required for the vorticity discharge from the wing to reach the tail (see ref. 13).

Since at low speeds the pitching moment of the tail far outweighs all other contributions, the results from steady-flow theory together with the term accounting for the vorticity lag satisfactorily predicted the dynamic longitudinal motions of wing-tail combinations, and it was concluded that the major aerodynamic effects had been accounted for. In recent years, however, numerous authors (in particular, Miles; see, e.g., ref. 11) have pointed out that the above-mentioned theory overlooks important contributions to the aerodynamic forces and moments which, though still within the first order in frequency approximation, arise from time-dependent boundary conditions and must be calculated from unsteady-flow theory. It has been shown by these authors that with proper inclusion in the equations of motion of these coefficients, the deterioration of damping in the short-period mode actually occurring for aircraft flying at speeds near the speed of sound can be successfully predicted. The consequences of the assumptions involved in the classical dynamic stability theory will be more evident from a brief review of the equation of motion and boundary conditions for the single-degree-of-freedom rotary oscillations of a rigid wing flying at constant supersonic speed. At the very outset, the assumption is generally made that the aerodynamic reactions to the motion of the airframe depend only on the angular position and angular velocity and not upon angular accelerations or higher time derivatives. The equation of motion for the change in pitching moment following a displacement from an equilibrium position is then written in the form of a power series:

$$\frac{I}{q_o S\bar{c}}\ddot{\alpha} = \left[\frac{\partial C_m}{\partial \alpha}\right]\Delta\alpha + \left\{\frac{\partial C_m}{\partial [\dot{\alpha}\bar{c}/2V_o]}\right\}\frac{\dot{\alpha}\bar{c}}{2V_o} + \left\{\frac{\partial C_m}{\partial [q\bar{c}/2V_o]}\right\}\frac{\dot{\alpha}\bar{c}}{2V_o} + \left[\frac{\partial^2 C_m}{\partial^2 \alpha}\right]\frac{[\Delta\alpha]^2}{2!} +$$

$$\left\{\frac{\partial^2 C_m}{\partial^2 [\dot{\alpha}\bar{c}/2V_o]}\right\}\frac{[\dot{\alpha}\bar{c}/2V_o]^2}{2!} + \left\{\frac{\partial^2 C_m}{\partial^2 [q\bar{c}/2V_o]}\right\}\frac{[\dot{\alpha}\bar{c}/2V_o]^2}{2!} + \cdots \quad (19)$$

It should be remembered that for the rotary-oscillation case, the airfoil is subjected to changes in both angle of attack α and angular velocity q, and that these motions produce normal velocity patterns at the airfoil surface which are different in character. Thus, although for the single-degree-of-freedom case, $\dot{\alpha}$ and q are equal, nevertheless their separate effects must be considered and it is therefore necessary to include both $\frac{\partial C_m}{\partial [q\bar{c}/2V_o]}$ and $\frac{\partial C_m}{\partial [\dot{\alpha}\bar{c}/2V_o]}$ in equation (19). Next, if it is assumed that the moments are linearly dependent on their respective variables, the higher-order terms in equation (19) may be discarded and the remaining partial derivatives considered as constants for the given wing. There remains, therefore, a linear second-order system with constant coefficients. In order to calculate the coefficients

(termed stability derivatives) theoretically it became necessary, for lack of more refined theoretical methods, to assume that the instantaneous normal velocity of the flow at the surface of the wing was fixed with respect to time. Thus, the partial derivative $\frac{\partial C_m}{\partial[q\bar{c}/2V_o]}$ could be calculated as the pitching moment due to a constant pitching rate, that is, $C_{m_q}(\sigma_a)$, while the derivative $\partial C_m/\partial\alpha$ becomes the pitching moment due to a constant angle of attack, that is, $C_{m_\alpha}(\sigma_a)$. As a consequence of fixing the normal velocity pattern in time, however, it was necessary to assume that the derivative $\frac{\partial C_m}{\partial[\dot{\alpha}\bar{c}/2V_o]}$ was zero. There was therefore no possibility for this theory to predict the occurrence of dynamic instability for a wing alone, since the only damping term remaining is $C_{m_q}(\sigma_a)$, which is always stabilizing. When the restriction of constant normal velocity with time is lifted, however, the assumption is then made that the stability derivatives in equation (19) may be calculated separately by fixing each of the independent variables α, $\dot{\alpha}$, and q in turn with respect to time. The derivatives $C_{m_q}(\sigma_a)$ and $C_{m_\alpha}(\sigma_a)$ thus remain unchanged, but the derivative $\frac{\partial C_m}{\partial[\dot{\alpha}\bar{c}/2V_o]}$ (or $C_{m_{\dot{\alpha}}}$) can now be included and calculated as the pitching moment due to a constant vertical acceleration, $\dot{\alpha}V_o$. It should be emphasized that while $C_{m_q}(\sigma_a)$ and $C_{m_\alpha}(\sigma_a)$ may be calculated from steady-flow theory by virtue of the assumed invariance with time of the normal velocity pattern, $C_{m_{\dot{\alpha}}}$ must be calculated from unsteady-flow theory since for constant $\dot{\alpha}$ the angle of attack varies linearly with time, as does the normal velocity of the flow at the surface.

It is clear that since the stability derivatives in equation (19) are assumed to be independent of the frequency, the result for the aerodynamic pitching-moment coefficient is thereby limited to one that is correct only to the first order in frequency. For the single-degree-of-freedom case, then, the in-phase and out-of-phase components of the total aerodynamic pitching-moment coefficient correct to the first order in frequency, become

$$\left.\begin{aligned} \frac{C_m}{\alpha} &= C_{m_\alpha}(\sigma_a) \\ \frac{C_m}{q\bar{c}/2V_o} &= C_{m_q}(\sigma_a) + C_{m_{\dot{\alpha}}}(\sigma_a) \end{aligned}\right\} \qquad (20)$$

By comparison with the first order in frequency result from the indicial response analysis (eq. (15)), it is evident that the two results are

identical if the quantity $-\int_0^{\sigma_a} F_s(\varphi)d\varphi$ can be shown to be equivalent to $C_{m_{\dot{\alpha}}}(\sigma_a)$. To show this equivalence, consider a wing, initially in level steady flight, which is suddenly forced down with constant vertical acceleration $\dot{\alpha}V_o$. As seen in sketch (1), the angle-of-attack variation in this case is $\alpha = \dot{\alpha}t$, where $\dot{\alpha}$ is a constant. Then applying the counterpart of equation (3) for the pitching moment

$$C_m(t) = \frac{d}{dt}\int_0^t C_{m_\alpha}(\tau)\alpha(t-\tau)d\tau$$

Inserting $\alpha(t-\tau) = \dot{\alpha}[t-\tau]$, and performing the indicated differentiation,

$$C_m(t) = \dot{\alpha}\int_0^t C_{m_\alpha}(\tau)d\tau$$

Now replace $C_{m_\alpha}(\tau)$ by $C_{m_\alpha}(t)-F_s(\tau)$ and let t be greater than t_a. Then

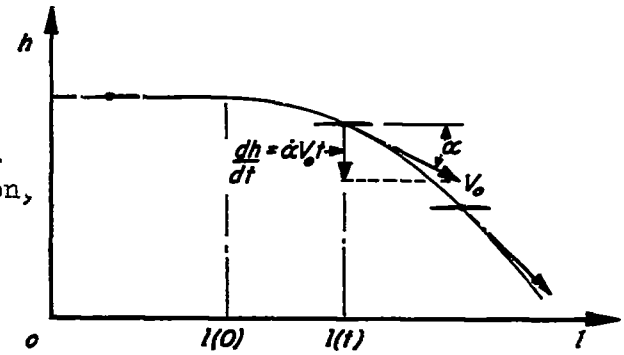

Sketch (1)

$$C_m(t) = \alpha(t)C_{m_\alpha}(t_a) - \dot{\alpha}\int_0^{t_a} F_s(\tau)d\tau$$

and nondimensionalizing, by replacing t and t_a by $\bar{c}\varphi/2V_o$ and $\bar{c}\sigma_a/2V_o$, we have

$$C_m(\varphi) = \alpha(\varphi)C_{m_\alpha}(\sigma_a) - \frac{\dot{\alpha}\bar{c}}{2V_o}\int_0^{\sigma_a} F_s(\varphi)d\varphi; \qquad \varphi \geq \sigma_a \qquad (21)$$

Thus, the pitching moment proportional to the constant vertical acceleration parameter $\dot{\alpha}\bar{c}/2V_o$, which is synonomous with the definition of the stability derivative $C_{m_{\dot{\alpha}}}$, is found to be equivalent to the pitching-moment contribution due to $\dot{\alpha}$ for the first order in frequency-rotary-oscillation case.[3] Therefore, the results of the indicial response method, when reduced to the first order in frequency for supersonic speeds, are identical to the results from the familiar first-order theory used in dynamic stability work.[4]

[3]By the same procedure, the stability derivative $C_{L_{\dot{\alpha}}}(\sigma_a)$ can be shown to be equivalent to the term $-\int_0^{\sigma_a} F_1(\varphi)d\varphi$.

[4]Notice in equation (21) that if σ_a is replaced by infinity, the results apply to subsonic speeds. For the two-dimensional wing, the analogy between $C_{m_{\dot{\alpha}}}$ and $-\int_0^{\infty} F_s(\varphi)d\varphi$ then gives only the previously mentioned singularity at infinity as $k \rightarrow 0$. If the area corresponding to $\int_0^{\infty} F_s(\varphi)d\varphi$ were finite, however, the analogy would be equally useful for subsonic as well as supersonic speeds.

Workers in the field of flutter, who were concerned with frequencies many times those encountered in dynamic stability analyses, required theoretical information showing the behavior of the forces and moments as affected by the frequency of oscillation, and therefore discarded the first-order theory for more precise methods of analysis. One of the most useful of these has been the "oscillating potential" theory, which is based on periodic solutions of the time-dependent linearized equation of compressible potential flow. The in-phase and out-of-phase lift and moments are thereby determined, generally as functions of powers of the reduced frequency, aspect ratio, Mach number, and position of the axis of rotation. The application of this method, which developed primarily as a result of Theodorsen's work for incompressible flow (ref. 14) has recently produced a number of useful papers covering a wide variety of wings at supersonic speeds (see, e.g., refs. 15 to 19). It has been shown by a number of authors, in particular, Garrick, in reference 7, that through the use of superposition methods the results for the aerodynamic coefficients obtained from the oscillating potential theory are wholly compatible with those of the indicial response method for harmonic motions (eqs. (12) and (14)).

Thus the indicial response method embraces both the first-order theory of dynamic stability and the oscillating potential theory, and, in effect, bridges the gap between the fields of dynamic stability and flutter. Furthermore, the indicial response method overcomes the disadvantages of the two methods described above since, unlike the first-order theory, the effects of frequency on the aerodynamic coefficients can be determined, and, unlike the oscillating potential theory, the method can be applied easily to the study of arbitrary motions. Finally, the indicial response method represents a fundamental approach to the problem of unsteady flow, and affords valuable insight into the physical nature of the aerodynamic phenomena taking place.

Physical concepts relating to the indicial loading.- It has been shown that for even small frequencies, the pitching moment of an airfoil in harmonic rotary motion can lag behind the angle of attack of the airfoil. The magnitude of the lag depends on the character of the indicial response to a step change in angle of attack. It is therefore of interest at this time to re-examine the physical nature of the flow that contributes this lag.

Consider first the lift and moment at the instant the angle of attack changes, assuming that previous to time zero the wing has been flying a level path at zero angle of attack. At $t = 0$, the wing begins to sink, without pitching, with constant downward velocity αV_o while maintaining its forward velocity. The angle of attack therefore changes discontinuously from zero to a constant α. At the same instant, the step change in angle of attack causes the emission of a compression wave from each point on the lower surface of the wing and expansion waves

from points on the upper surface. In the infinitesimal time during which the starting action occurs, each section of the wing experiences the same impulsive force, and by equating the impulse to the momentum transmitted to the mass of fluid affected by the starting waves, the starting lift coefficient can easily be derived as $4\alpha/M_0$ (see ref. 3). During the infinitesimal starting time, the pressure disturbances from the edges of the airfoil, propagated at the speed of sound, travel an insignificant distance and do not influence the remainder of the airfoil. The lift coefficient is therefore independent of the wing plan form. This remarkably simple result for the starting lift coefficient, which is valid for both subsonic and supersonic speeds, is thus dependent solely on the flight Mach number. The starting pitching moment follows directly from the above result, since by virtue of the uniformity of loading the aerodynamic center is located at the wing centroid of area.

For values of time greater than zero, however, the situation differs radically for the supersonic and subsonic speed ranges. Consider first the supersonic case. As time passes, the spherical sound waves emitted at $t = 0$ grow in size with radius $a_0 t$. The wing, however, is moving forward at a faster rate than the rate of growth of the starting sound waves and thus begins to emerge from the influence of these waves. This is shown schematically in sketch (m).

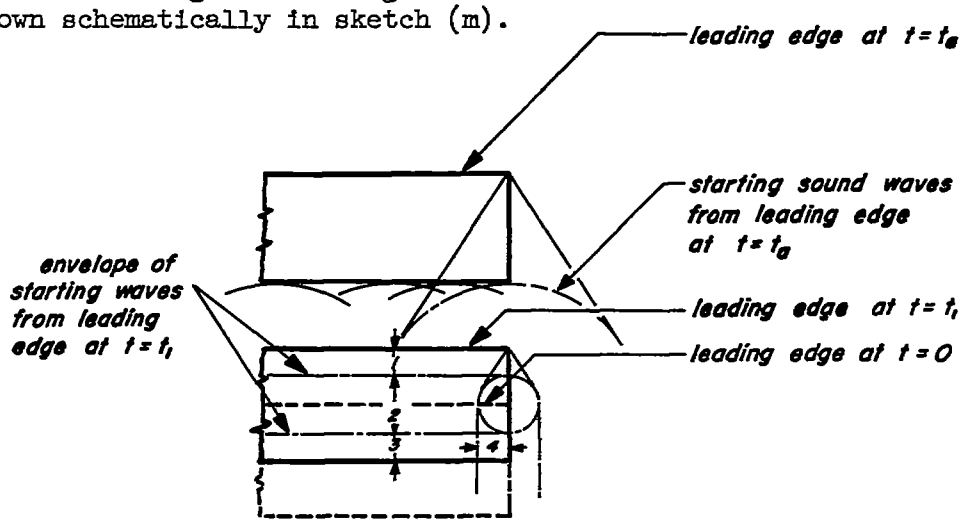

Sketch (m)

At $t = 0$, the starting waves just cover the wing and the loading is uniform as described previously. At $t = t_1$, the starting waves have grown in radius and the wing has begun to emerge from their influence. On that portion of the wing which has emerged, region (1) in sketch (m), the loading has already reached its steady-state value. Notice that in this region the characteristic tip Mach cone has already formed. On the portion of the wing uninfluenced by the starting waves from the edges, region (3) in sketch (m), the loading is still uniform as at $t = 0$. In regions (2) and (4), the loading is influenced by the starting waves

from the leading and side edges, and in these regions is thus different from the loading in either regions (1) or (3). As time increases still further, the uniform starting load quickly disappears as the sound waves from the leading edge grow in size and as the wing moves forward. Finally, at time t_a, the envelope of the starting waves from the leading edge is coincident with the trailing edge of the wing, and the steady-state loading corresponding to the new angle of attack α has been completely established over the wing.

The above relationships can be shown more clearly for the entire time interval zero to t_a for a two-dimensional wing by plotting as a function of time the position of the wing leading and trailing edges and position of the envelopes of the sound waves which emanate from the leading and trailing edges at $t = 0$. Such a plot is shown in sketch (n).

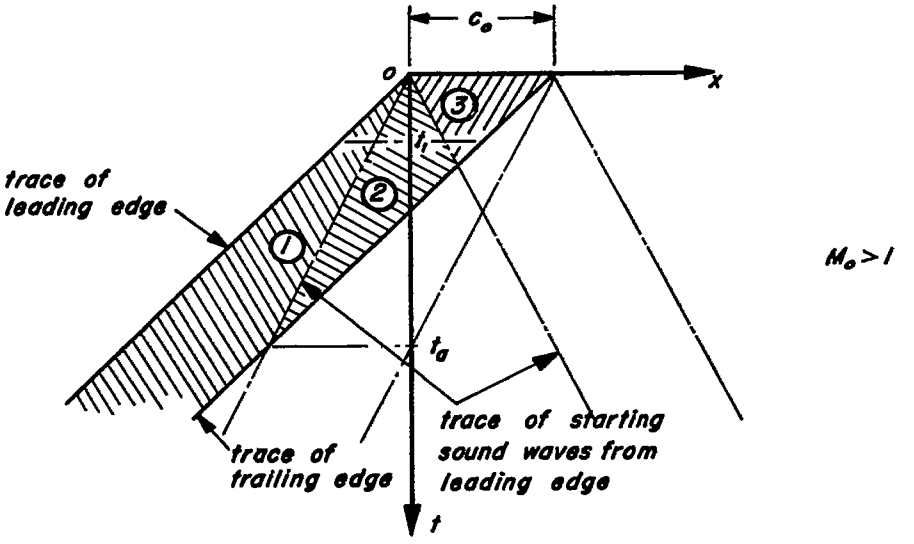

Sketch (n)

It is clear that at $t = t_1$ the regions of the wing (1), (2), and (3) correspond to the same regions at $t = t_1$ for the wing shown in sketch (m). For $t = 0$ and in region (3) the loading is uniform and is given by $4\alpha/M_o$. For $t > t_a$ and in region (1) the wing has outstripped the starting waves from the leading edge and has attained its steady-state loading. For $t < t_a$ the chordwise loading is composed of combinations of the loading in each of the three regions as shown in sketch (o).[5]

[5]The reader will note the similarity between sketch (n) and sketches depicting the boundary conditions for three-dimensional wings in steady supersonic flow. Many researchers have pointed out the analogy and it has been used to calculate the pressure over a wing impulsively starting from rest (refs. 3 and 4).

Since the loading on the wing attains its final steady-state distribution at precisely the time when the wing has emerged entirely from the influence of the starting sound waves from the leading edge (or apex), the time to reach steady state may be easily calculated for any type of wing by means of the geometric relationships shown in sketch (p).

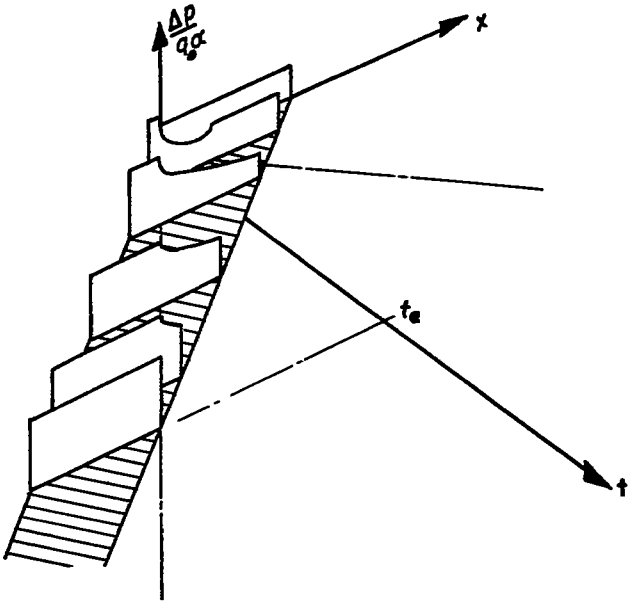

Sketch (o)

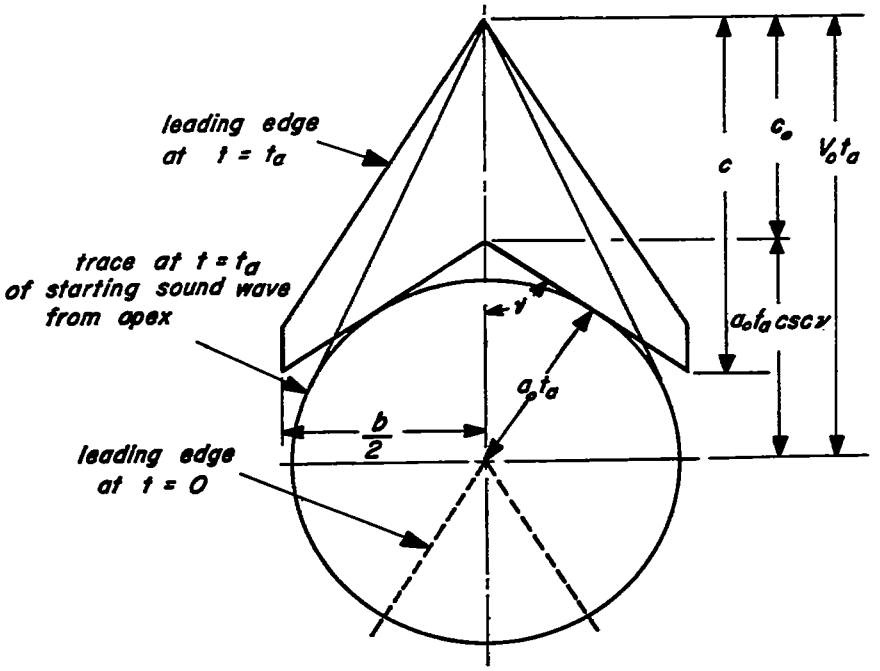

Sketch (p)

[redacted]

It may be easily verified that t_a, the time required for the wing to attain its steady-state loading, is given by the following relationship:

$$t_a = \frac{c_o M_o}{V_o[M_o - \csc \nu]} \qquad \nu \leq \frac{\pi}{2} \tag{22}$$

Notice that for wings having straight or swept-forward trailing edges and straight or swept-back leading edges, equation (22) reduces to

$$t_a = \frac{c_o M_o}{V_o[M_o - 1]} \tag{23}$$

In terms of the number of half M.A.C. lengths of travel, it thus appears that for wings having straight or swept-forward trailing edges and straight or swept-back leading edges,

$$\sigma_a = \frac{2V_o}{\bar{c}} t_a = \frac{2c_o}{\bar{c}} \frac{M_o}{[M_o - 1]} \tag{24}$$

whereas for wings having swept-back trailing edges and straight or swept-back leading edges,

$$\left.\begin{aligned} \sigma_a &= \frac{2c_o}{\bar{c}} \frac{M_o}{[M_o - \csc \nu]}, \qquad M_o \geq \csc \nu + \frac{2c_o}{b} \cos \nu \\ \sigma_a &= 2M_o \frac{c}{\bar{c}} \left\{ \frac{M_o + \sqrt{1 - \frac{b^2}{4c^2}[M_o^2 - 1]}}{M_o^2 - 1} \right\}, \qquad M_o \leq \csc \nu + \frac{2c_o}{b} \cos \nu \end{aligned}\right\} \tag{25}$$

The second of equations (25) applies to that range of Mach numbers for which the trace of the starting sound wave from the apex is not tangent to the trailing edge at $t = t_a$.

Now consider the subsonic case. Here the situation is more complicated in that since the starting sound waves travel faster than the wing, the wing never escapes their influence. Furthermore, the vorticity shed by the wing at $t = 0$ can also influence the loading on the wing since the disturbances created by the shed vorticity travel forward at a faster rate than the wing. For these reasons, the indicial loading at subsonic speeds approaches its steady-state distribution asymptotically with time. The situation for subsonic speeds will be more clearly

evident from examination of sketch (q), which shows the relationship of the traces versus time of the leading and trailing edges of a two-dimensional wing flying at a subsonic Mach number to the traces of the envelopes of the starting sound waves.

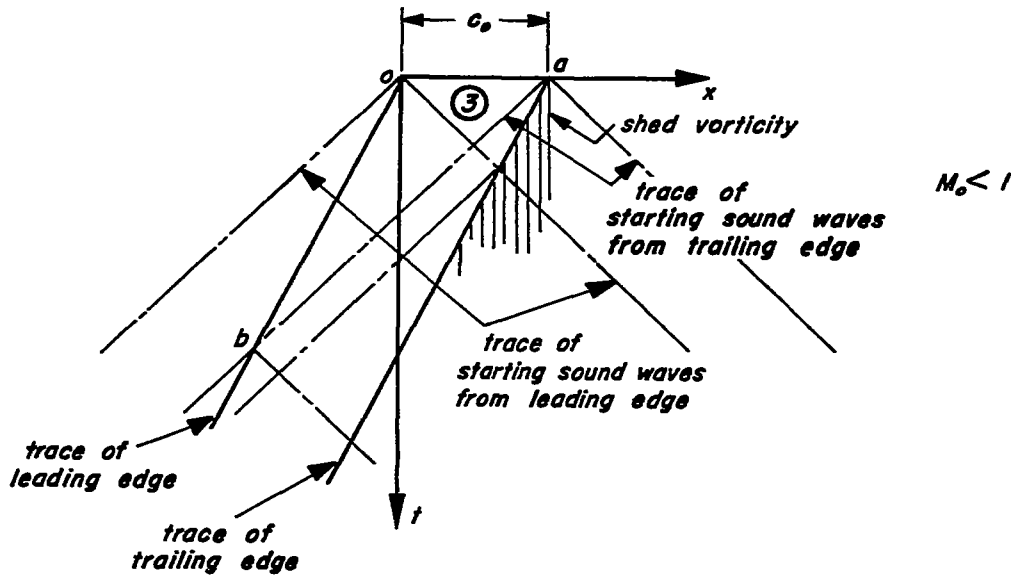

Sketch (q)

Notice in sketch (q) that the starting sound waves intersect the edges of the wing and that each intersection causes a new sound wave to be emitted, which in turn will intersect an edge. Furthermore, notice that the vorticity shed from the trailing edge at time zero can influence that portion of the wing behind the sound wave trace labeled a-b. The influence of each successive sound wave reflection, however, is weaker than the last, and as the wing moves away from the starting vortices their influence diminishes, so that at $t = \infty$ the loading on the wing attains its steady-state distribution. The variation of the chordwise loading with time for the two-dimensional wing flying at a subsonic Mach number is shown in sketch (r). Notice that for $t > 0$, the chordwise loading is markedly different from the loading at supersonic speeds (sketch (o)). However, for $t = 0$

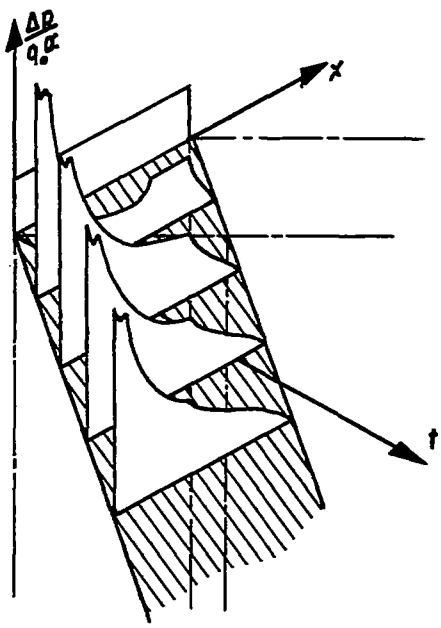

Sketch (r)

and in the region corresponding to region (3) of sketch (q), the loading is uniform and equal to $4\alpha/M_o$, as in the supersonic case.

Damping in Pitch of Low-Aspect-Ratio Wings

Previously (eq. (20)), it was shown that for single-degree-of-freedom, slow-frequency, pitching oscillations of a wing, the principal parameter contributing to the damping of the motion is the damping coefficient $C_{m_q} + C_{m_{\dot{\alpha}}}$. This result, however, is not directly applicable to the case of an aircraft in flight, since generally additional damping is provided by virtue of the fact that the aircraft experiences harmonic vertical translatory oscillations as well as the rotary oscillations. For the slow-frequency case, however, the effect of the second degree of freedom on the damping can be determined by use of the relationships given in reference 10. It is further shown in reference 10 that although the effect of the translatory oscillation is usually to increase the total damping, nevertheless, the parameter of primary importance in determining the magnitude and duration of the motion remains the damping-in-pitch coefficient $C_{m_q} + C_{m_{\dot{\alpha}}}$. The remainder of this section is therefore concerned with a study of the effect on this parameter of certain important variables. In particular, the effect of the position of the center of gravity, and the effects of Mach number, aspect ratio, plan-form shape, frequency, and thickness will be examined, principally by inspection of the indicial lift and moment responses to a change in angle of attack.

Effect of static margin.- From the previous discussion, it will be remembered that at supersonic speeds the stability derivatives $C_{L_{\dot{\alpha}}}(\sigma_a)$ and $C_{m_{\dot{\alpha}}}(\sigma_a)$ were shown to be equivalent to the indicial lift and moment expressions, $-\int_o^{\sigma_a} F_1(\varphi)d\varphi$ and $-\int_o^{\sigma_a} F_3(\varphi)d\varphi$. Furthermore, it was shown that these were the contributions which could cause the total lift and moment during the short-period oscillation to lag behind the angle of attack. Hence, by inspection of equation (15), it is evident that since $C_{m_q}(\sigma_a)$ is always stabilizing, when $C_{m_\alpha}(\sigma_a)$ is negative (corresponding to a statically stable condition) the possibility of dynamic instability in the form of negatively damped rotary oscillations arises when $C_{m_{\dot{\alpha}}}(\sigma_a)$, the shaded area in sketch (k-ii), is larger than $C_{m_q}(\sigma_a)$. Now since the normal velocity at the surface of the wing due to the instantaneous angle of attack is constant over the wing, the lift derivative $C_{L_{\dot{\alpha}}}$ which arises from this boundary condition is independent of the axis position and $C_{m_{\dot{\alpha}}}$ will therefore vary linearly with

axis position. This variation is illustrated in sketch (s), where Δx_o represents the distance of the center of gravity from the aerodynamic center, measured positive forward of the aerodynamic center.

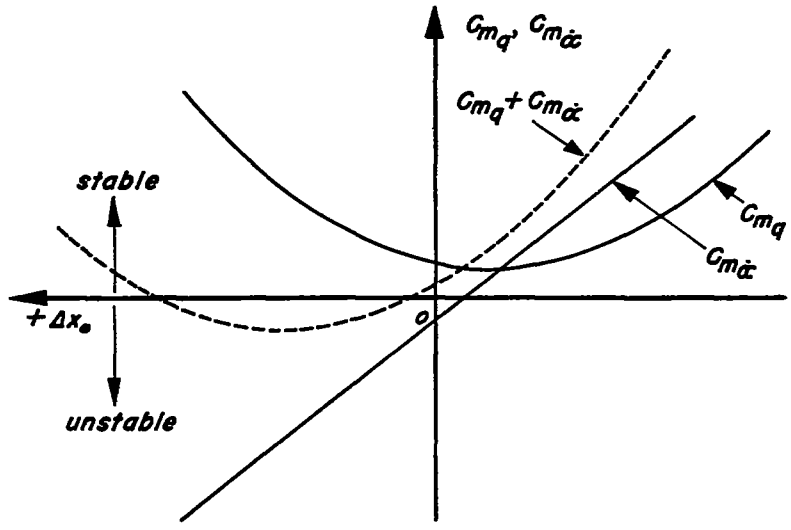

Sketch (s)

The parameter C_{L_q}, on the other hand, is a direct function of the axis position, since it arises from a normal velocity distribution that varies directly as the distance from the axis. The moment coefficient C_{m_q} will therefore vary as the second power of the axis position, and describes the parabolic shape shown also in sketch (s). It is evident from sketch (s) that the sum of C_{m_q} and $C_{m_{\dot{\alpha}}}$ will be a minimum at some value of the static margin, and that the sign of $C_{m_q} + C_{m_{\dot{\alpha}}}$ at that point determines whether or not a region of axis positions will exist over which the wing can experience negatively damped rotary oscillations. These qualitative statements may be written explicitly by considering the equation for the damping in pitch about an arbitrary axis,

$$C_{m_q} + C_{m_{\dot{\alpha}}} = \left[C_{m_q}\right]_o + \left[C_{m_{\dot{\alpha}}}\right]_o - \frac{\Delta x_o}{\bar{c}} \left\{\left[C_{L_q}\right]_o + C_{L_{\dot{\alpha}}}\right\} - 2\left[\frac{\Delta x_o}{\bar{c}}\right]^2 C_{L_\alpha} \tag{26}$$

where again Δx_o refers to the distance of the center of gravity from the aerodynamic center, and the subscripted terms are referred to an axis through the aerodynamic center.

[redacted]

Taking the derivative of equation (26) with respect to $\Delta x_o/\bar{c}$, and setting the result equal to zero, there is obtained the axis location at which the damping in pitch is a minimum

$$\left.\begin{aligned} \frac{d\left[C_{m_q}+C_{m_{\dot{\alpha}}}\right]}{d\left[\Delta x_o/\bar{c}\right]} &= -\left\{\left[C_{L_q}\right]_o + C_{L_{\dot{\alpha}}}\right\} - 4\,\frac{\Delta x_o}{\bar{c}}\,C_{L_\alpha} = 0 \\ \frac{\Delta x_o}{\bar{c}} &= -\frac{\left\{\left[C_{L_q}\right]_o + C_{L_{\dot{\alpha}}}\right\}}{4C_{L_\alpha}} \end{aligned}\right\} \tag{27}$$

When equation (27) is inserted into equation (26), the minimum value of the damping in pitch is given as

$$\left[C_{m_q}+C_{m_{\dot{\alpha}}}\right]_{min.} = \left\{\left[C_{m_q}\right]_o + \left[C_{m_{\dot{\alpha}}}\right]_o\right\} + \frac{1}{8C_{L_\alpha}}\left\{\left[C_{L_q}\right]_o + C_{L_{\dot{\alpha}}}\right\}^2 \tag{28}$$

and hence, a region of instability will exist if

$$\left\{\left[C_{m_q}\right]_o + \left[C_{m_{\dot{\alpha}}}\right]_o\right\} + \frac{1}{8C_{L_\alpha}}\left\{\left[C_{L_q}\right]_o + C_{L_{\dot{\alpha}}}\right\}^2 > 0 \tag{29}$$

If equation (29) is greater than zero, the boundaries of the region of axis positions over which instability is possible are of course given by setting equation (26) equal to zero and solving for $\Delta x_o/\bar{c}$.

$$\frac{\Delta x_o}{\bar{c}} = -\frac{\left\{\left[C_{L_q}\right]_o + C_{L_{\dot{\alpha}}}\right\}}{4C_{L_\alpha}} \mp \sqrt{\left\{\frac{\left[C_{L_q}\right]_o + C_{L_{\dot{\alpha}}}}{4C_{L_\alpha}}\right\}^2 + \left\{\frac{\left[C_{m_q}\right]_o + \left[C_{m_{\dot{\alpha}}}\right]_o}{2C_{L_\alpha}}\right\}} \tag{30}$$

Notice in both sketch (s) and equation (30) that for a given Mach number there will be two axis positions at which the damping in pitch vanishes. Then if the above procedure is carried out for a series of Mach numbers, one may trace out a curve as shown in sketch (t) which forms the locus of Mach numbers and axis positions at which the damping in pitch is zero. This locus thus delineates the regions of Mach number and axis position for which dynamic instability is and is not theoretically possible. Such loci, covering a wide variety of wings at supersonic speeds, have been presented by a number of authors. Watkins, for example, presents supersonic boundary curves for rectangular and triangular wings in references 16 and 17. At subsonic speeds, Miles' reduction of Possio's development to first order in frequency (ref. 11) can be used to form a

stability boundary curve for the two-dimensional wing for a given (small) reduced frequency. Such a curve is presented for the entire Mach number range in figure 1, where, here $+ x_o$ is the distance of the axis of rotation behind the leading edge and k, the reduced frequency, is 0.011 for subsonic speeds and approaches zero for supersonic speeds. Notice in figure 1 that at both subsonic and supersonic speeds, the range of Mach numbers over which dynamic instability is possible is largest for center-of-gravity positions forward of the aerodynamic center. Further, the largest range of axis positions over which dynamic instability is possible occurs near $M_o = 1$. Both of these characteristics are true as well for three-dimensional wings at supersonic speeds (see, e.g., refs. 16 to 19).

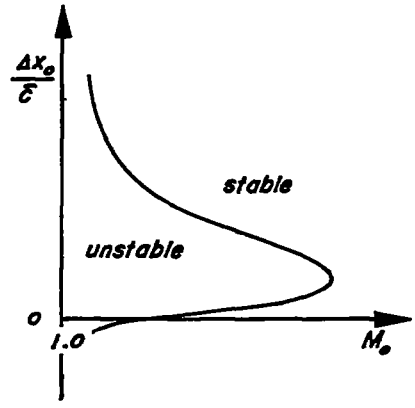

Sketch (t)

Effect of Mach number.- Next consider the effect of Mach number on the damping in pitch of a two-dimensional wing with axis at the leading edge. The variation with Mach number of the indicial pitching-moment response to a change in α will first be examined, using the information given in the previous sections and the indicial curves given in reference 4. At supersonic speeds, the manner in which $-\int_0^{\sigma_a} F_s(\varphi)d\varphi$, the area corresponding to $C_{m_{\dot{\alpha}}}$, is affected can then be assessed and compared with $C_{m_q}(\sigma_a)$. At subsonic speeds, use is made of equation (18b). It is evident in equation (18b) that by fixing k and choosing φ_1, such that the quantity $\frac{1}{4} G(\varphi_1,k)$ is the same at each Mach number, one is free to compare finite areas $-\int_0^{\varphi_1} F_s(\varphi)d\varphi$ on an equivalent basis.

As has been mentioned previously, the starting lift, at any Mach number, is $4\alpha/M_o$ and is concentrated at the midchord. At $M_o = 0$, therefore, there is an initial infinite pulse in the pitching moment about an axis coincident with the leading edge after which the indicial curve drops to $\pi/4$ and begins to grow asympotically toward its steady-state value $\pi/2$. At low subsonic Mach numbers other than zero, the initial pitching moment is less than infinite but very large, being $2/M_o$, and then falls before growing toward the steady value $\pi/2\beta$. As the Mach number increases toward 1.0, the starting pitching moment falls while the asymptotic value grows, until at $M_o = 1.0$ the indicial curve becomes unbounded in asymptotic moment.

As seen in sketch (u), the effect of increasing the Mach number at subsonic speeds is therefore to increase rapidly the area corresponding to the destabilizing moment contribution, $-\int_0^{\varphi_1} F_3(\varphi)d\varphi$.

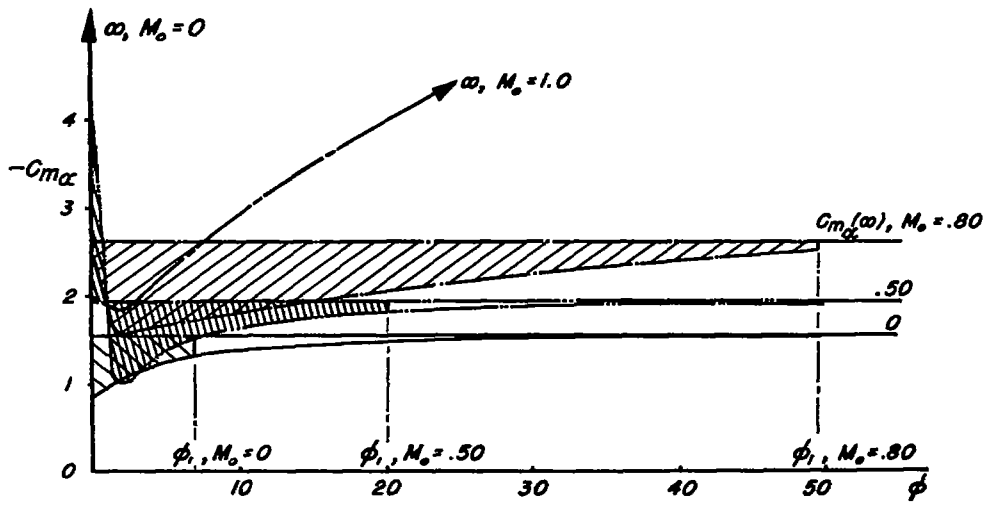

Sketch (u)

In sketch (u), k was chosen to be 0.011 and the values of φ_1 were picked such that $-\frac{1}{4}G(\varphi_1,k)$ was +4.88 at each Mach number. In the following discussion, the damping moment $-\int_0^{\varphi_1} F_3(\varphi)d\varphi + 4.88$ will be referred to as $C_{m_{\dot\alpha}}$ for convenience.

At supersonic speeds, the initial value of the pitching moment $2/M_0$ continues to drop with increasing Mach number, but here the steady-state pitching moment also begins to fall and at a faster rate than the starting moment, being $2/\beta$. Even more important, as the Mach number increases, the number of half-chord lengths traveled to reach steady state decreases rapidly, being 22, for example, at $M_0 = 1.1$, as compared to 4 at $M_0 = 2$. As seen in sketch (v), the area representing $C_{m_{\dot\alpha}}$ therefore shrinks rapidly with increasing supersonic Mach number and becomes relatively unimportant at Mach numbers greater than 2. The trend of $C_{m_{\dot\alpha}}$ with Mach number through the range $0 < M_0 < 2$ is more clearly evident in sketch (w). It is seen that $C_{m_{\dot\alpha}}$ is positive, or destabilizing, throughout the Mach number range and that its effect is most important at Mach numbers near 1.0. Also shown plotted for comparison in sketch (w) is the variation of C_{m_q} with Mach number. When the parameters are added, it is evident that the damping moment $C_{m_q} + C_{m_{\dot\alpha}}$ for the two-dimensional wing with axis at the leading edge is destabilizing in the Mach number range $0 < M_0 < 1.414$.

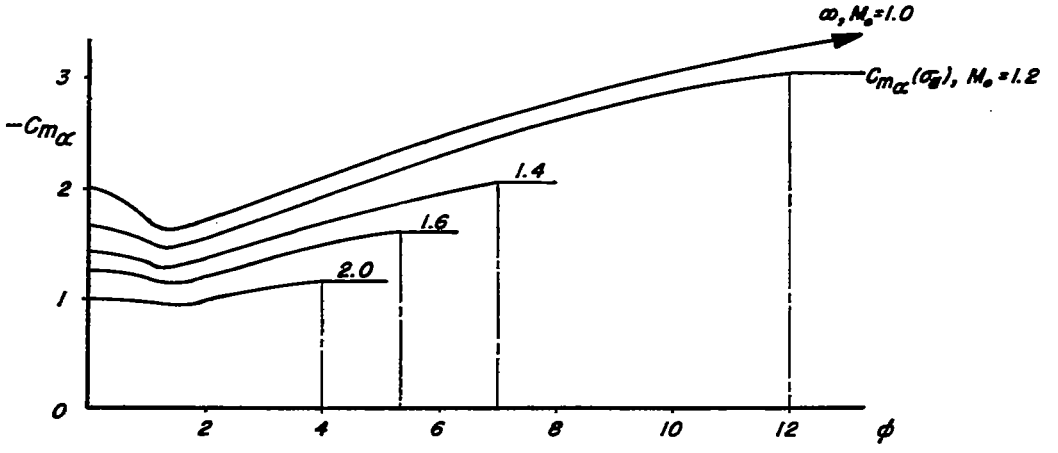

Sketch (v)

Effect of aspect ratio.- To illustrate the effect of aspect ratio, it is convenient to compare the supersonic damping-in-pitch characteristics of a group of triangular wings having subsonic leading edges. The wings are of equal area and differ only in aspect ratio. As was done previously, the indicial lift responses to a change in angle of attack will first be examined. The effect of aspect ratio on the characteristic area representing $C_{L_{\dot{\alpha}}}$ can then be assessed.

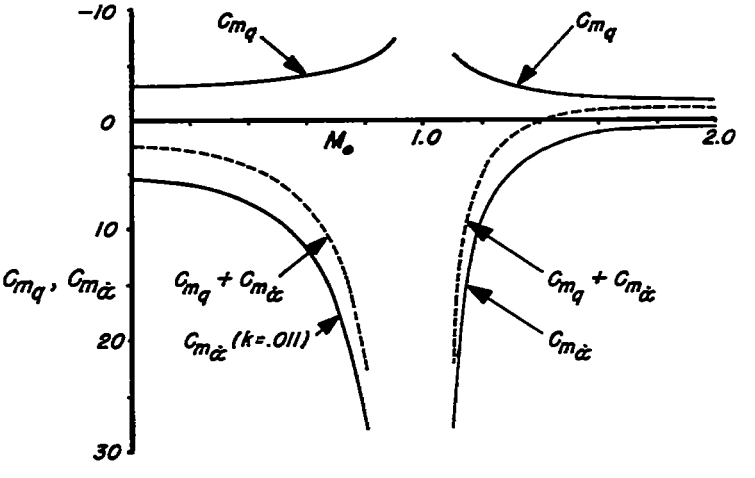

Sketch (w)

As has been mentioned previously, the starting lift coefficient after a step change in α is independent of aspect ratio and is therefore equal to $4\alpha/M_o$ for each wing. The parameter σ_a, the number of half M.A.C. lengths required to reach steady state, is also the same for each wing, being a function only of Mach number. The steady-state lift coefficient, on the other hand, is a function of aspect ratio and

decreases as the aspect ratio is reduced. Thus, as shown schematically in sketch (x), as the aspect ratio becomes smaller, the characteristic

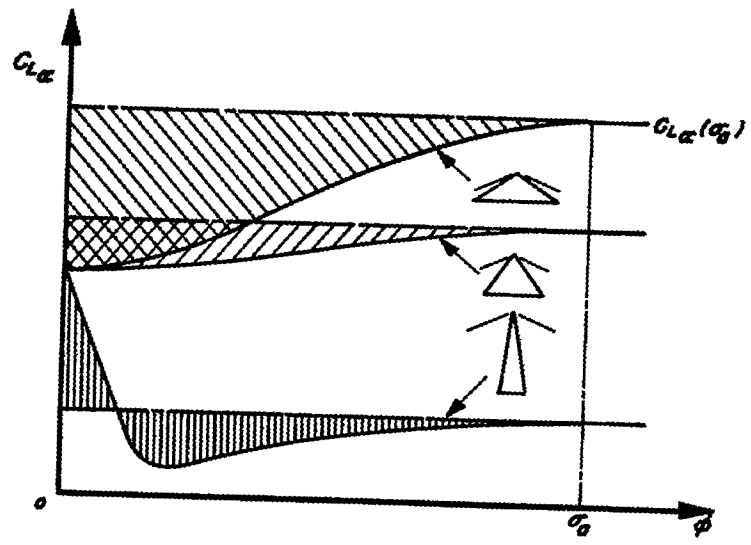

Sketch (x)

area representing $C_{L_{\dot{\alpha}}}$ decreases rapidly.[e] For the wing of smallest aspect ratio, $C_{L_{\dot{\alpha}}}$ may be positive since the area below the steady-state lift coefficient is more than compensated for by the area above. It is evident, therefore, that a reduction in aspect ratio has a highly stabilizing effect on the damping in pitch, since for positive values of the static margin the development of a destabilizing damping moment is possible only when $C_{L_{\dot{\alpha}}}$ is negative. This result is shown in sketch (y) where, for an axis of rotation located at $0.25\ \bar{c}$ and $M_o=1.2$, the damping parameters are presented as functions of aspect ratio. Since for triangular wings the lift due to $\dot{\alpha}$ is concentrated at $\frac{5}{8}\bar{c}$, $C_{m_{\dot{\alpha}}}$ is equal to $-\frac{3}{8}C_{L_{\dot{\alpha}}}$. The variation of $C_{m_{\dot{\alpha}}}$ with aspect ratio shown in sketch (y) then follows directly from the trend of $C_{L_{\dot{\alpha}}}$ shown in sketch (x). Also plotted in sketch (y) is the variation of C_{m_q}

[e] Theoretical indicial curves have not yet been calculated for the triangular wing with subsonic leading edges. The curves drawn in sketch (x) are estimates of the true shapes, and are intended only to indicate the trend of the characteristic area with aspect ratio. The exact variation of $C_{L_{\dot{\alpha}}}$ with aspect ratio can be computed from the results of reference 20.

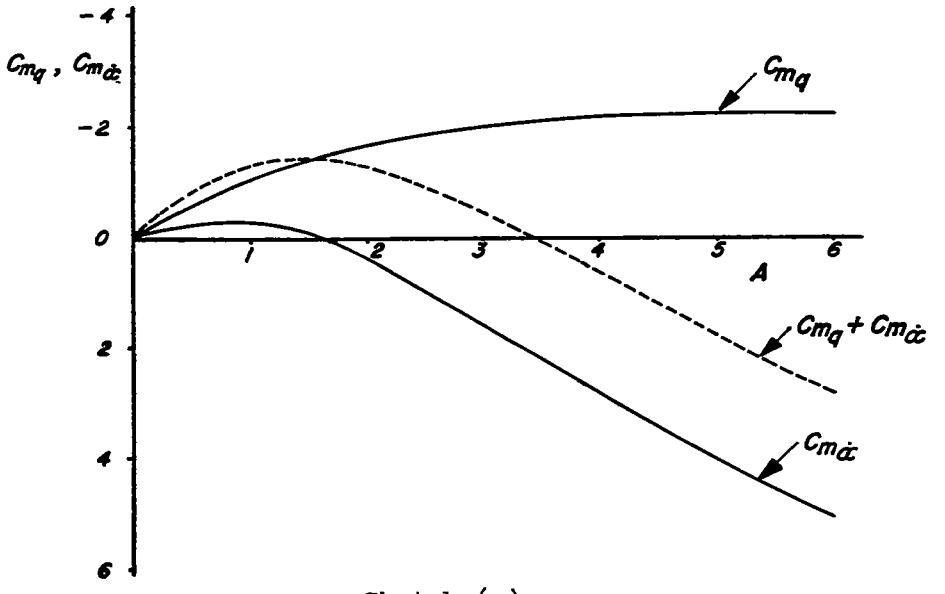

Sketch (y)

with aspect ratio (ref. 20). It is apparent that although C_{m_q} becomes more stabilizing with increasing aspect ratio, the destabilizing effect of $C_{m_{\dot{\alpha}}}$ predominates, and the trend of the net damping moment is seen to become highly destabilizing as the aspect ratio is increased.

By the same reasoning, the variation with aspect ratio of the damping moments of other types of wings can be shown to be similar (see, e.g., refs. 11, 21, 22, and 23). A notable exception, however, is the triangular wing with supersonic leading edges, whose damping in pitch has been shown to be independent of aspect ratio (see refs. 18 and 19). This characteristic may be anticipated from a study of the indicial response curves, since not only are the initial pitching moment $C_{m_\alpha}(o)$ and the half M.A.C. lengths traveled to reach steady state (σ_a) independent of aspect ratio, but, unlike the subsonic-edged triangular wing, the steady-state pitching moment $C_{m_\alpha}(\sigma_a)$ is also independent of aspect ratio, being $-\frac{4}{\beta}\left[\frac{\Delta x_o}{\bar{c}}\right]$. Inspection of the results of reference 4 then reveals that the indicial variation $C_{m_\alpha}(\varphi)$ between zero and σ_a and the steady-state parameter $C_{m_q}(\sigma_a)$ are likewise independent of aspect ratio.

Effect of plan-form shape.- Next, consider the effect of plan-form shape on the supersonic damping in pitch of a group of wings having the same aspect ratio. In order to make use of readily available theoretical results and yet compare these results with the experimental data to be

given later, three wings of aspect ratio 3 are chosen, having the triangular, swept, and rectangular plan forms shown in sketch (z).

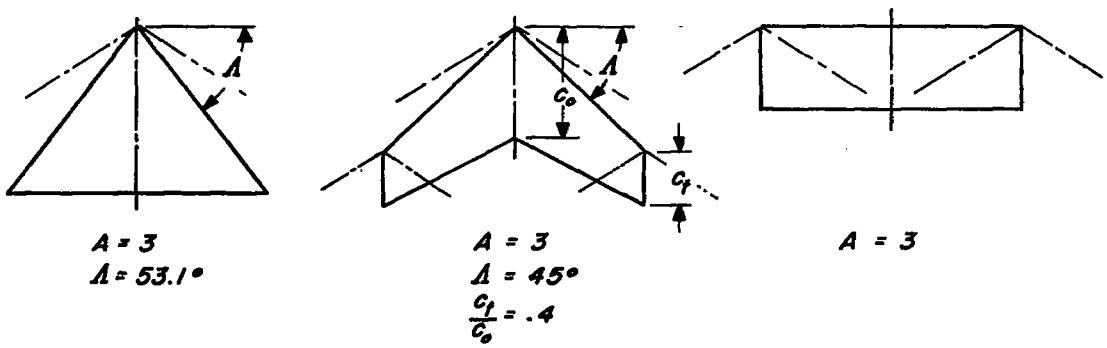

Sketch (z)

As has been shown in the section entitled "Effect of static margin," the tendencies of the wings toward dynamic instability can be compared comprehensively by plotting their stability boundaries. For this comparison, then, use is made of equation (30). The stability derivatives which appear in equation (30) were computed from the theoretical results of references 11, 20, 22, and 23. Results of these calculations are shown in figure 2, wherein the stability boundaries for the three wings are shown as a function of axis position and Mach number. (Note that the axis position for each wing is measured as the distance from the leading edge of the M.A.C. of the wing, and that the dimensions are nondimensionalized on an equivalent basis by referring them to the M.A.C. of the triangular wing.) It is clear from inspection of figure 2 that at any Mach number the triangular wing has the smallest range of axis positions over which dynamic instability is possible and the rectangular wing, the largest.

The differences in the damping characteristics of the triangular and rectangular wings will be more clearly understood by a qualitative study of their indicial lift responses for a Mach number of 1.2, and an examination of the distribution of loading due to $\dot{\alpha}$ for the two wings. Consider first the indicial lift responses.

Again, the starting lift coefficient is independent of plan-form shape and is $4\alpha/M_o$ for each wing. For the rectangular wing, the lift drops abruptly after time zero due to the loss in lift in the regions of the wing influenced by the formation of the tip Mach cones and the starting waves from the side edges (see sketch (m)). Then as the wing begins to emerge from the influence of the starting waves, the lift begins to recover, rises toward its steady-state value (given by eq. 6.3-2 of ref. 11), and attains this value after 12 half-chord

lengths of travel (eq. (24)). The variation is shown in reference 4 and is redrawn in sketch (aa). As mentioned previously, theoretical indicial

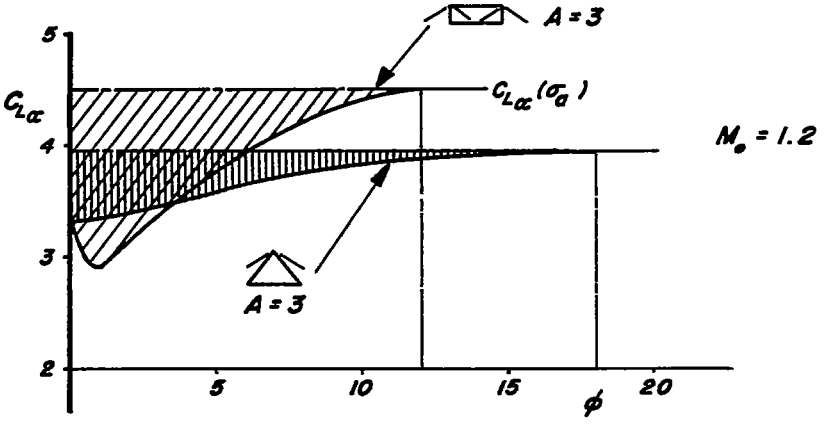

Sketch (aa)

lift results have not yet been developed for triangular wings having subsonic leading edges. However, the variation shown in sketch (aa) is considered to be a reasonable estimate of the true shape, being based on knowledge of the steady-state lift (ref. 20), the time to reach steady state (eq. (24)), and the assumption that the shape of the variation would be similar to that of the wide triangular wing (ref. 4). The curve was adjusted within the known end points until the area corresponding to $C_{L_{\dot{\alpha}}}$ agreed with that given for this parameter in reference 20. It is evident from examination of sketch (aa) that because of the initial loss in lift and the larger steady-state lift for the rectangular wing, $C_{L_{\dot{\alpha}}}$ for this wing is significantly more negative than that for the triangular wing. Next, it is shown in references 11 and 21 that with the exception of regions influenced by tip Mach cones, the loading due to $\dot{\alpha}$ (for $\varphi > \sigma_a$) for wings having swept-back leading edges increases linearly from zero along rays from the apex; whereas for rectangular wings the loading due to $\dot{\alpha}$ increases linearly from zero along chord lines. These characteristics place the center of loading due to $\dot{\alpha}$ at $\frac{3}{4}\,c_o$ for the triangular wing and approximately $\frac{2}{3}\,c_o$ for the rectangular wing.[7] Then for an axis of rotation passing through the aerodynamic centers of the wings, the moment arm for the lift due to $\dot{\alpha}$ for the triangular

[7] Due to the influence of the tip Mach cones, the center of loading due to $\dot{\alpha}$ is shifted forward somewhat from the position it has for the two-dimensional wing. Calculations for the $A = 3$ rectangular wing at $M_o = 1.2$ show that the center of loading is at $0.605\,c_o$.

wing is $\frac{1}{12} c_o$ or $\frac{1}{8} \bar{c}$; whereas for the rectangular wing it is approximately $\frac{1}{6} c_o$.[8] Thus, not only is the negative out-of-phase lift contribution $C_{L_{\dot{\alpha}}}$ for the rectangular wing significantly larger than that for the triangular wing, but the destabilizing damping moment $-\frac{x}{\bar{c}} C_{L_{\dot{\alpha}}}$ is larger yet, due to the larger moment arm. Calculations for the steady pitching parameter C_{m_q} for an axis through the aerodynamic center (refs. 11 and 20) then reveal that C_{m_q} for the triangular wing is more negative than for the rectangular wing. The net result is therefore a considerably larger damping moment for the triangular wing than for the rectangular wing. The result of this comparison, however, should not be interpreted as a recommendation that the triangular rather than the rectangular wing be used on aircraft from a dynamic stability standpoint. To obtain adequate static stability, the rectangular wing would generally be employed in combination with a tail surface, whereas the triangular plan form may be sufficiently airworthy without the use of a tail. The addition of a tail surface in effect reduces the aspect ratio of the rectangular wing, which reduction, as noted previously, has a highly stabilizing effect on the damping in pitch. The tailless triangular wing may therefore experience more difficulty at Mach numbers near 1.0 than a rectangular wing-tail combination.

Effect of frequency.- The previous discussion has been restricted to the analysis of a harmonic motion that is of vanishingly small frequency. This limitation arose as a consequence of discarding all but first order in frequency terms in the expansions of equations (12) and (14). The question arises: when the frequency can no longer be considered small, what effect has the frequency on the damping in pitch?

Previously, the trigonometric terms in equation (14) were expanded and, assuming k to be very small, terms of order k^2 and higher were eliminated. It was then found that the loss in damping from that provided by the steady damping parameter $C_{m_q}(\sigma_a)$ was associated with the destabilizing moment contribution corresponding to the term $-\int_o^{\sigma_a} F_3(\varphi) d\varphi$. Now, however, we discard the restriction of small k and perform graphically the integrations evident in equation (14) for supersonic speeds for several values of k. The procedure is indicated in sketch (bb). It is apparent from sketch (bb) that the effect of increasing k is to reduce the area corresponding to the destabilizing moment contribution $-\int_o^{\sigma_a} F_3(\varphi) \cos k\varphi d\varphi$. There appears another

[8] Again, due to the influence of tip Mach cones, the aerodynamic center is shifted forward from $\frac{1}{2} c_o$ to $0.443\, c_o$. The moment arm is therefore $0.163\, c_o$.

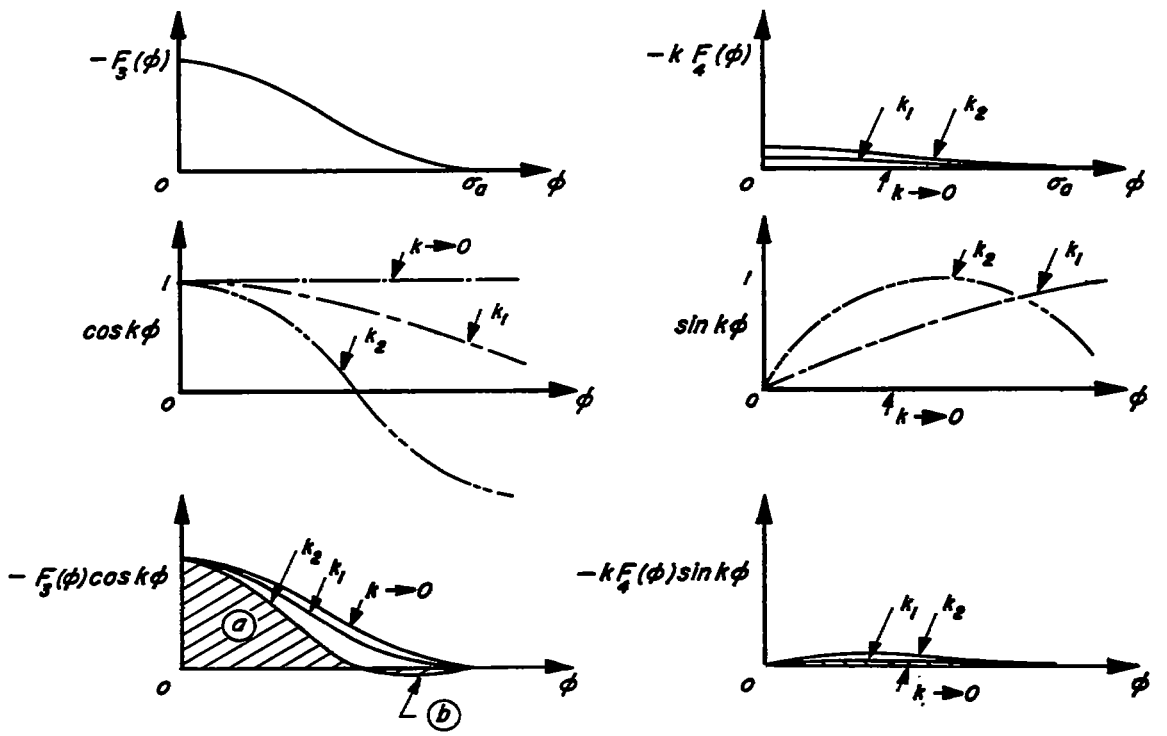

Sketch (bb)

destabilizing contribution, $-k\int_0^{\sigma_a} F_4(\varphi)\sin k\varphi d\varphi$, but quite evidently its effect is small compared to the reduction in the term $-\int_0^{\sigma_a} F_3(\varphi)\cos k\varphi d\varphi$. Notice further in sketch (bb) that the effect of increasing k becomes of marked importance when the half-period of oscillation is the same order of magnitude as the time for the indicial response to reach steady state. As shown in sketch (bb) for the frequency k_2, the area (b) then begins to subtract from (a), so that the destabilizing contribution $-\int_0^{\sigma_a} F_3(\varphi)\cos k\varphi d\varphi$ can be very small. We may therefore expect that increasing the frequency of oscillation has a stabilizing effect on the damping in pitch. This conjecture is substantiated in figures 3 and 4, where the supersonic stability boundary curves for aspect ratio 4 triangular and rectangular wings are shown plotted for various reduced frequencies. These curves were obtained from calculations based on the results of references 16 and 17. Notice that for both wings the region of possible instability is diminished as the frequency is increased.

From the results of the analysis for supersonic speeds, we may further expect that the stabilizing effect of increasing the frequency

will be of even more importance at subsonic speeds, for here the indicial variation $F_3(\Phi)$ dies out at infinity. The half-period of oscillation is therefore always smaller than the time to reach steady state. The situation for the term $-\int_0^\infty F_3(\Phi) \cos k\Phi d\Phi$ is shown in sketch (cc).

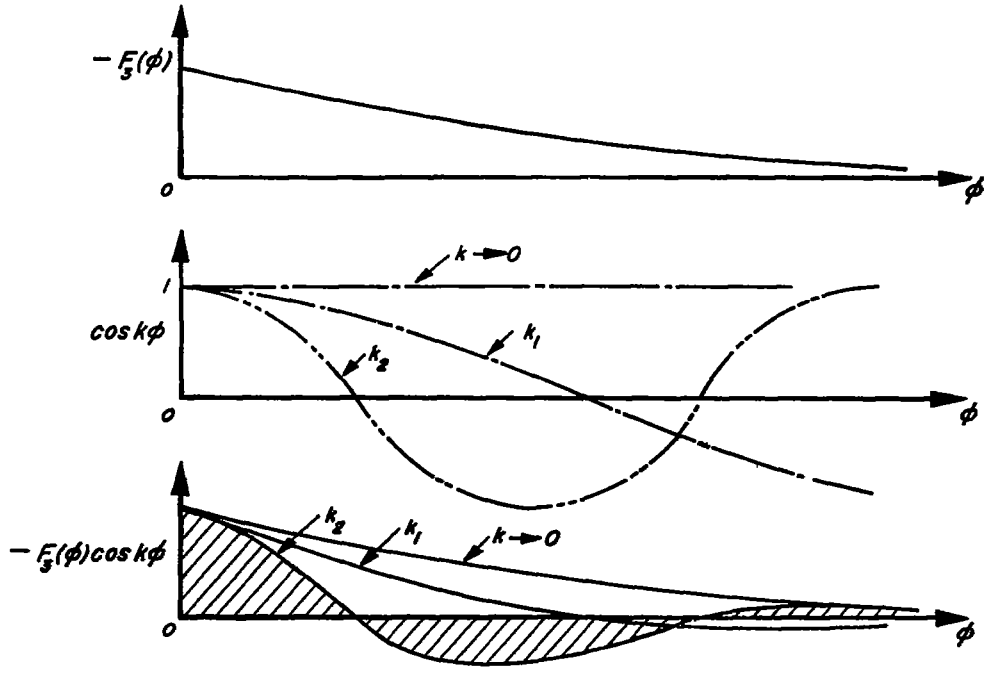

Sketch (cc)

It is evident in sketch (cc) that the destabilizing moment $-\int_0^\infty F_3(\Phi) \cos k\Phi d\Phi$ diminishes rapidly as the frequency is increased. The effect of this reduction on the damping in pitch can be illustrated by plotting the subsonic damping-moment coefficient against reduced frequency for the two-dimensional wing (with axis at the leading edge) for Mach numbers 0, 0.5, and 0.8. The results, which were obtained from reference 4, are shown in figure 5. It is seen in figure 5 that the large destabilizing effects of the moment contributions $-\int_0^\infty F_3(\Phi) \cos k\Phi d\Phi$ and $-k\int_0^\infty F_4(\Phi) \sin k\Phi d\Phi$ are confined to a relatively narrow range of reduced frequencies. Notice further in figure 5 that the range of frequencies for which instability is possible is small at $M_0 = 0$ $(0 < k < 0.04)$ and grows with increasing Mach number. This is believed to be the primary reason why unsteady lift effects were found to be unimportant at low speeds but are of great importance at speeds near the sonic speed.

Effect of thickness.- In this section, the concepts regarding the indicial functions discussed in previous paragraphs will be used to examine the effect of profile thickness on the damping in pitch of a two-dimensional wing flying at a supersonic Mach number.

It will be recalled that for low frequencies the damping in pitch may be considered to be the sum of the damping moment due to steady pitching, $C_{m_q}(\sigma_a)$, and the area representing $C_{m_{\dot{\alpha}}}$ on the plot of the pitching-moment response to a step change in angle of attack (sketch (k-ii)). The airfoil thickness, of course, influences both these parameters. For the purpose of this analysis, it will be considered sufficiently accurate to study the effects of thickness only on the steady parameter $C_{m_q}(\sigma_a)$ and on the end values $C_{m_\alpha}(o)$, $C_{m_\alpha}(\sigma_a)$ and σ_a of the indicial response curve. It will then be assumed that shape of the indicial response curve is not appreciably altered by thickness effects, whereupon the major effect of thickness on $C_{m_{\dot{\alpha}}}$ can be assessed by adjusting the response curve given by the linearized theory to fit the corrected values of $C_{m_\alpha}(o)$, $C_{m_\alpha}(\sigma_a)$ and σ_a.

It has been shown by Busemann (see, e.g., ref. 24) that the loading at an element of a lifting airfoil may be represented by

$$\frac{\Delta p}{q_o} = C_1[\sigma_u - \sigma_l + 2\alpha] + C_2\left\{\sigma_u^2 - \sigma_l^2 + 2\alpha\,[\sigma_u + \sigma_l]\right\} \tag{31}$$

where

$$C_1 = \frac{2}{\sqrt{M_o^2 - 1}}$$

$$C_2 = \frac{[\gamma+1]M_o^4 - 4[M_o^2 - 1]}{2[M_o^2 - 1]^2}$$

and σ_u and σ_l are the local slopes of the upper and lower surfaces, respectively, measured with respect to the chord line. For the special case of an airfoil that is symmetrical about the chord line, σ_u equals σ_l and equation (31) reduces to the following:

$$\frac{\Delta p}{q_o} = 2\alpha C_1 + 4\alpha C_2 \sigma_u \tag{32}$$

For the sake of simplicity, in what follows equation (32) will be used for the local loading rather than equation (31). The results will therefore be valid only for airfoils that are symmetrical about the chord line.

[redacted]

The lift on the airfoil due to angle of attack is obtained simply by integration of equation (32) across the chord.

$$C_L(\sigma_a) = \frac{1}{c_o} \int_o^{c_o} \frac{\Delta p}{q_o} dx$$

$$C_{L_\alpha}(\sigma_a) = \frac{C_L(\sigma_a)}{\alpha} = 2C_1 + \frac{4C_2}{c_o} \int_o^{c_o} \sigma_u dx \tag{33}$$

Similarly, the moment due to angle of attack, measured about the leading edge, is

$$C_m'(\sigma_a) = - \frac{1}{c_o^2} \int_o^{c_o} \frac{\Delta p}{q_o} x \, dx$$

$$C_{m_\alpha}'(\sigma_a) = \frac{C_m'(\sigma_a)}{\alpha} = - C_1 - \frac{4C_2}{c_o^2} \int_o^{c_o} \sigma_u x \, dx \tag{34}$$

When both the leading and trailing edges are on the chord line, equations (33) and (34) reduce to the following:

$$\left.\begin{aligned} C_{L_\alpha}(\sigma_a) &= 2C_1 \\ C_{m_\alpha}'(\sigma_a) &= - C_1 + \frac{2\Omega C_2}{c_o^2} \end{aligned}\right\} \tag{35}$$

where Ω is the enclosed area of the airfoil section.

The local loading given by equation (32) is still applicable for the steady pitching case with this added provision: that now α represents the local angle of attack. For an airfoil pitching about its leading edge, the variation of α with chordwise distance is given by $\alpha = qx/V_o$, where q is the pitching velocity. Then again, for the lift due to pitching,

$$C_L'(\sigma_a) = \frac{1}{c_o} \int_o^{c_o} \frac{\Delta p}{q_o} dx$$

$$C_{L_q}'(\sigma_a) = \frac{C_L'(\sigma_a)}{qc_o/2V_o} = 2C_1 + \frac{8C_2}{c_o^2} \int_o^{c_o} \sigma_u x \, dx \tag{36}$$

Likewise, the pitching moment due to pitching about the leading edge is

$$C_{m}'(\sigma_a) = -\frac{1}{c_o^2}\int_o^{c_o} \frac{\Delta p}{q_o}\, x\, dx$$

$$C_{m_q}'(\sigma_a) = \frac{C_{m}'(\sigma_a)}{qc_o/2V_o} = -\frac{4}{3}C_1 - \frac{8C_2}{c_o^3}\int_o^{c_o} \sigma_u x^2 dx \qquad (37)$$

The primes on the parameters indicate that the moments are measured about and the wing is pitching about the leading edge.

In order to illustrate the result given by equation (37), the damping moment due to steady pitching has been computed for a family of airfoils having symmetrical biconvex parabolic arc sections. The results are presented in figure 6. The dashed line in figure 6 represents the theoretical locus of Mach number and leading-edge angle for bow-wave detachment (ref. 24). Since the requirements of the second-order theory are violated to the left of this line, the damping curves there are not rigorously correct, and therefore are terminated a short distance beyond the line.

To determine the effect of thickness on the parameter, $C_{m_{\dot{\alpha}}}'$, it is assumed that the shape of the indicial pitching-moment variation is not significantly affected by thickness. When this assumption is made, it becomes necessary only to correct the initial and final ordinates of the indicial curve $C_{m_\alpha}'(o)$ and $C_{m_\alpha}'(\sigma_a)$ and the number of half-chord lengths traveled to reach steady state, σ_a. The response curve is adjusted to fit these new end values, so that the area representing the corrected $C_{m_{\dot{\alpha}}}'$ can then be determined.

The effect of thickness on the final ordinate of the indicial curve, $C_{m_\alpha}'(\sigma_a)$, has already been determined (eq. (34)). Now consider the starting lift and moment.

Assume first a thin flat wing to be flying at zero angle of attack in a uniform stream of density ρ_o. At time zero, it starts to sink with downward velocity $V_o\alpha$. The impulsive start causes a plane compression wave to be emitted from the lower surface at the speed of sound, which is constant throughout the stream. (The pressure and therefore the temperature is sensibly constant.) At the same instant, a plane expansion wave is emitted from the upper surface and travels at the same velocity in the opposite direction. At the end of an infinitesimal time period Δt, the wing has sunk a distance $V_o\alpha\Delta t$. The sound waves have

moved a distance $a_o\Delta t$ in both directions. The mass of fluid affected is $2\rho_o c_o a_o \Delta t$. Then, from Newton's second law, one may write

$$(f_u - f_l)\,\Delta t = 2\rho_o c_o a_o \Delta t\, V_o \alpha$$

where f_u and f_l are the forces per unit span on the upper and lower surfaces, respectively. Converting to coefficient form, it then appears that

$$\frac{C_L(o)}{\alpha} = \frac{f_u - f_l}{\frac{1}{2}\rho_o V_o^2 c_o \alpha} = \frac{4}{M_o}$$

For the wing of finite thickness for which the pressure varies along the chord, a different result is expected. The wing is assumed to have been flying at zero angle of attack for a period of time long enough for the flow to have established itself around the surface. In this case, the density, temperature, and therefore the speed of sound, vary along the chord due to the curvature of the surface. At time zero the wing again starts to sink, but the compression and expansion waves are propagated at different rates at various chordwise positions so that

$$\Delta t\,[f_u - f_l](x) = 2\,\frac{\rho}{\rho_o}(x)\,\frac{a}{a_o}(x)\,\rho_o a_o \Delta t\, V_o \alpha$$

and the starting lift becomes

$$\frac{C_L(o)}{\alpha} = \frac{4}{M_o c_o}\int_o^{c_o} \frac{\rho}{\rho_o}\frac{a}{a_o}\,dx \tag{38}$$

From reference 24, the variation of $\rho/\rho_o\ a/a_o$ with C_p is found to be

$$\frac{\rho}{\rho_o}\frac{a}{a_o} = \left[1 + \frac{\gamma M_o^2}{2} C_p\right]^{\frac{\gamma+1}{2\gamma}} \tag{39}$$

where C_p is the pressure coefficient at a point on the surface when the airfoil is at zero angle of attack. Again, from reference 24,

$$C_p = \frac{p - p_o}{q_o} = C_1\sigma_u + C_2\sigma_u^2 \tag{40}$$

where p and p_o are, respectively, the pressure at a point on the surface of the airfoil and the free-stream static pressure.

For the symmetrical biconvex parabolic arc airfoil considered earlier, the local slope σ_u is given by

$$\sigma_u = 2\delta\left[1 - \frac{2x}{c_o}\right] \tag{41}$$

where δ is the thickness ratio.

Then expanding equation (39) in a binomial series, retaining terms through the second order in σ_u, and performing the integration indicated by equation (38), there results for the starting lift coefficient

$$C_{L_\alpha}(o) = \frac{4}{M_o}\left\{1+0.04M_o^2\delta^2[20C_2-M_o^2C_1^2]\right\} \tag{42}$$

A similar procedure can be carried out for the starting pitching-moment coefficient, measured about the leading edge

$$C_{m_\alpha}'(o) = -\frac{4}{M_o c_o^2}\int_o^{c_o}\frac{\rho}{\rho_o}\frac{a}{a_o}\,x\,dx$$

$$C_{m_\alpha}'(o) = -\frac{2}{M_o}\left\{1+0.04M_o^2[20C_2\delta^2-M_o^2C_1^2\delta^2-10C_1\delta]\right\} \tag{43}$$

It is necessary also to consider the effect of thickness on the time required for the loading on the airfoil subjected to a step change in angle of attack to reach steady state. As was seen in sketches (n) and (p), the time to reach steady state is exactly equivalent to the time required for the wing to escape the influence of the sound waves emitted from the leading edge at the start of the motion. For purposes of analysis, the situation is reversed by requiring that the wing remain stationary in a fluid moving with supersonic velocity V_o, and causing a sound wave to be emitted at the leading edge of the wing. To an observer standing on the upper surface of the airfoil, there will appear to be two wave fronts whose velocities tangent to the surface are $[V+a]$ and $[V-a]$, where V and a are the local stream velocity and local speed of sound, respectively. Then the time required for the slower wave front to clear the airfoil is given by

$$t_a = \int_o^{t_a} dt = \int_o^{c_o}\frac{dx}{[V-a]\cos[\tan^{-1}\sigma_u]} = \frac{M_o}{V_o}\int_o^{c_o}\frac{\sqrt{1+\sigma_u^2}\,dx}{[V/a_o-a/a_o]} \tag{44}$$

[redacted]

It is therefore necessary to obtain V/a_o and a/a_o as functions of chordwise location x. Again, in reference 24 these quantities are found to be functions of the local pressure coefficient C_p.

$$\left.\begin{aligned} \frac{a}{a_o} &= \left[1 + \frac{\gamma M_o^2}{2} C_p\right]^{\frac{\gamma-1}{2\gamma}} \\ \frac{V}{a_o} &= \left[\frac{2}{\gamma-1}\left\{1 - \left[\frac{a}{a_o}\right]^2\right\} + M_o^2\right]^{\frac{1}{2}} \end{aligned}\right\} \tag{45}$$

Expanding equations (45) through the second power of C_p and $\sqrt{1+\sigma_u^2}$ through the second power of σ_u, there is obtained

$$t_a = \frac{M_o}{V_o[M_o-1]} \int_o^{c_o} \frac{\left[1 + \frac{1}{2}\sigma_u^2\right] dx}{1-\kappa_1 C_p+\kappa_2 C_p^2} \tag{46}$$

where

$$\kappa_1 = \frac{0.50M_o + 0.10M_o^2}{M_o - 1}$$

$$\kappa_2 = \frac{0.125M_o[M_o^2-1] + 0.03M_o^4}{M_o - 1}$$

The pressure coefficient C_p is now assumed to be that existing at a point on the surface when the airfoil is at zero angle of attack. This assumption, of course, introduces some error since the angle of attack has changed discontinuously from zero to α at $t = 0$. However, if we require that α be less than δ^2, then the error introduced through neglect of the effect of the change in α on the pressure coefficient is negligible. Then, as in the starting lift problem,

$$C_p = C_1\sigma_u + C_2\sigma_u^2 \tag{47}$$

Inserting equation (47) into equation (46), dividing numerator by denominator, and again retaining terms through the second power in σ_u, there results

$$t_a = \frac{M_o}{V_o[M_o-1]} \int_o^{c_o} \left[1+C_1\kappa_1\sigma_u + \left\{\kappa_1 C_2+[\kappa_1^2-\kappa_2]C_1^2 + \frac{1}{2}\right\}\sigma_u^2\right] dx \tag{48}$$

For the symmetrical biconvex parabolic arc airfoil, σ_u is replaced by equation (41), whereupon for this airfoil the time to reach steady state becomes

$$t_a = \frac{c_o M_o}{V_o[M_o-1]}\,[1+\xi] \tag{49}$$

where

$$\xi = \frac{4\delta^2}{3}\left\{\kappa_1 C_2 + [\kappa_1^2 - \kappa_2]C_1^2 + \frac{1}{2}\right\}$$

Alternatively, in terms of the number of half-chord lengths of travel,

$$\sigma_a = \frac{2V_o}{c_o}\,t_a = \frac{2M_o}{M_o-1}\,[1+\xi] \tag{50}$$

The effect of thickness on the damping parameter $C_{m_{\dot{\alpha}}}'$ can now be estimated approximately by adjusting the indicial pitching-moment curve obtained from the linearized theory to the end values given by equations (34), (43), and (50), and then measuring the area corresponding to the "corrected" $C_{m_{\dot{\alpha}}}$. The process is indicated in sketch (dd) below, and the adjustment formulas are given by equations (51).

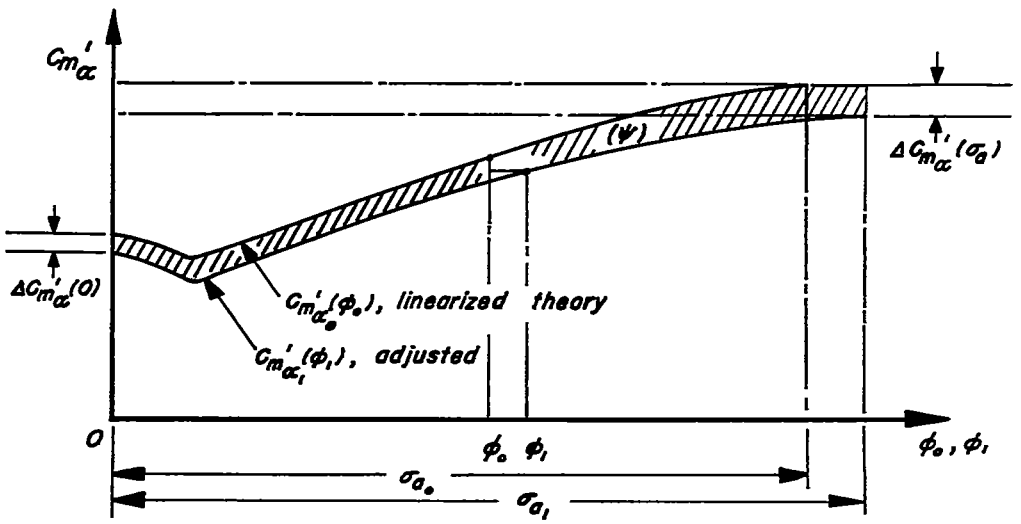

Sketch (dd)

[redacted]

$$\left.\begin{aligned} C_{m_{\alpha_1}}'(\varphi_1) &= C_{m_{\alpha_o}}'(\varphi_o) - \Delta C_{m_\alpha}'(o) - \frac{\varphi_o}{\sigma_{a_o}}\left[\Delta C_{m_\alpha}'(\sigma_a) - \Delta C_{m_\alpha}'(o)\right] \\ \varphi_1 &= \frac{\varphi_o}{\sigma_{a_o}}\sigma_{a_1} \end{aligned}\right\} \quad (51)$$

where

$$\Delta C_{m_\alpha}'(o) = C_{m_{\alpha_o}}'(o) - C_{m_{\alpha_1}}'(o)$$

$$\Delta C_{m_\alpha}'(\sigma_a) = C_{m_{\alpha_o}}'(\sigma_{a_o}) - C_{m_{\alpha_1}}'(\sigma_{a_1})$$

and the subscripts o and 1 indicate values corresponding to the linearized theory and the adjusted theory, respectively. Notice also in sketch (dd) that the area corresponding to the adjusted value of $C_{m_{\dot\alpha}}'$ is given by the following expression:

$$C_{m_{\dot\alpha_1}}' = C_{m_{\dot\alpha_o}}' + (\Psi) - \sigma_{a_1}\Delta C_{m_\alpha}'(\sigma_a) \quad (52)$$

The parameter $C_{m_{\dot\alpha}}'$ for pitching about the leading edge has been computed, using equations (35) to (52) for the same family of airfoils as that discussed previously and the results added to those obtained for C_{m_q}' (eq. (37)). The total damping moment $C_{m_q}' + C_{m_{\dot\alpha}}'$ is shown plotted as a function of Mach number in figure 7. It is evident from examination of figure 7 that the effects of thickness are small and are in the destabilizing direction with increasing thickness ratio. It should be noted that this result does not agree with those of Jones and of Wylly in references 25 and 26 which indicate that the effect of thickness is extremely stabilizing. In reference 27, however, Van Dyke takes issue with the results of references 25 and 26, and offers an alternate solution correct to the second order in thickness. From this result, the following relationship for the damping-moment coefficient for pitching about the leading edge can be deduced:

$$\left[C_{m_q}'+C_{m_{\dot\alpha}}'\right]_1 = \left[C_{m_q}'+C_{m_{\dot\alpha}}'\right]_o \left[1 + \left\{\frac{\lambda\beta[M_o^2 N-2]}{2-M_o^2}\,\delta\right\}\right] \quad (53)$$

where $\left[C_{m_q}'+C_{m_{\dot\alpha}}'\right]_o$ is the damping-moment coefficient obtained from the linearized theory and

$$N = \frac{\gamma+1}{2}\frac{M_o^2}{\beta^2}$$

$\lambda = 1$ for biconvex airfoils

$\lambda = \frac{3}{4}$ for double-wedge airfoils

The trend of the damping-moment coefficient with thickness obtained from this result agrees closely with that obtained in the present paper.

EXPERIMENT

Wind Tunnel

The experimental investigation of the damping-in-pitch characteristics of the various model configurations was conducted in the Ames 6- by 6-foot supersonic wind tunnel. In this tunnel, the Mach number can be varied continuously within the subsonic speed limits 0.60 to choking, and at supersonic speeds from 1.20 to 2.00. The total pressure can also be changed at any time within the limits 3 pounds per square inch absolute to atmospheric. A complete description of the wind tunnel is given in reference 28.

Models

The pertinent dimensions of the five wing-body configurations investigated in the present report are shown in figure 8. All the wings had sections which were symmetrical in streamwise planes and 3 percent thick. Wings having leading-edge sweep angles less than or equal to 45° (wings c, d, and e in fig. 8) had biconvex circular-arc sections in streamwise planes with maximum thickness at 50-percent chord. Wings having leading-edge sweep angles greater than 45° (wings a and b in fig. 8) had NACA 0003-63 sections in streamwise planes. The wings were identical in plan form and section shape to those investigated in the series of force tests reported in references 29 to 33. Strength considerations required that wings c, d, and e be built of steel. Wings a and b were built of aluminum.

The models were fitted with bodies such that the distance from the apex of the body to the wing-body intersection was the same for each model. Also, the ratio of wing area to body maximum cross-sectional area was 17.9 for each model. Forward of the point of maximum radius, the

bodies were of thin laminated wood construction and were identical in shape to those of references 29 to 33. The aluminum afterbodies were cylindrical in shape and terminated at the trailing edges of the wings to permit the models to be deflected with sufficient amplitude when mounted on the support structure.

Model Support System

The support system used in the present investigation was the same as that developed for the single-degree-of-freedom free-oscillation experiments of reference 10. The interested reader is referred to that report for a detailed description of the oscillation mechanism. For the present tests, two changes were made in the system which served to improve the accuracy of the data. The changes and the reasons for them are as follows:

1. The vertical flexure pivots which provided vertical restraint in the tests of reference 10 were replaced by bearings after it was found that the heavier models of this investigation caused the pivots to twist laterally when the model was given its initial displacement. An undesirable yawing oscillation was thereby induced which destroyed the linearity of the system. Installation of the bearings entirely eliminated this yawing tendency. The damping due to friction in the bearings was somewhat larger than that of the flexure pivots, but by frequent checking of the wind-off damping and regular replacement of the bearings it was possible to maintain the tare damping well within acceptable limits.

2. A stiffening strut was installed between the sting support and the tunnel ceiling in order to remove the possibility of coupling between the model oscillation and the resonant mode of the sting support. The influence of the strut on the aerodynamic forces at subsonic speeds was investigated by removing the strut and recording data for one of the models at a frequency sufficiently below the sting resonant frequency to avoid excessive sting vibrations. Results obtained with the strut installed and removed agreed within the experimental accuracy.

By effectively eliminating both yawing tendencies of the model and vibrations of the sting support, it can be seen from comparison of the present results with those of reference 10 that the deviations between a number of observations at a given Mach number were markedly reduced.

Scope of Tests

Investigation of the damping-in-pitch characteristics of the various model configurations was conducted over a supersonic Mach number range of 1.20 to 1.90 and, where possible, over a subsonic Mach number range of 0.60 to 0.90. The Reynolds number for the major portion of the tests was held constant at 1.6×10^6 per foot. Additional data for one of the models was obtained at Reynolds numbers of 1.0×10^6 per foot and 3.2×10^6 per foot.

All the tests were conducted with the models at a mean angle of attack of 0°, the angle being measured from the mean line of the sting support to the axis of the test section. For each oscillation, an initial displacement of $\pm 5^\circ$ was imparted to the model by means of the pneumatically actuated pawl arrangement described in reference 10.

Other important variables are listed below for the five wing-body configurations investigated:

Model	Range of moment of inertia, slug - ft^2	Axes of rotation, % M.A.C.	Range of reduced frequency
A = 2 triangular	0.0534 - 0.0589	35, 45	0.012 - 0.037
A = 3 triangular	.0368 - .0402	25, 35	.018 - .050
A = 4 triangular	.0491 - .0512	25, 35, 45	.007 - .041
A = 3 swept	.0549 - .0576	25, 35	.011 - .025
A = 3 unswept	.0422 - .0488	20, 35, 40	.007 - .025

Reduction of Data

The technique used in this investigation for reducing an experimental oscillation-decay record to the damping-in-pitch coefficient $C_{m_q} + C_{m_{\dot{\alpha}}}$ was identical to that described in reference 10. Briefly, this technique involves plotting the envelope of the oscillation-decay curve against time on semilogarithmic graph paper. If the damping of the system is a linear function of the angular velocity, this plot will be a straight line, the slope of which is proportional to the damping term. Calibrations for the model moment of inertia and the damping due to internal friction, and standard measurements for the density and velocity of the air stream then enable one to reduce the aerodynamic damping term to coefficient form. The aerodynamic restoring moment C_{m_α} can be obtained from measurements of the frequency of oscillation and a calibration for the static spring constant of the system. Results for

the restoring moment about two axes of rotation a known distance apart then permit calculation of the lift-curve slope C_{L_α}.

Corrections to Data

No wind-tunnel-wall corrections were made to the subsonic results for any of the measured stability derivatives. To the author's knowledge, no corrections have been developed for application to the forces acting on a finite-span wing oscillating in a compressible fluid. Tunnel-resonant-frequency effects were investigated by use of reference 34, and it was found that the range of frequencies used in this investigation was well below the lowest calculated tunnel resonant frequency. In view of the fact that the subsonic damping moments measured for the $A = 4$ triangular wing in the present investigation agreed reasonably well with the results for a similar wing obtained during an investigation in the Ames 12-foot wind tunnel (ref. 35), it is believed that the effect of the tunnel walls on the damping in pitch was not significant.

A subsonic correction could have been made to the static parameters C_{L_α} and C_{m_α}. However, since this correction would have been very small, and in view of the uncertainty involved in applying static corrections to the results of dynamic measurements, it was decided not to make the correction.

The effects of constriction of the flow at subsonic speeds by the tunnel walls were taken into account by the method of reference 36. This correction amounted to, at most, a 2-percent increase in the Mach number and in the dynamic pressure over that determined from a calibration of the wind tunnel without a model in place.

For the tests at supersonic speeds, no corrections were required to be made on either the aerodynamic measurements or the air-stream properties.

The reader is referred to reference 10 for a discussion of the precision of the data. Since the method of reduction of the data was the same as that of reference 10, the uncertainty in the recorded value of a given damping coefficient remained of the order of ± 0.02. However, by virtue of the elimination of yawing tendencies in the model and sting-support vibrations, the standard deviation of a number of observations at a given Mach number was reduced from ± 0.06 to ± 0.03.

RESULTS

Damping Coefficients

The basic experimental results for the damping coefficient $C_{m_q} + C_{m_{\dot{\alpha}}}$ for the five wing-body configurations investigated are shown in figures 9 to 13. In cases where data could be obtained at subsonic as well as supersonic speeds, these results are shown plotted through the Mach number range 0.60 to 1.90 for ready comparison of the magnitudes of the coefficients in the two speed ranges. Also shown plotted in figures 9 to 13 are the theoretical results for the damping coefficient $C_{m_q} + C_{m_{\dot{\alpha}}}$ at supersonic speeds for the wings alone. In addition, theoretical results for the triangular wing-body combinations, considering interference effects, are shown in figures 9 to 11. The sources of these theoretical results are references 11, 16 through 23, and 37. The experimental results for subsonic speeds are not compared with theory, since a rigorous linearized theory for triangular, swept, or unswept wings oscillating in a subsonic compressible flow has not yet been developed. A very approximate analysis for C_{m_q} and $C_{m_{\dot{\alpha}}}$ for the aspect ratio 4 triangular wing was presented in reference 10. In this development, the parameter $C_{m_{\dot{\alpha}}}$ was approximated using the incompressible theory of reference 8 for the elliptic wing. However, a more rigorous analysis for the elliptic wing in compressible flow (ref. 11) has indicated that the result of reference 10 for $C_{m_{\dot{\alpha}}}$ may be incorrect. The good agreement between the experimental subsonic results of reference 10 and the subsonic theory of reference 10 may be fortuitous.

The results for the three triangular wings (figs. 9 to 11) and the swept wing (fig. 12) show that in the supersonic speed range, in every case, the linearized first-order-in-frequency theory provides a reliable guide for obtaining both the magnitude and trend with Mach number of the damping coefficients. Of particular importance are the theoretical predictions of ranges of Mach number over which the wings could experience negatively damped oscillations. The experimental results for the $A = 3$ triangular wing (fig. 10) are inconclusive in this regard since the theoretically predicted unstable range occurs in the low supersonic Mach number range, 1.0 to about 1.08, where it was not possible to obtain data. The predictions by the theory of larger unstable ranges for the $A = 4$ triangular wing and the $A = 3$ swept wing were borne out by the experimental results, as shown in figures 11 and 12 by the experimental points plotted below the abcissas. In the absence of available theoretical results for unswept wings, the experimental results for the unswept wing are compared with theoretical damping coefficients for a rectangular wing of aspect ratio 3 (fig. 13). It is seen from examination of figure 13 that the theoretical prediction of a rather large region of instability for an axis of rotation at $0.20\bar{c}$ (fig. 13(a)) is

borne out by the experimental results but that the theory fails to predict the reversal in trend of the damping coefficients at low supersonic Mach numbers for axes of rotation closer to the aerodynamic center (figs. 13(b) and (c)). It is clear from these results that the effects of taper can be important and should be considered for an accurate theoretical appraisal of the damping-in-pitch characteristics of unswept wings.

It should be mentioned that at a Mach number of 0.90, the damping of the $A = 4$ triangular wing (fig. 11) and the $A = 3$ triangular and swept wings (figs. 10 and 12) were highly nonlinear with angle of attack, being stabilizing for angles of attack of 5° and decreasing steadily to zero at about 1°. The dashed lines for this Mach number shown in figures 10, 11, and 12 are intended to indicate the range of this nonlinear variation. Further discussion of the phenomenon is withheld to a later section of this report. The above-mentioned difficulty was not encountered with the $A = 2$ triangular wing, and the value of $C_{m_q} + C_{m_{\dot{\alpha}}}$ at $M_o = 0.9$ for this wing (fig. 9) represents the damping throughout the amplitude range. Subsonic results for the unswept wing could not be obtained due to the highly erratic behavior of the aerodynamic restoring moment which generally was so strongly destabilizing as to counterbalance the spring restoring moment and force the model against its stops.

Reynolds Number Effects

For the $A = 2$ triangular wing at supersonic speeds (fig. 9), damping coefficients have been obtained at three Reynolds numbers ranging from 1.18×10^6 to 3.77×10^6, while at subsonic speeds (fig. 9) they have been obtained at 1.18×10^6 and 1.89×10^6. In both cases, it is evident that at least within the range of Reynolds numbers at which data were recorded there is no significant effect of scale. It is reasonable to assume that a similar lack of scale effects exists for the other wings as well.

Aeroelastic Effects

In figures 14 to 23, the static parameters C_{m_α} and C_{L_α} for the five wings are compared with force-test measurements of similar wings (refs. 29 to 33). Such a comparison is useful as an indication of the importance of aeroelastic effects on the aerodynamic properties of the less rigid models of the present tests. The fact that at supersonic speeds there is excellent agreement between the two experiments for the lift-curve slope C_{L_α}, whereas the present results for C_{m_α} are

consistently smaller, is attributed primarily to the difference in the body shapes of the models of the two investigations. In the force-test investigation, the afterbodies were carried beyond the trailing edges of the wings, which would tend to shift the centers of pressure of the wing-body combinations farther rearward while leaving the total lift essentially unchanged. From this reasoning, it is concluded that aeroelastic effects on the aerodynamic coefficients of the present tests are of secondary importance. At subsonic speeds, there are differences in magnitude of both C_{L_α} and C_{m_α}. However, in view of the fact that no large effects of aeroelasticity were found at supersonic speeds where the dynamic pressure is greatest, it is believed that the differences in C_{L_α} and C_{m_α} at subsonic speeds are not due to aeroelastic effects. It must therefore be stated that at the present time the differences at subsonic speeds are not understood.

Transfer of Axes

Sufficient information has been given in figures 9 to 23 to permit the transfer of the damping-in-pitch results at supersonic speeds to axes of rotation other than those used during the tests. Such a transfer, if valid, of course greatly increases the range of applicability of the given data. The validity of the transfer equation (given in appendix A) depends primarily on the invariance of the stability derivatives with changes in angle of attack and angular velocity and could be best checked by experimental means. Checks on the method are provided in figures 11(c) and 13(c) for the $A = 4$ triangular wing and $A = 3$ unswept wing, respectively. Shown in these figures are the experimental damping coefficients obtained during the investigation and coefficients for the same axis position computed, by means of the transfer equation, from the results of experiments at two other axis positions. It is evident that the transferred results portray the actual data with sufficient accuracy to establish the validity of the method.

DISCUSSION

Effect of Aspect Ratio

It will be remembered from the discussion in the theoretical section of this report that the linearized theory indicates that a decrease in aspect ratio has a highly stabilizing effect on the damping in pitch of a triangular wing with subsonic leading edges. This indication is confirmed in figure 24, wherein the damping in pitch is shown as a function of Mach number for the three triangular wings having their axes at $0.35\bar{c}$. It is noteworthy that the $A = 2$ wing shows no tendency toward dynamic

instability in the Mach number range 1.2 to 1.9, that for $M_o < 1.2$ the trend of the damping coefficients of the $A = 3$ wing is toward instability, and that a range of instability exists for the $A = 4$ wing. It is of further interest to note that for Mach numbers greater than 1.67, in which range the leading edges of the $A = 3$ and $A = 4$ wings are supersonic, the damping coefficients for these wings are essentially the same. This serves as a partial confirmation of the theoretical prediction of reference 19, wherein it is shown that the damping coefficients of triangular wings having supersonic leading edges are independent of aspect ratio.

A more comprehensive way of comparing the tendencies of the wings toward dynamic instability would be to show the entire ranges of axis positions and Mach numbers over which dynamic instability is possible, that is, to plot the stability boundary curves for the three wings. In the Mach number range 1.2 to 1.9, however, only the $A = 4$ wing has a region of instability and this curve is shown, compared with the theoretical curve, in figure 25.

The preceding comparison (fig. 24) was useful primarily for verifying the theoretical prediction regarding the role played by aspect ratio in determining the tendency of a triangular wing toward dynamic instability. A comparison of the actual magnitudes of the damping moments was masked, however, by the fact that the coefficients for the three wings were referred to their own respective characteristic lengths. In the following comparison, an attempt is made to overcome this difficulty by posing the question: Given three triangular wings of aspect ratios 2, 3, and 4, of equal area, and required to have the same restoring moment (in ft-lb) at a Mach number of 1.4, how do the physical magnitudes of the damping moments compare? For this purpose, the aspect ratio 3 wing is chosen as a standard, required to have a static margin of 0.05 at $M_o = 1.4$, and the damping moments of all the wings referred to the M.A.C. of the aspect ratio 3 wing. The comparison on this basis is shown in figure 26. It is evident from examination of figure 26 that on this basis also, the effect of decreasing the aspect ratio is beneficial to the damping in pitch, the aspect ratio 2 wing having the largest damping moments throughout the range of test Mach numbers, and the aspect ratio 4 wing the smallest.

Effect of Plan-Form Shape

For this comparison, use is made of the results for the aspect ratio 3 triangular, swept, and unswept wings. First, the prediction made in the section entitled "Theory" regarding the tendencies of three similar wings toward dynamic instability is examined by comparing their stability boundaries. From the preceding section, it will be

recalled, however, that no region of instability exists for the $A = 3$ triangular wing in the Mach number range 1.2 to 1.9. It is apparent, therefore, that as predicted by the theory the triangular wing is superior in this regard. The stability boundary curves for the swept and unswept wings, with axis position referred to the leading edge of the M.A.C., are compared in figure 27. Again, the theoretical prediction is borne out for, as seen in figure 27, a considerably larger region of instability exists for the unswept wing.

Next, the magnitudes of the damping moments are compared by choosing the $A = 3$ triangular wing as a standard, with a static margin of 0.05 at $M_o = 1.4$, and, as in the previous section, requiring that the wings have equal restoring moments at this Mach number. The comparison is shown in figure 28. On this basis, it is again apparent that the triangular wing is the superior wing, followed in order by the swept and unswept wings.

Notice in figures 26 and 28 that since the damping coefficients of all five wings investigated are referred to the M.A.C. of the $A = 3$ triangular wing and since all wings have equal restoring moments at $M_o = 1.4$, the results of figures 26 and 28 may be compared directly. Here it appears that the $A = 2$ triangular wing is the most desirable wing from a longitudinal-dynamic-stability standpoint, and the $A = 3$ unswept wing the least desirable. As mentioned previously, however, it should not be inferred that the result of this comparison implies a recommendation for the use of triangular rather than unswept wings. Obviously, the addition of tail surfaces could alter considerably the relative damping-in-pitch merits of the wings investigated.

Effect of Thickness

It has been shown by the results of experiments (figs. 9 to 12) that the supersonic linearized potential theory provides a reliable basis for predicting the low-frequency damping-in-pitch characteristics of thin wings of finite span. Considerable doubt has been shed, however, over the ability of the linearized theory to predict the dynamic behavior of wings that cannot be classified as thin. In recent years, a number of reports have been issued (refs. 25, 26, and 38) which indicate that second-order thickness effects have a profoundly stabilizing effect on the damping in pitch of two-dimensional wings. In particular, reference 26 indicates that by increasing the thickness of an infinite-span wing from zero to only 4-1/2 percent, the rather large region of instability predicted by the linearized theory is completely eliminated. In contrast to these results, the approximate analysis of this paper (see Theory) indicates that thickness effects are relatively small, the destabilizing effect on C_{m_q} being partially canceled by a stabilizing

effect on $C_{m_{\dot{\alpha}}}$. In view of these conflicting results, it is of some interest to obtain additional experimental data which would serve to clarify the issue. Of particular interest are the effects of thickness for finite-span wings. In this case, a limited comparison can be made between the experimental results for the 3-percent $A = 4$ triangular wing of this report and the results of reference 10 for two 6-percent triangular wings having the same aspect ratio. Aside from the differences in profile and small differences in the dimensions of the bodies, the models and test conditions of the two experiments were almost identical. The comparison is shown in figure 29. It is seen that for this wing, the effects of thickness are small and are in the direction of decreasing stability with increasing thickness. Of primary importance is the fact that all the wings exhibit regions of Mach number over which dynamic instability is experienced.

Although admittedly the experimental evidence in figure 29 is not conclusive, nevertheless in the light of these results it is difficult to accept those results which indicate that large stabilizing effects of thickness are present on infinite-span wings, especially in view of the fact that the behavior of a triangular wing with supersonic edges is in many ways quite similar to that of an infinite-span wing.

Effect of Nonlinearities

From examination of the experimental oscillation-decay records at both low subsonic and all supersonic speeds, it was evident that the assumption of a linear second-order system was well justified. Aside from a moderate amount of scatter, a decay curve could be fitted by an exponential curve over a wide range of amplitudes, verifying that the damping parameter was essentially independent of amplitude. At high subsonic speeds, however, this linear behavior was no longer true for most of the wings tested. As an example, figure 30 shows the oscillation-decay record for the $A = 3$ triangular wing at $M_o = 0.90$. It is seen that after an initial displacement the amplitude of oscillation quickly dies out to a low level, but there sustains itself indefinitely. Similar phenomena have also been reported in the forced oscillation experiments of reference 35 for a wing-body combination having a triangular wing of aspect ratio 4 and in flight tests of various high-speed aircraft, particularly tailless aircraft. The deleterious effects of such sustained oscillations on the qualities of an aircraft as a gun platform or from a structural standpoint are obvious. It is therefore of considerable importance to gain an understanding of the phenomenon, with a view toward advancing means of eliminating it.

At the present time, insufficient information, either theoretical or experimental, is available to enable a complete and authoritative

description of the physical event; a tentative hypothesis is therefore advanced instead, which would appear to fit the observed facts. It must be emphasized, however, that in the light of additional information, the assumptions and conclusions drawn here may require considerable revision.

Specifically, the observed facts are these: (1) The damping coefficient is highly nonlinear, being negative or stabilizing for angles of attack greater than about 1°, and zero at 1°. The possibility that the nonlinearity is caused entirely by scale effects and/or wind-tunnel-wall interference is ruled out by the fact that similar behavior is observed in full-scale flight tests. (2) The frequency of oscillation is essentially constant throughout the amplitude range, implying that the restoring moment is a linear or nearly linear function of the angle of attack.

From these observations, it is hypothesized that the characteristic differential equation governing the motion is of the form

$$I\ddot{\alpha} + \varphi(\alpha,\dot{\alpha})\ \dot{\alpha} + K^2\alpha = 0$$

where $\varphi(\alpha,\dot{\alpha})$ represents the damping coefficient as a nonlinear function of the angle of attack and angular velocity, and I and K are constants. It is therefore necessary to search for a mechanism that can affect the damping moment to a much larger degree than it does the restoring moment. In this regard, it is pertinent to first review some of the characteristics of wings in steady transonic flow. It is well known that at high subsonic Mach numbers, the essential feature of the flow is the appearance of shock waves on the wing as the speed of air over the wing surface exceeds the local speed of sound. These shock waves cause large changes in the pressure and also promote flow separation near the shock wave, due to the presence of adverse pressure gradients. The effects of these disturbances on the pitching-moment characteristics of an unswept wing of aspect ratio 3 are shown in reference 39 and reproduced as curve (a) in sketch (ee). Notice that the slope of the pitching moment is positive for small angles of attack, indicating that the aircraft would be statically unstable in that range. It was also illustrated in reference 39 that by reducing the curvature of the wing profile near the trailing edge, thereby reducing the tendency toward separation, the positive slope through zero could be eliminated. This result is shown as curve (b) in sketch (ee). By virtue of the beneficial effect of reducing separation, it is argued

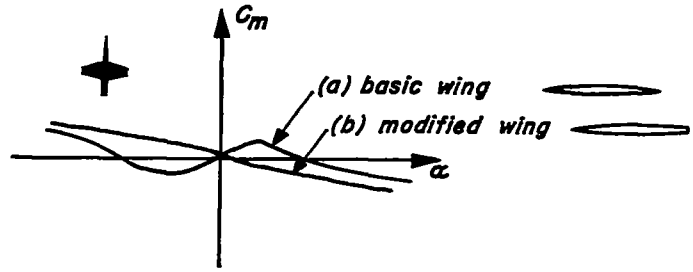

Sketch (ee)

here that in the absence of separation and strong shocks on the basic wing, the variation of pitching moment with angle of attack would be nearly linear, as shown by curve (a) in sketch (ff), and that the effects of these disturbances can be lumped into an additional moment variation, curve (b), such that the sum of (a) and (b) then gives the observed nonlinear variation.

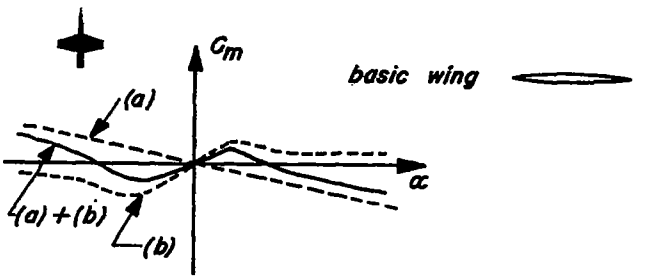

Sketch (ff)

For triangular wings, the reversal in slope of the pitching moment at small angles of attack does not appear (see refs. 29, 30, and 31). This, however, does not preclude the presence of the nonlinear variation due to separation. For a triangular wing with center of gravity at, say, the quarter M.A.C. point, the slope of the pitching-moment curve can be quite large. As seen in sketch (gg), the linear variation (a) can then greatly outweigh the effect of the nonlinear curve (b), with the result that a scarcely evident nonlinearity appears in the combined curve.

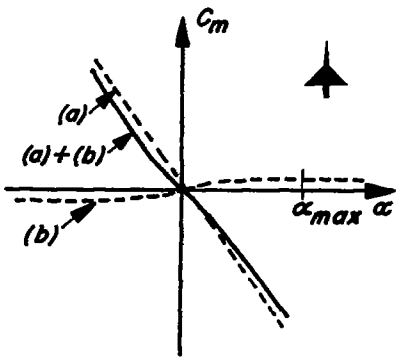

Sketch (gg)

The preceding examples were taken from the results of static measurements, where the angle of attack is simply the angle between the chord line of the wing and the free-stream direction. When the wing is oscillating, however, each point ξ measured from the axis of rotation experiences an additional angle of attack $\dot{\alpha}\xi/V_o$, due to the angular velocity. Then if the steady-state pitching-moment variation caused by the separation (curve (b) in sketch (gg)) is approximated in the range $0<\alpha<\alpha_{max}$ by

$$C_m(\alpha) = a\alpha - b\alpha^3$$

in the unsteady case it is,

$$C_m\left(\alpha + \frac{\dot{\alpha}\xi}{V_o}\right) = a\left[\alpha + \frac{\dot{\alpha}\xi}{V_o}\right] - b\left[\alpha + \frac{\dot{\alpha}\xi}{V_o}\right]^3 \qquad (54)$$

where now ξ is assumed to be the distance from the axis to the point at which the additional lift due to separation is concentrated.[9] Now, since for slow frequencies $\dot{\alpha}\xi/V_o$ is much smaller than α, all but first-order terms in $\dot{\alpha}$ are neglected so that equation (54) becomes

$$C_m = \alpha\,[a-b\alpha^2] + \frac{\dot{\alpha}\xi}{V_o}\,[a-3b\alpha^2] \tag{55}$$

The characteristic equation of motion then becomes

$$I\ddot{\alpha} - \frac{\dot{\alpha}\bar{c}}{2V_o}\left\{[C_{m_q}+C_{m_{\dot{\alpha}}}] + \frac{2\xi}{\bar{c}}\,[a-3b\alpha^2]\right\} - \alpha\left\{C_{m_\alpha}+[a-b\alpha^2]\right\} = 0 \tag{56}$$

where $[C_{m_q}+C_{m_{\dot{\alpha}}}]$ and C_{m_α} are the (constant) stability derivatives which would be present in the absence of separation. Thus, it appears that although the effect of the nonlinearity on the restoring moment can be insignificant, the possibility still remains that the damping moment can be profoundly affected in the event that $[C_{m_q}+C_{m_{\dot{\alpha}}}]$ is sufficiently small. Notice that when $[C_{m_q}+C_{m_{\dot{\alpha}}}] + 2\xi a/\bar{c}$ is greater than zero and if the nonlinear term in the restoring moment can be ignored, equation (56) takes on the form

$$\ddot{\alpha} - 2\delta\dot{\alpha}(1-\mu\alpha^2) + \kappa^2\alpha = 0 \tag{57}$$

Equation (57) is then recognized as being the well-known Van Der Pol equation of nonlinear mechanics. It is evident that for small values of α the damping term is negative, leading to a divergent oscillation, whereas for larger α, the damping term is positive. A stable regime therefore will exist where $\alpha = \sqrt{1/\mu}$ and oscillations of either large or small amplitude will converge to that regime.

Thus, by the assumptions of an additional nonlinear pitching-moment variation caused by flow separation and a sufficiently small damping moment in the absence of separation, the observed phenomenon of a small-amplitude self-sustained oscillation can be hypothetically explained as being due to the destabilizing effect of the nonlinearity in the restoring moment on the damping moment.

[9]It is recognized that usually the nonlinear effects of shock-wave boundary-layer interaction and flow separation are markedly reduced during nonsteady motions. However, for the low-frequency oscillations of the present tests (of the order of one cycle per 100 chord lengths of travel), it is believed that the effects of separation, though perhaps less severe than for the steady case, are nevertheless still present.

CONCLUSIONS

The results of a theoretical and experimental investigation of the single-degree-of-freedom damping in pitch of a series of low-aspect-ratio wing-body combinations made at subsonic and supersonic speeds lead to the following conclusions:

1. In the Mach number range 1.2 to 1.9, theoretical and experimental values of the damping-in-pitch coefficient $C_{m_q} + C_{m_{\dot{\alpha}}}$ were in good agreement for triangular wings of aspect ratios 2, 3, and 4, and swept wing of aspect ratio 3.

2. Theoretical predictions of the existence of ranges of center-of-gravity positions for a range of Mach numbers greater than 1.2 over which dynamic instability may be expected for the aspect ratio 4 triangular wing and the aspect ratio 3 swept and unswept wings were confirmed by the experimental results.

3. The prediction by the theory of the beneficial effect on the damping in pitch at supersonic speeds of a reduction in aspect ratio was borne out by the results of experiments for the triangular wings having aspect ratios 2, 3, and 4. In the Mach number range 1.2 to 1.9, the aspect ratio 2 wing had the largest damping moments throughout the range of Mach numbers and the aspect ratio 4 wing, the smallest.

4. Experimental results for the stability boundaries in the supersonic speed range of three wings of aspect ratio 3 having triangular, swept, and unswept plan forms confirmed the theoretical prediction regarding the relative magnitudes of the region of Mach number and center-of-gravity position in which dynamic instability could be experienced. In the Mach number range 1.2 to 1.9, no region of instability existed for the triangular wing. The region of instability for the unswept wing was considerably larger than for the swept wing.

5. The effects of profile thickness on the damping in pitch at supersonic speeds of triangular wings of aspect ratio 4 and thickness ratios of 3 percent and 6 percent were found to be small and in the direction of decreasing stability with increasing thickness ratio.

6. The occurrence at a Mach number of 0.9 of small-amplitude self-sustained oscillations of the triangular wing of aspect ratio 4 and the triangular and swept wings of aspect ratio 3 was attributed to a destabilizing effect on the damping moment of nonlinearities in the aerodynamic restoring moment.

Ames Aeronautical Laboratory
National Advisory Committee for Aeronautics
Moffett Field, Calif.

APPENDIX A

TRANSFER OF AXES

The problem to be solved may be posed as: Given the damping coefficient $C_{m_q} + C_{m_{\dot{\alpha}}}$ and the restoring-moment coefficient C_{m_α} about two axes of rotation, a known distance apart, find the damping coefficient about an arbitrary axis.

For single-degree-of-freedom rotary oscillations about axis (1) the damping coefficient is written as

$$\left[C_{m_q} + C_{m_{\dot{\alpha}}}\right]_1 = \left[C_{m_q} + C_{m_{\dot{\alpha}}}\right]_o + 2\bar{x}_1\left[C_{m_\alpha}\right]_o - \bar{x}_1\left[C_{L_q} + C_{L_{\dot{\alpha}}}\right]_o - 2\bar{x}_1^2 C_{L_\alpha} \quad (A1)$$

where the axis (o) is chosen as a reference axis, $\left[C_{m_q} + C_{m_{\dot{\alpha}}}\right]_1$ is known, and $\bar{x}_1$ is the known (nondimensionalized) distance of axis (1) ahead of axis (o). For pitching about axis (2), the damping coefficient is

$$\left[C_{m_q} + C_{m_{\dot{\alpha}}}\right]_2 = \left[C_{m_q} + C_{m_{\dot{\alpha}}}\right]_o + 2\bar{x}_2\left[C_{m_\alpha}\right]_o - \bar{x}_2\left[C_{L_q} + C_{L_{\dot{\alpha}}}\right]_o - 2\bar{x}_2^2 C_{L_\alpha} \quad (A2)$$

where $\left[C_{m_q} + C_{m_{\dot{\alpha}}}\right]_2$ and $\bar{x}_2$ are known.

The relationship of the axes (1) and (2) to the reference axis (o) is shown in sketch (hh). Note that if the reference axis (o) is chosen to be coincident with the axis passing through the aerodynamic center, then the quantities $2\bar{x}_1\left[C_{m_\alpha}\right]_o$ and $2\bar{x}_2\left[C_{m_\alpha}\right]_o$ in equations (A1) and (A2) are zero. Since $C_{m_{\alpha_1}}$ and $C_{m_{\alpha_2}}$ are known, the parameters C_{L_α} and $C_{m_{\alpha_o}}$ may be determined from

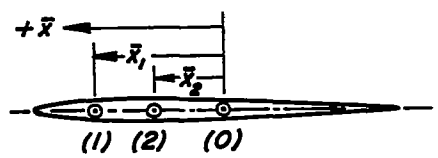

Sketch (hh)

$$\left.\begin{aligned} C_{L_\alpha} &= \frac{\left[C_{m_\alpha}\right]_2 - \left[C_{m_\alpha}\right]_1}{\bar{x}_1 - \bar{x}_2} \\ \left[C_{m_\alpha}\right]_o &= \left[C_{m_\alpha}\right]_1 + \bar{x}_1 C_{L_\alpha} \end{aligned}\right\} \quad (A3)$$

With C_{L_α} and $\left[C_{m_\alpha}\right]_o$ determined, it is now possible to solve equations (A1) and (A2) simultaneously.

Let

$$\left[C_{m_q} + C_{m_{\dot{\alpha}}}\right]_1 = a$$

$$\left[C_{m_q} + C_{m_{\dot{\alpha}}}\right]_2 = b$$

$$2\left[C_{m_\alpha}\right]_o = c$$

$$2C_{L_\alpha} = d$$

Then

$$\left.\begin{aligned} \left[C_{L_q} + C_{L_{\dot{\alpha}}}\right]_o &= -\left\{\frac{a-b - c[\bar{x}_1 - \bar{x}_2] + d[\bar{x}_1^2 - \bar{x}_2^2]}{\bar{x}_1 - \bar{x}_2}\right\} = e \\ \left[C_{m_q} + C_{m_{\dot{\alpha}}}\right]_o &= a - \bar{x}_1[c-e] + d\bar{x}_1^2 = f \end{aligned}\right\} \quad (A4)$$

The damping coefficient about an arbitrary axis, with $\bar{x}$ referred to axis (o) and measured as positive ahead of axis (o), is therefore,

$$\left[C_{m_q} + C_{m_{\dot{\alpha}}}\right] = f + \bar{x}c - \bar{x}e - \bar{x}^2 d \quad (A5)$$

REFERENCES

1. Zimmerman, Charles H.: An Analysis of Longitudinal Stability in Power-Off Flight with Charts for Use in Design. NACA Rep. 521, 1935.

2. Wagner, Herbert: Über die Entstehung des dynamischen Auftriebes von Tragflügeln. z.f.a.M.M. Bd. 5, Heft 1, Feb. 1925, S. 17-35.

3. Heaslet, Max.A., and Lomax, Harvard: Two-Dimensional Unsteady Lift Problems in Supersonic Flight. NACA Rep. 945, 1949.

4. Lomax, Harvard, Fuller, Franklyn B., and Sluder, Loma: Two- and Three-Dimensional Unsteady Lift Problems in High-Speed Flight. NACA Rep. 1077, 1952. (Supersedes NACA TN's 2403, 2387, and 2256)

5. Miles, John W.: Transient Loading of Wide Delta Airfoils at Supersonic Speeds. NAVORD Rep. 1235, 1950.

6. Miles, John W.: Transient Loading of Supersonic Rectangular Airfoils. Jour. Aero. Sci., vol. 17, no. 10, Oct. 1950, pp. 647-652.

7. Garrick, I. E.: On Some Reciprocal Relations in the Theory of Nonstationary Flows. NACA Rep. 629, 1938.

8. Jones, Robert T.: The Unsteady Lift of a Wing of Finite Aspect Ratio. NACA Rep. 681, 1940.

9. Churchill, R. V.: Modern Operational Mathematics in Engineering. McGraw-Hill Book Company, N.Y., 1944.

10. Tobak, Murray, Reese, David E., Jr., and Beam, Benjamin H.: Experimental Damping in Pitch of 45° Triangular Wings. NACA RM A50J26, 1950.

11. Miles, John W.: The Application of Unsteady Flow Theory to the Calculation of Dynamic Stability Derivatives. North American Aviation Rep. AL-957, 1950.

12. Jahnke, Eugen, and Emde, Fritz: Tables of Functions with Formulae and Curves. Fourth ed., Dover Pub., N.Y. 1945.

13. Durand, W. F., ed.: Aerodynamic Theory. Vol. V, Julius Springer (Berlin), 1935. (Available as CIT Reprint, 1943)

14. Theodorsen, Theodore: General Theory of Aerodynamic Instability and the Mechanism of Flutter. NACA Rep. 496, 1935.

15. Garrick, I. E., and Rubinow, S. I.: Flutter and Oscillating Air-Force Calculations for an Airfoil in a Two-Dimensional Supersonic Flow. NACA Rep. 846, 1946.

16. Watkins, Charles E.: Effect of Aspect Ratio on the Air Forces and Moments of Harmonically Oscillating Thin Rectangular Wings in Supersonic Potential Flow. NACA TN 2064, 1950.

17. Watkins, Charles E.: Air Forces and Moments on Triangular and Related Wings With Subsonic Leading Edges Oscillating in Supersonic Potential Flow. NACA TN 2457, 1951.

18. Nelson, Herbert C.: Lift and Moment on Oscillating Triangular and Related Wings With Supersonic Edges. NACA TN 2494, 1951.

19. Miles, John W.: On Harmonic Motion of Wide Delta Airfoils at Supersonic Speeds. NAVORD Rep. 1234, 1950.

20. Ribner, Herbert S., and Malvestuto, Frank S., Jr.: Stability Derivatives of Triangular Wings at Supersonic Speeds. NACA Rep. 908, 1948.

21. Malvestuto, Frank S., Jr., and Margolis, Kenneth: Theoretical Stability Derivatives of Thin Sweptback Wings Tapered to a Point with Sweptback or Sweptforward Trailing Edges for a Limited Range of Supersonic Speeds. NACA Rep. 971, 1950. (Supersedes NACA TN 1761)

22. Malvestuto, Frank S., Jr., and Hoover, Dorothy M.: Lift and Pitching Derivatives of Thin Sweptback Tapered Wings with Streamwise Tips and Subsonic Leading Edges at Supersonic Speeds. NACA TN 2294, 1951.

23. Malvestuto, Frank S., Jr., and Hoover, Dorothy M.: Supersonic Lift and Pitching Moment of Thin Sweptback Tapered Wings Produced by Constant Vertical Acceleration. Subsonic Leading Edges and Supersonic Trailing Edges. NACA TN 2315, 1951.

24. Staff of the Ames 1- by 3-Foot Supersonic Wind-Tunnel Section: Notes and Tables for Use in the Analysis of Supersonic Flow. NACA TN 1428, 1947.

25. Jones, W. Prichard, and Skan, Sylvia W.: Aerodynamic Forces on Biconvex Aerofoils Oscillating in a Supersonic Airstream. British A.R.C. 13, 162, 1950.

26. Wylly, Alexander: A Second-Order Solution for an Oscillating, Two-Dimensional, Supersonic Airfoil. RAND Corp. Rep., 1951.

27. Van Dyke, Milton D.: On Second-Order Supersonic Flow Past a Slowly Oscillating Airfoil. Reader's Forum, Jour. Aero. Sci, vol. 20, no. 1, Jan. 1953.

28. Frick, Charles W., and Olson, Robert N.: Flow Studies in the Asymmetric Adjustable Nozzle of the Ames 6- by 6-Foot Supersonic Wind Tunnel. NACA RM A9E24, 1949.

29. Heitmeyer, John C., and Smith, Willard G.: Lift, Drag, and Pitching Moment of Low-Aspect-Ratio Wings at Subsonic and Supersonic Speeds - Plane Triangular Wing of Aspect Ratio 2 With NACA 0003-63 Section. NACA RM A50K24a, 1951.

30. Heitmeyer, John C.: Lift, Drag, and Pitching Moment of Low-Aspect-Ratio Wings at Subsonic and Supersonic Speeds - Plane Triangular Wing of Aspect Ratio 3 With NACA 0003-63 Section. NACA RM A51H02, 1951.

31. Heitmeyer, John C.: Lift, Drag, and Pitching Moment of Low-Aspect-Ratio Wings at Subsonic and Supersonic Speeds - Plane Triangular Wing of Aspect Ratio 4 With 3-Percent-Thick, Biconvex Section. NACA RM A51D30, 1951.

32. Heitmeyer, John C.: Lift, Drag, and Pitching Moment of Low-Aspect-Ratio Wings at Subsonic and Supersonic Speeds - Plane 45° Swept-Back Wing of Aspect Ratio 3, Taper Ratio 0.4 With 3-Percent-Thick, Biconvex Section. NACA RM A51H10, 1951.

33. Reese, David E., Jr., and Phelps, E. Ray: Lift, Drag, and Pitching Moment of Low-Aspect-Ratio Wings at Subsonic and Supersonic Speeds - Plane Tapered Wing of Aspect Ratio 3.1 With 3-Percent-Thick, Biconvex Section. NACA RM A50K28, 1951.

34. Runyan, Harry L., and Watkins, Charles E.: Considerations on the Effect of Wind-Tunnel Walls on Oscillating Air Forces for Two-Dimensional Subsonic Compressible Flow. NACA TN 2552, 1951.

35. Beam, Benjamin H.: The Effects of Oscillation Amplitude and Frequency on the Experimental Damping in Pitch of a Triangular Wing Having an Aspect Ratio of 4. NACA RM A52G07, 1952.

36. Herriot, John G.: Blockage Corrections for Three-Dimensional-Flow Closed-Throat Wind Tunnels With Consideration of the Effect of Compressibility. NACA Rep. 995, 1950. (Supersedes NACA RM A7B28)

37. Henderson, Arthur, Jr.: Pitching-Moment Derivatives C_{m_q} and $C_{m_{\dot{\alpha}}}$ at Supersonic Speeds for a Slender-Delta-Wing and Slender-Body Combination and Approximate Solutions for Broad-Delta-Wing and Slender-Body Combinations. NACA TN 2553, 1951.

38. Bratt, J. B., and Chinneck, A.: Information Report on Measurements of Mid-Chord Pitching Moment Derivatives at High-Speed. British A.R.C. Rep. 10,710, 1947.

39. Dugan, Duane W.: Effects of Three Types of Blunt Trailing Edges on the Aerodynamic Characteristics of a Plane Tapered Wing of Aspect Ratio 3.1, With a 3-Percent-Thick Biconvex Section. NACA RM A52E01, 1952.

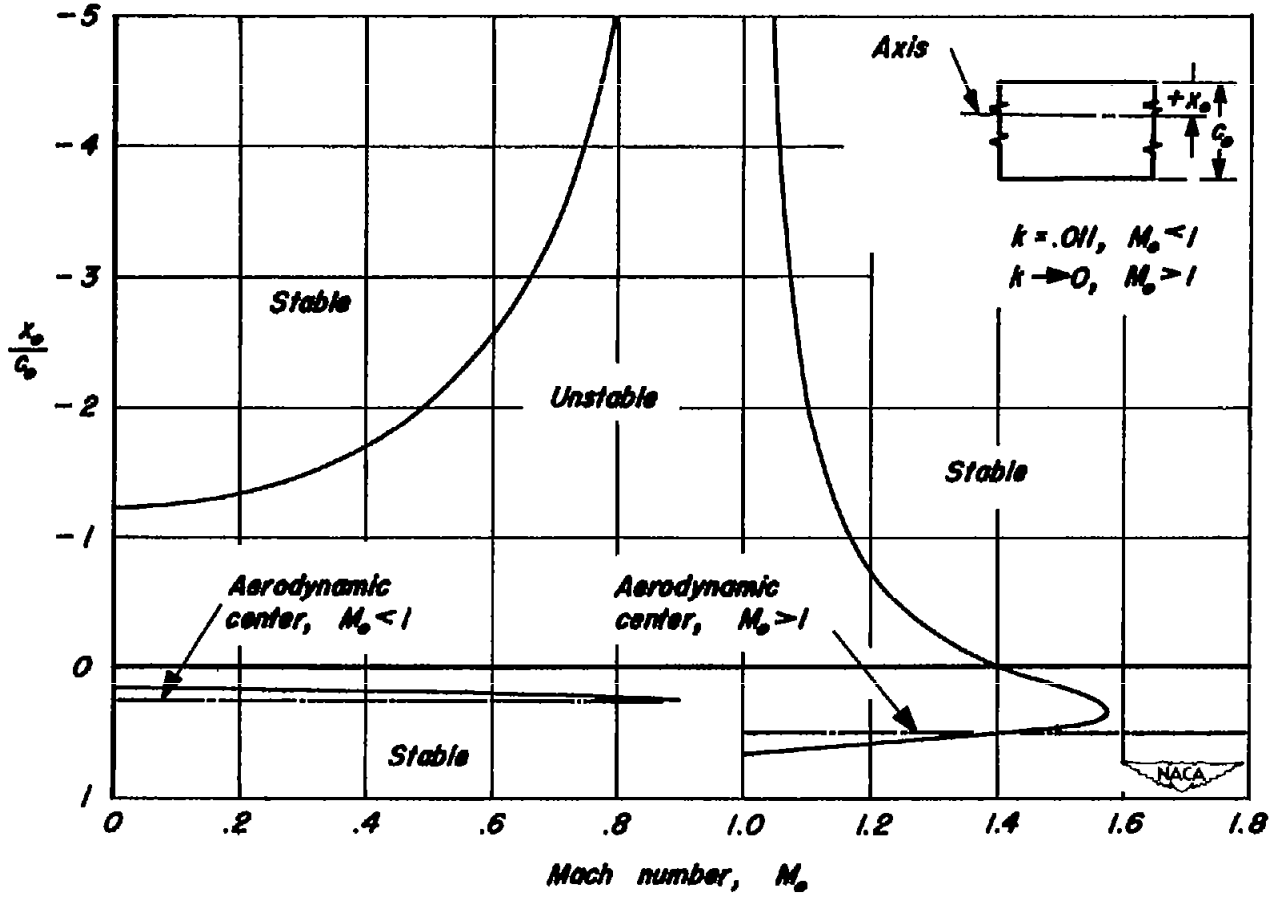

Figure 1.— Theoretical single-degree-of-freedom short-period pitching stability boundaries for the two-dimensional wing at subsonic and supersonic speeds.

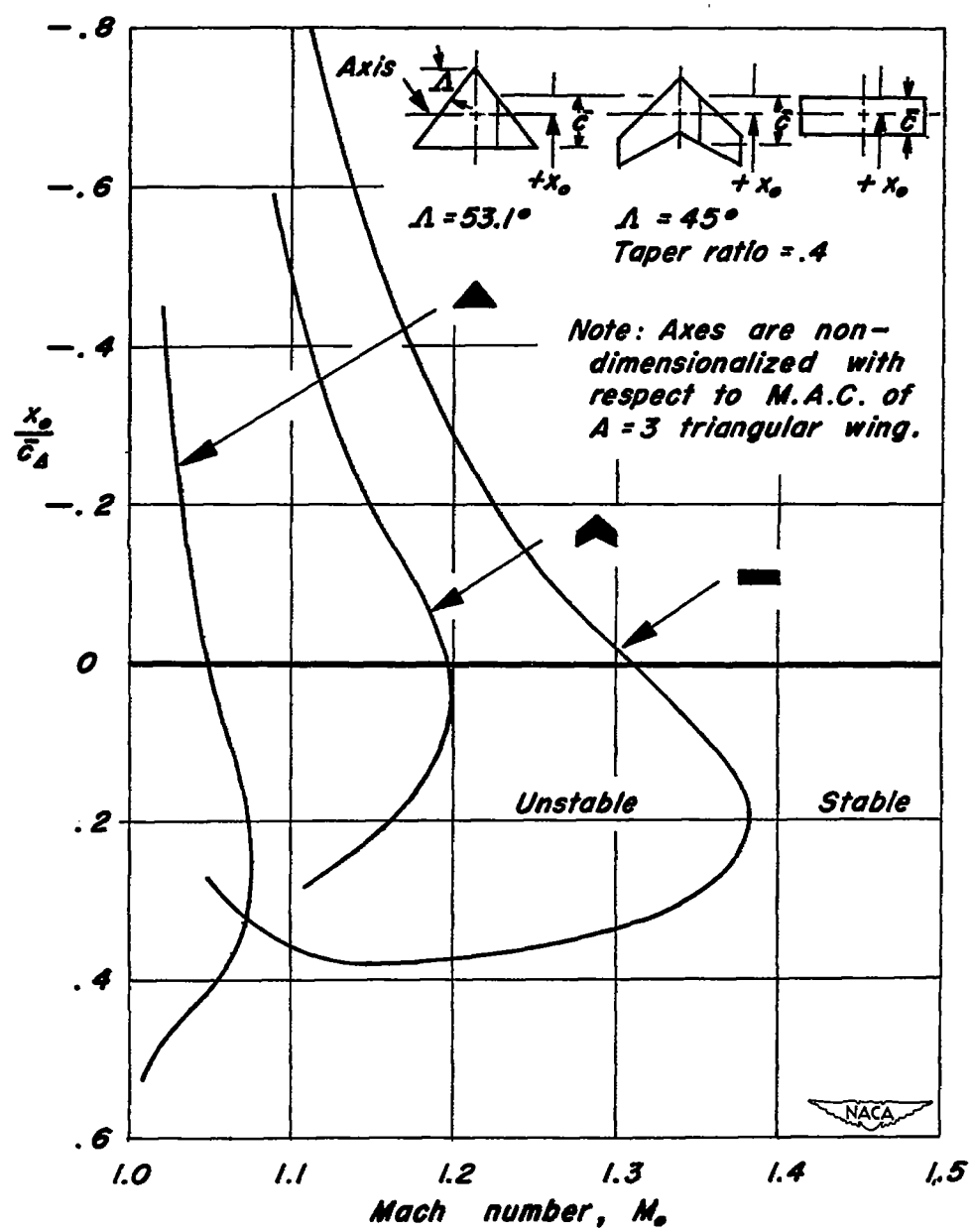

Figure 2.– Comparison of theoretical single-degree-of-freedom short-period pitching stability boundaries at supersonic speeds for three wings of aspect ratio 3, having triangular, swept, and rectangular plan forms.

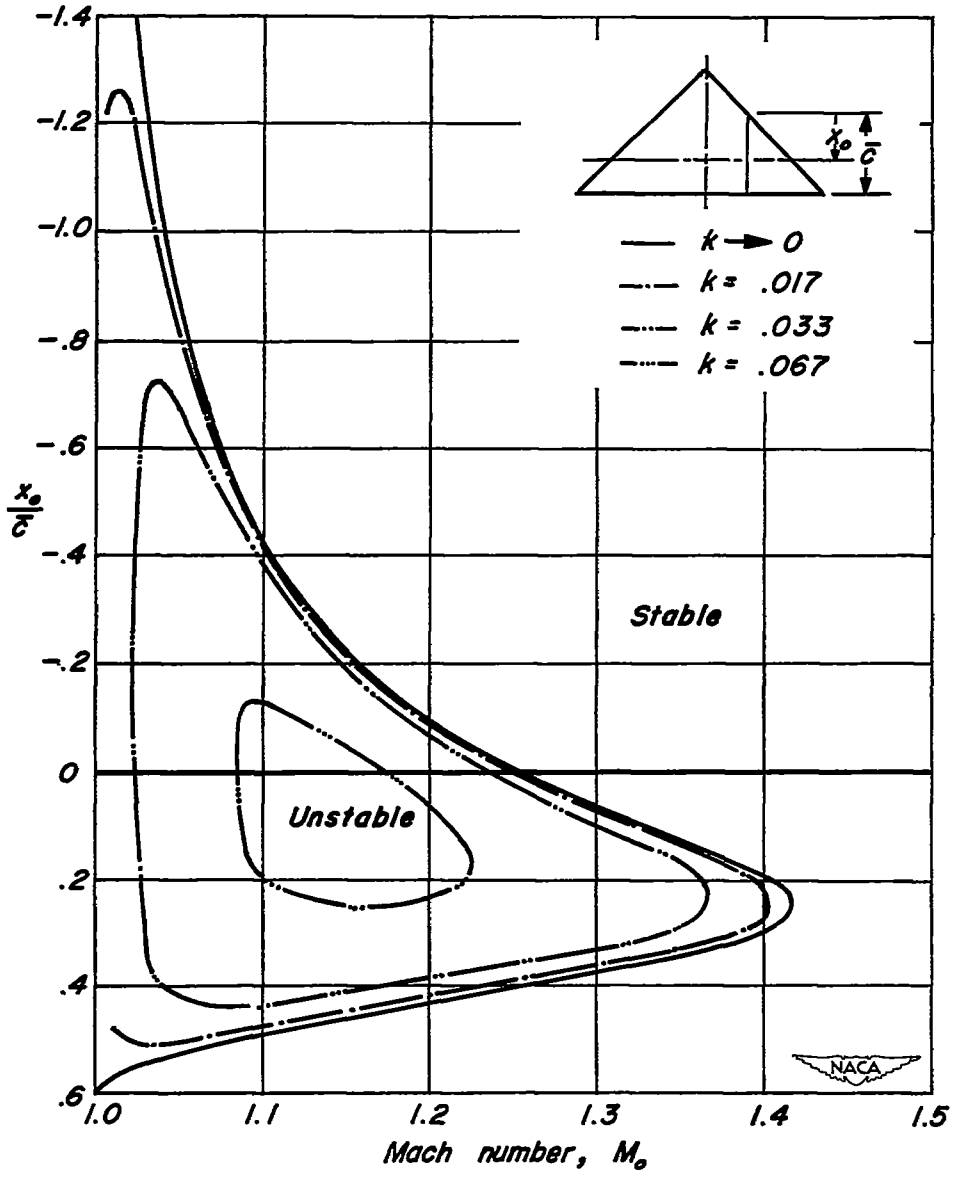

Figure 3.— The effect of frequency on the theoretical single-degree-of-freedom short-period pitching stability boundaries at supersonic speeds for a triangular wing of aspect ratio 4.

[redacted]

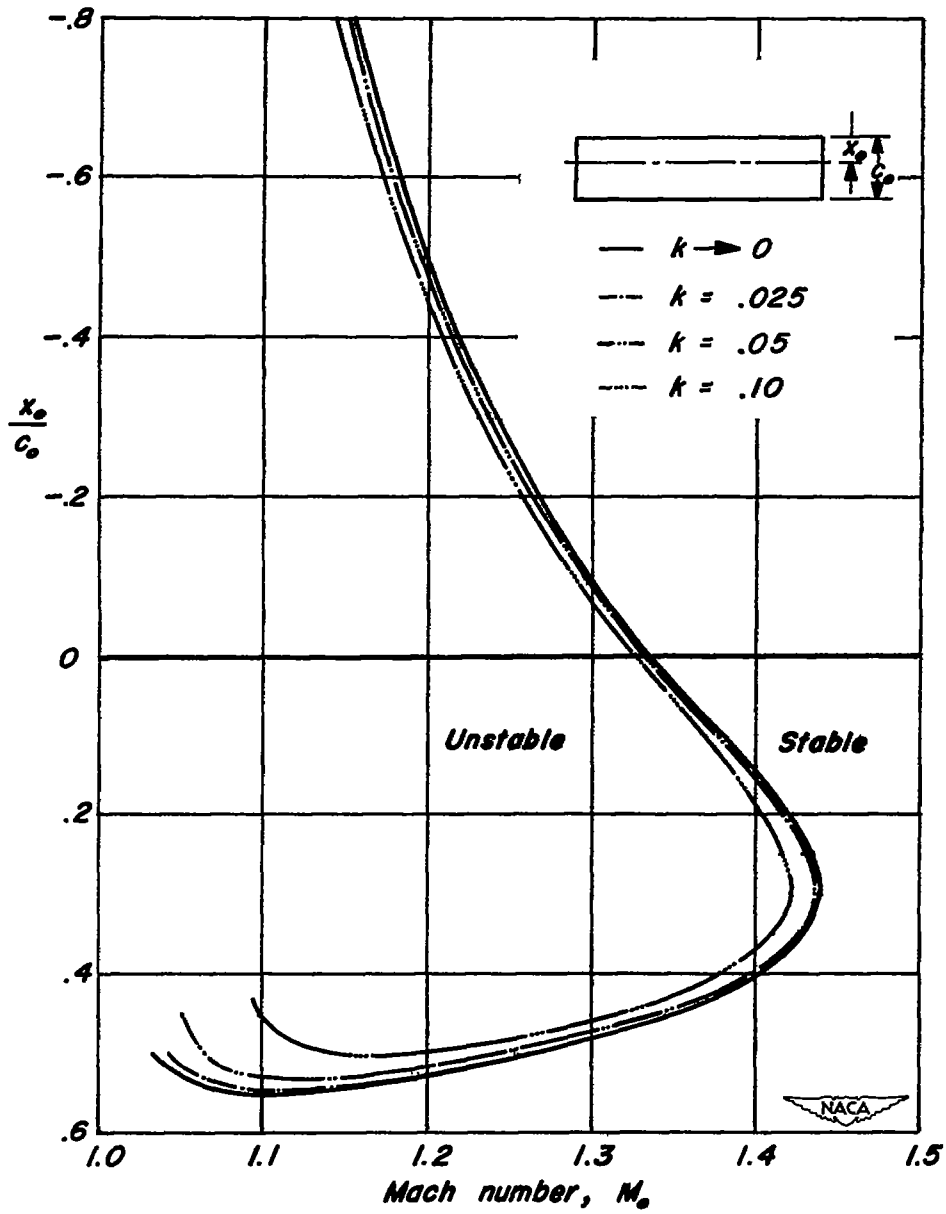

Figure 4.— The effect of frequency on the theoretical single-degree-of-freedom short-period pitching stability boundaries at supersonic speeds for a rectangular wing of aspect ratio 4.

[redacted]

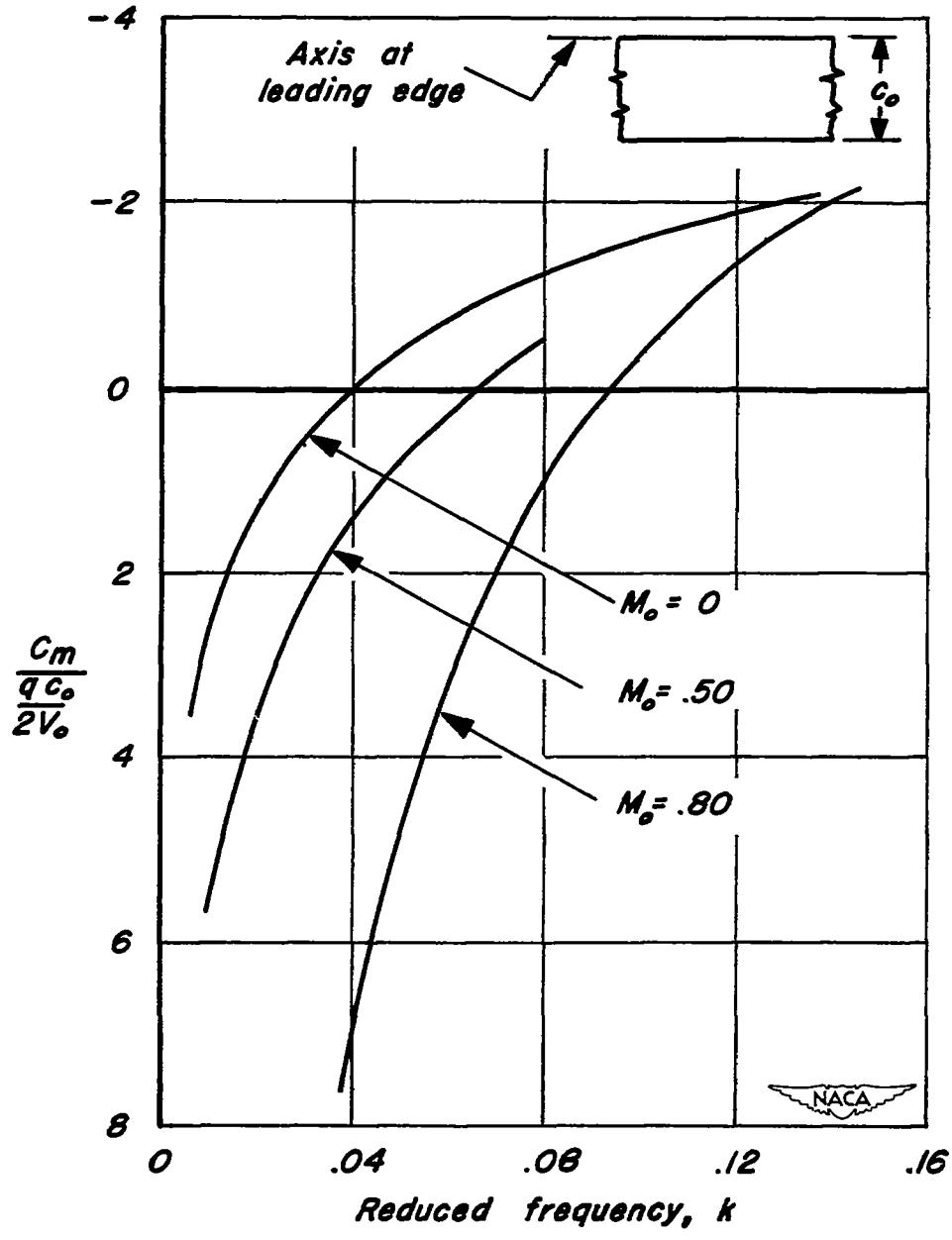

Figure 5.— The variation with reduced frequency of the single-degree-of-freedom rotary damping — moment coefficient for the two-dimensional wing at Mach numbers 0, 0.50, and 0.80. Axis at leading edge.

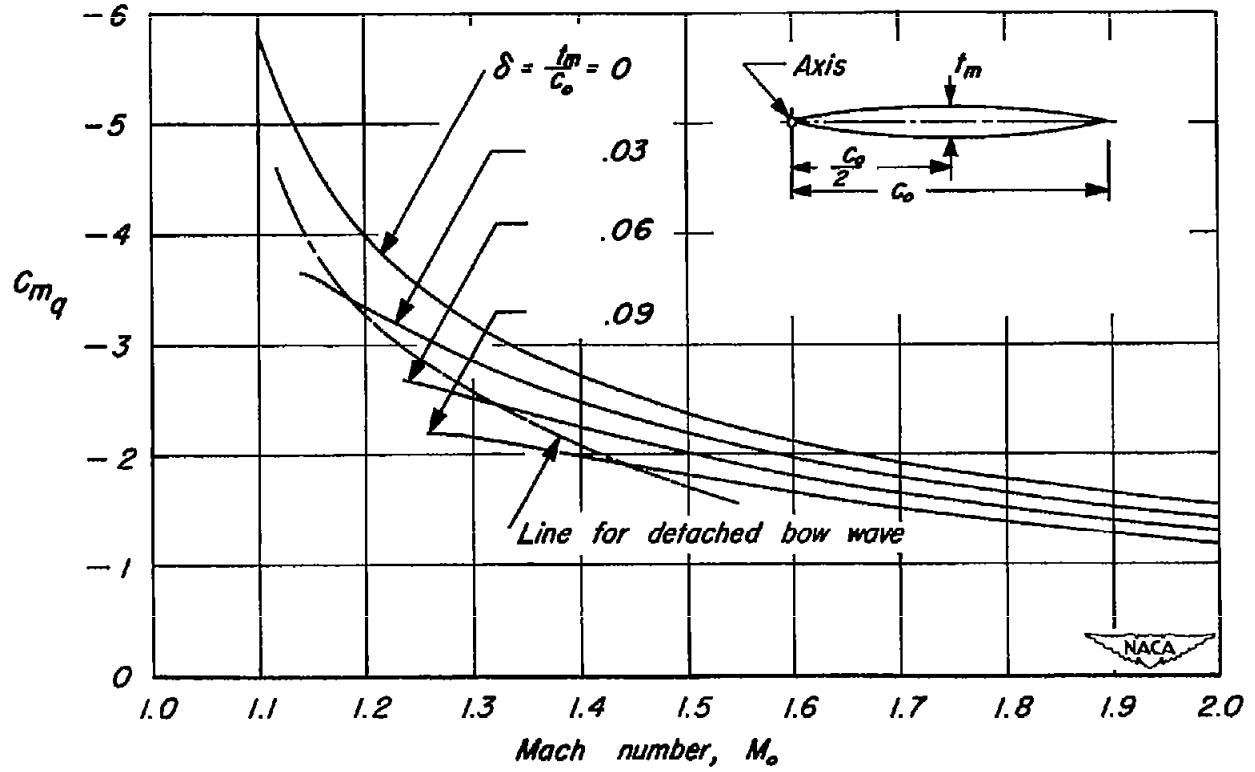

Figure 6.– The effect of thickness on the damping-in-pitch coefficient C_{m_q} for a two-dimensional wing having a symmetrical biconvex parabolic-arc section. Axis at leading edge.

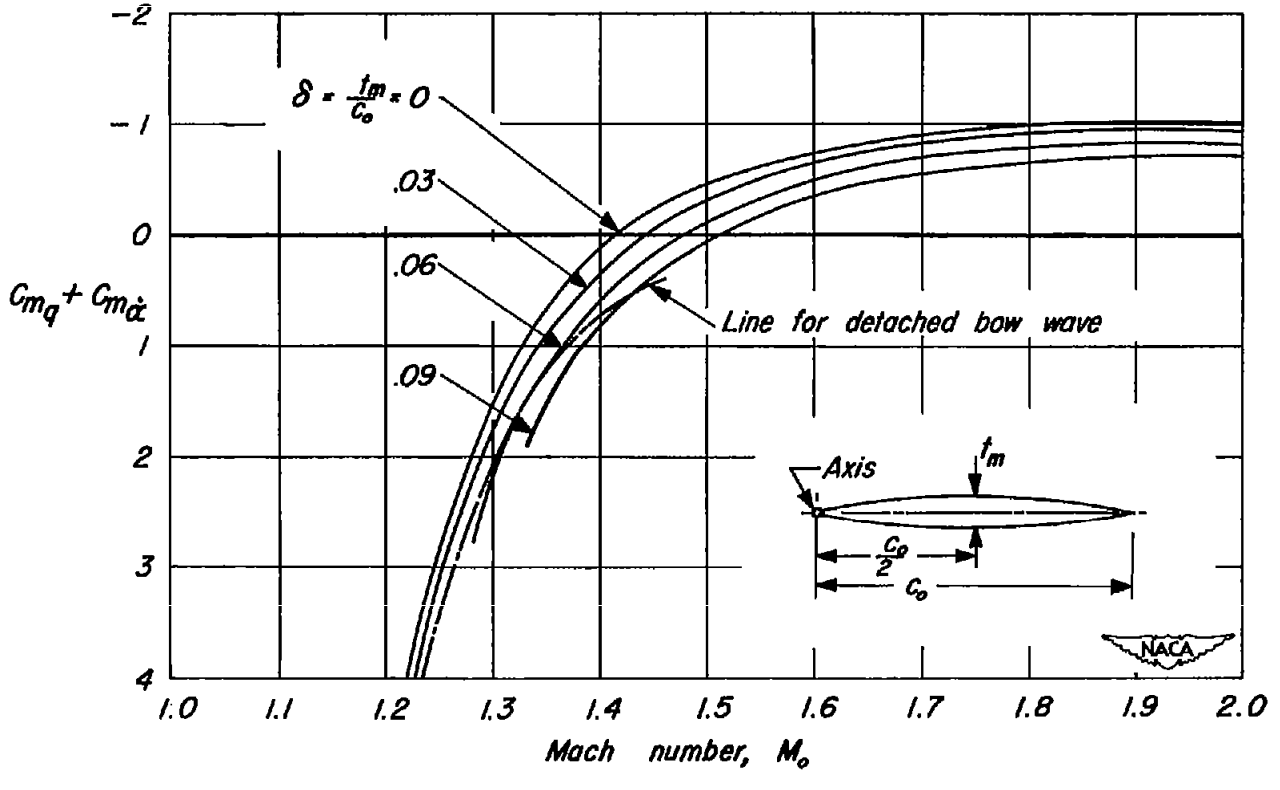

Figure 7.—The effect of thickness on the damping-in-pitch coefficient $C_{m_q} + C_{m_{\dot{\alpha}}}$ for a two-dimensional wing having a symmetrical biconvex parabolic-arc section. Axis at leading edge.

Equation of forebodies: $r = r_0\left[1-\left(1-\frac{2x}{l}\right)^2\right]^{3/4}$

$r_0 = 2''$

$l = 50''$

$0 < x < 25''$

Equation of afterbodies: $r = r_0$

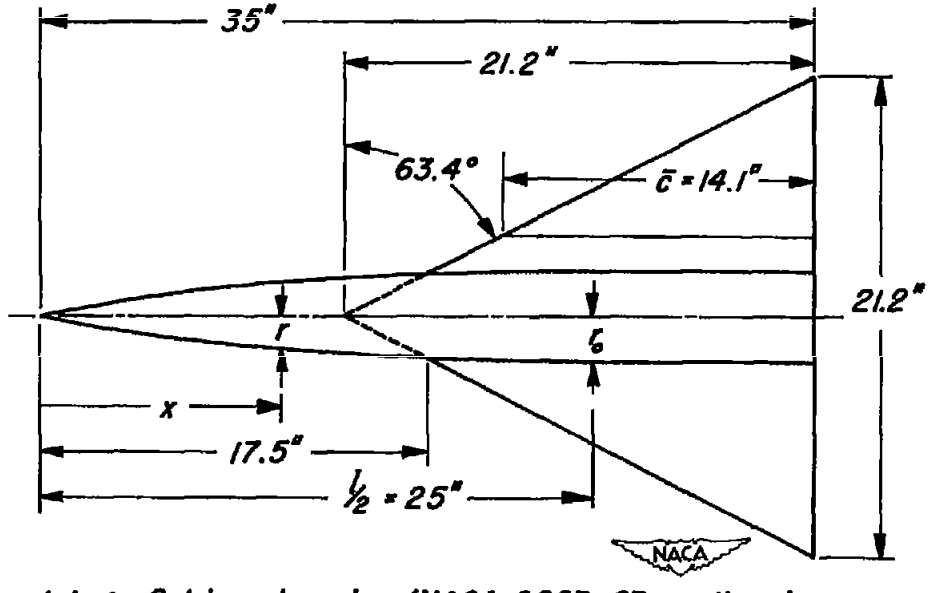

(a) A = 2 triangular wing (NACA 0003-63 sections).

Figure 8.– Sketch of models investigated.

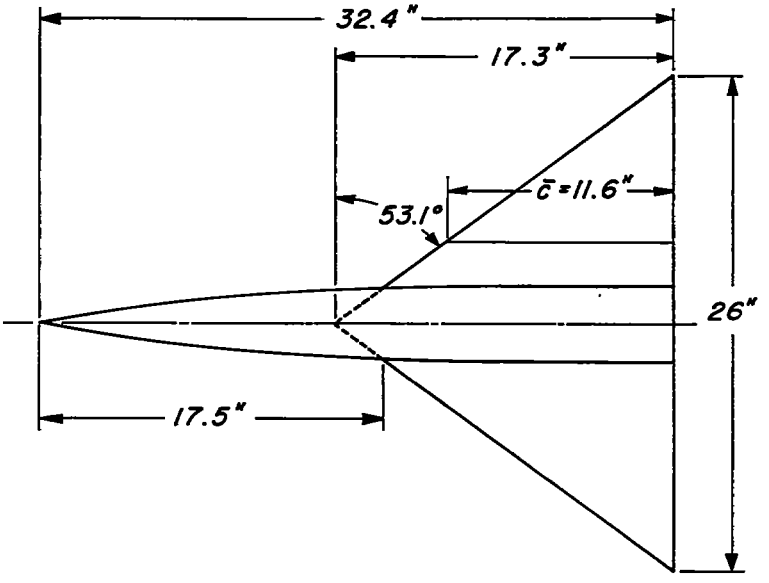

(b) A = 3 triangular wing (NACA 0003-63 sections).

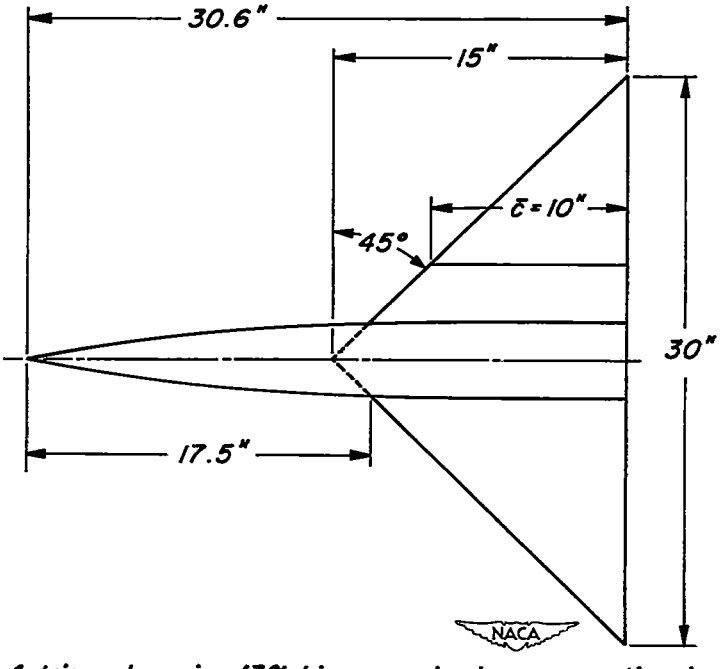

(c) A = 4 triangular wing (3% biconvex circular-arc sections).

Figure 8.- Continued.

[redacted]

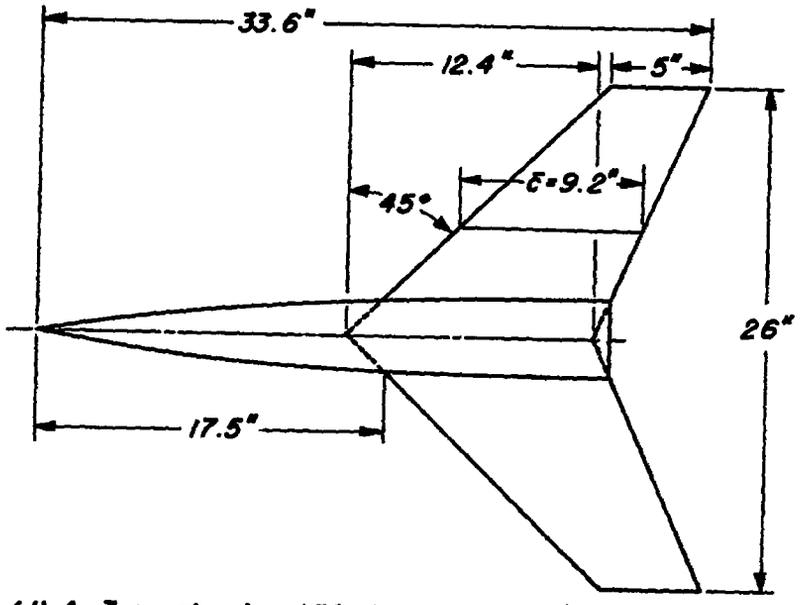

(d) A=3 swept wing (3% biconvex circular-arc sections).

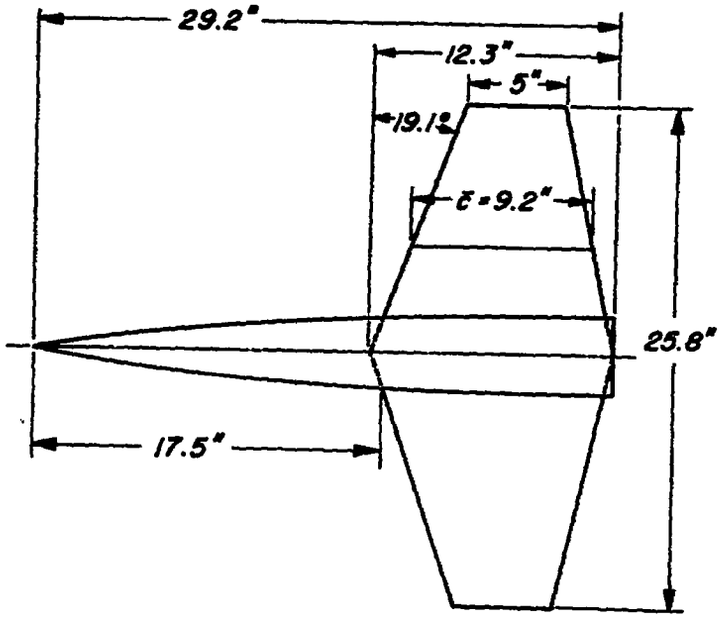

(e) A=3 unswept wing (3% biconvex circular-arc sections).

NACA

Figure 8.- Concluded.

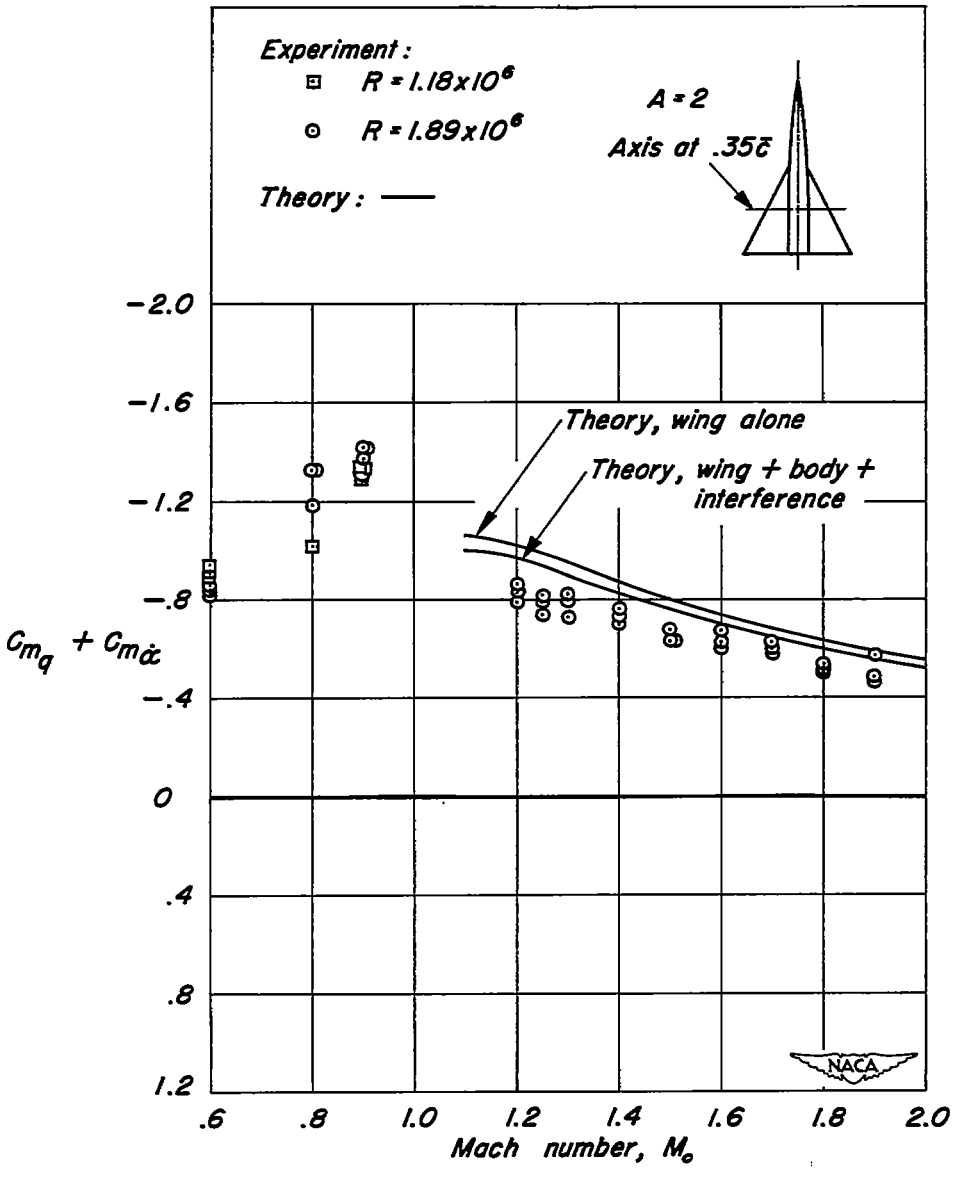

(a) Axis at 0.35c̄

Figure 9.— Experimental damping-in-pitch coefficients for the wing-body combination having a triangular wing of aspect ratio 2.

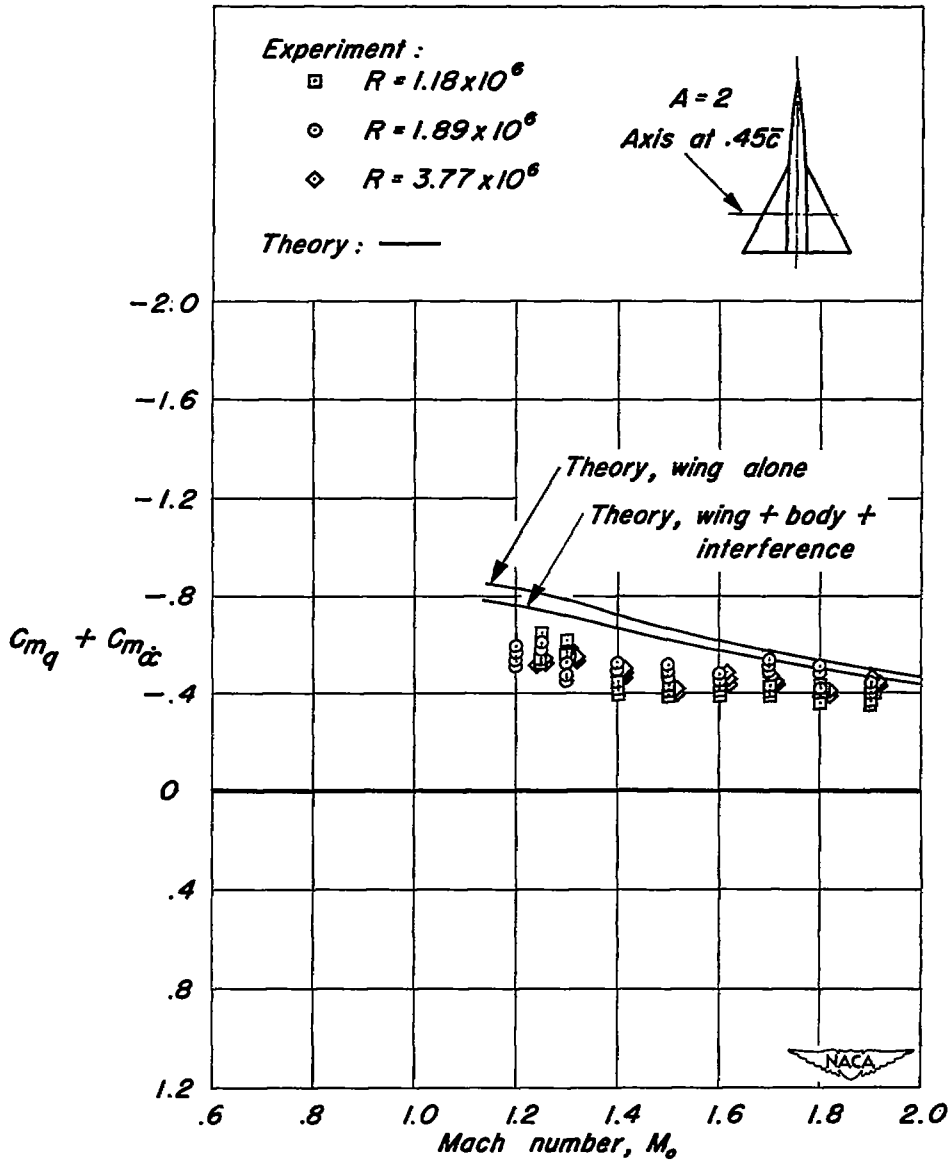

(b) Axis at 0.45c̄.

Figure 9.— Concluded.

[redacted]

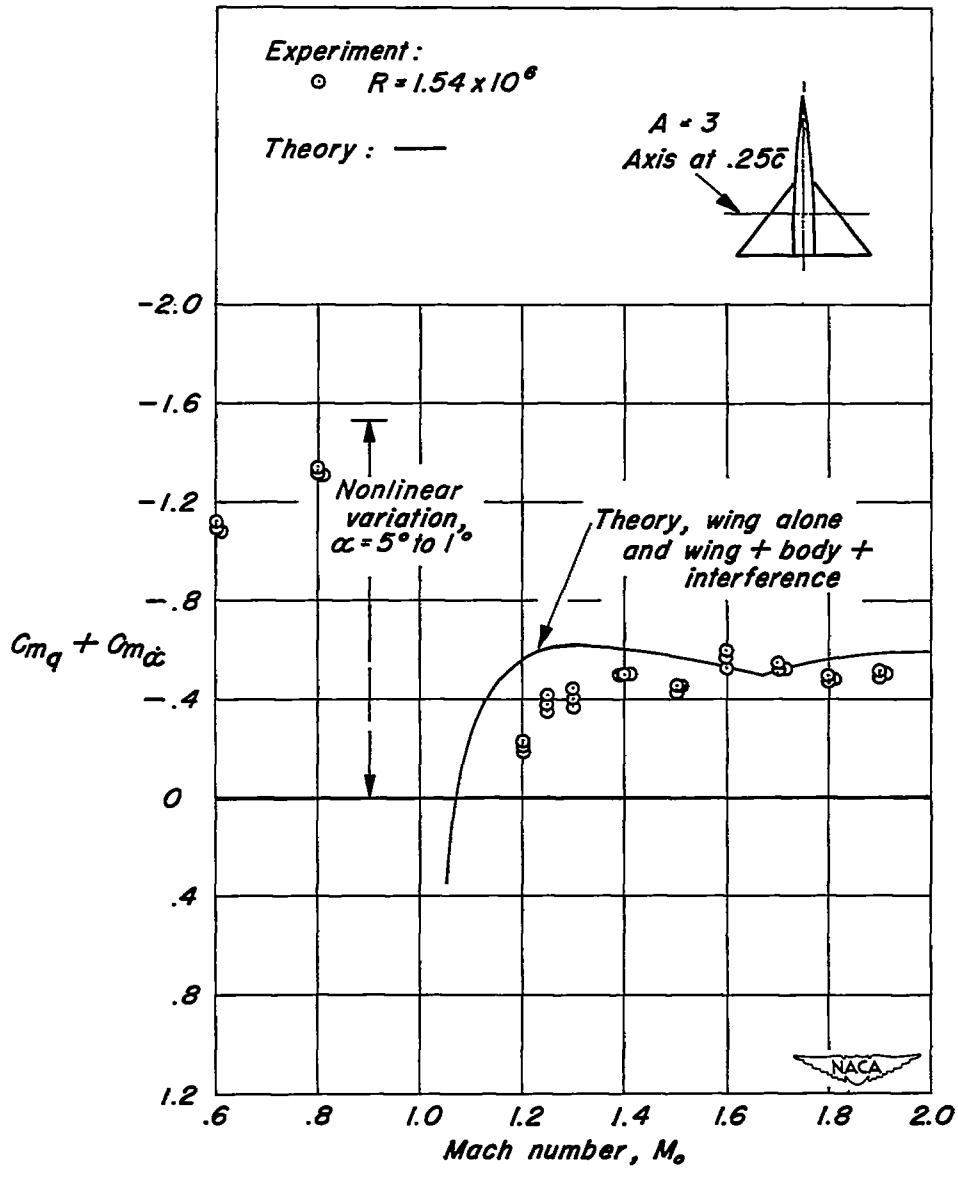

(a) Axis at 0.25c̄.

Figure 10.— Experimental damping-in-pitch coefficients for the wing-body combination having a triangular wing of aspect ratio 3.

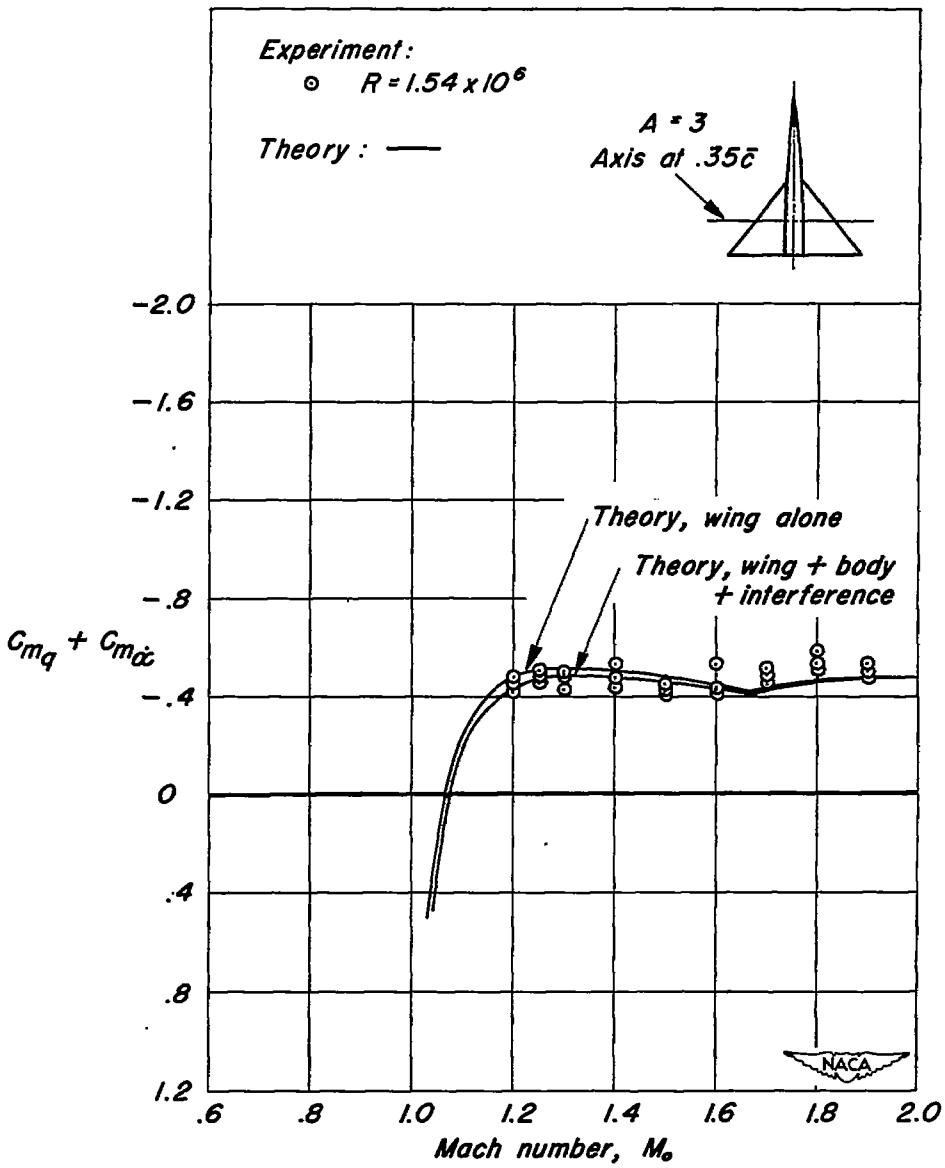

(b) Axis at 0.35c̄.

Figure 10.– Concluded.

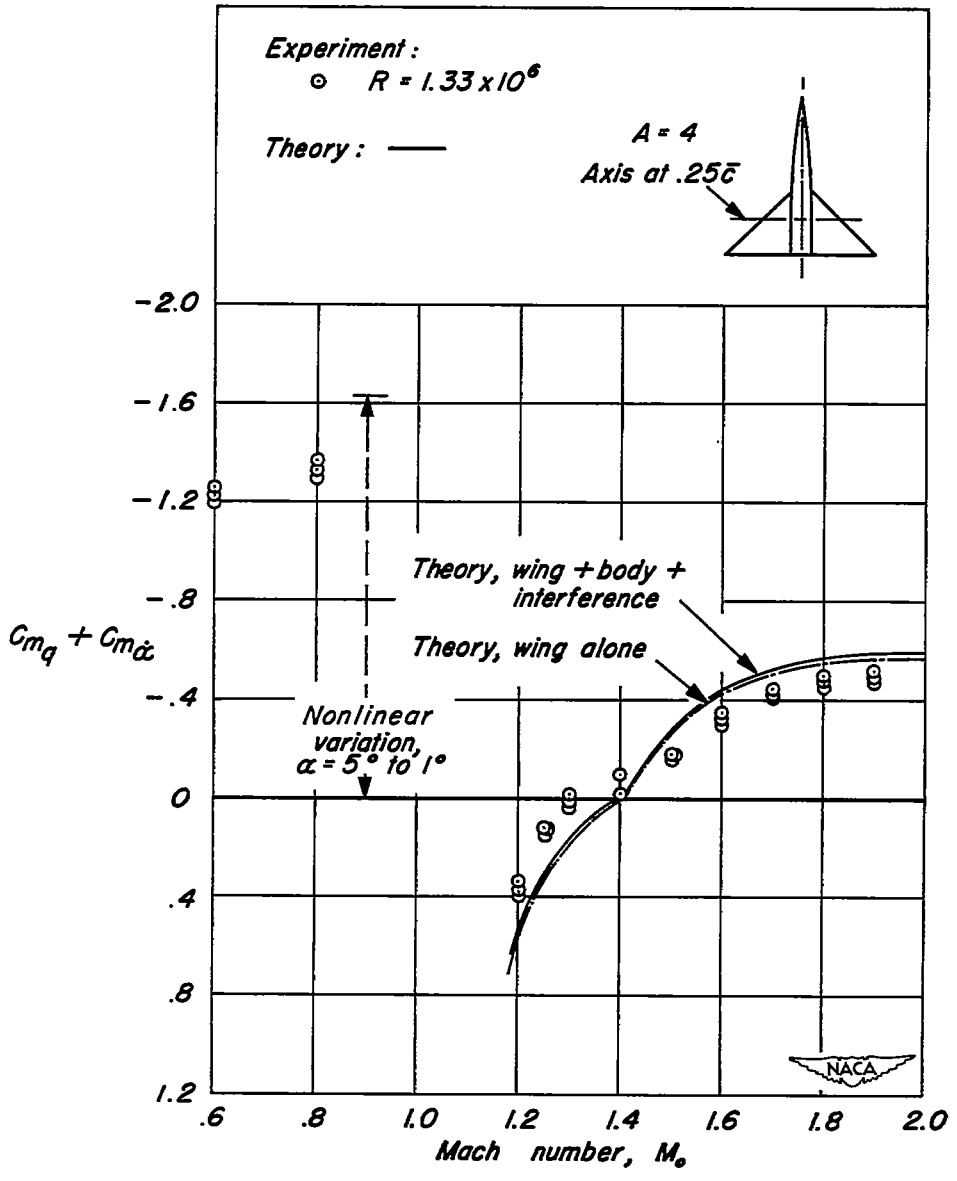

(a) Axis at 0.25$\bar{c}$.

Figure 11.— Experimental damping-in-pitch coefficients for the wing-body combination having a triangular wing of aspect ratio 4.

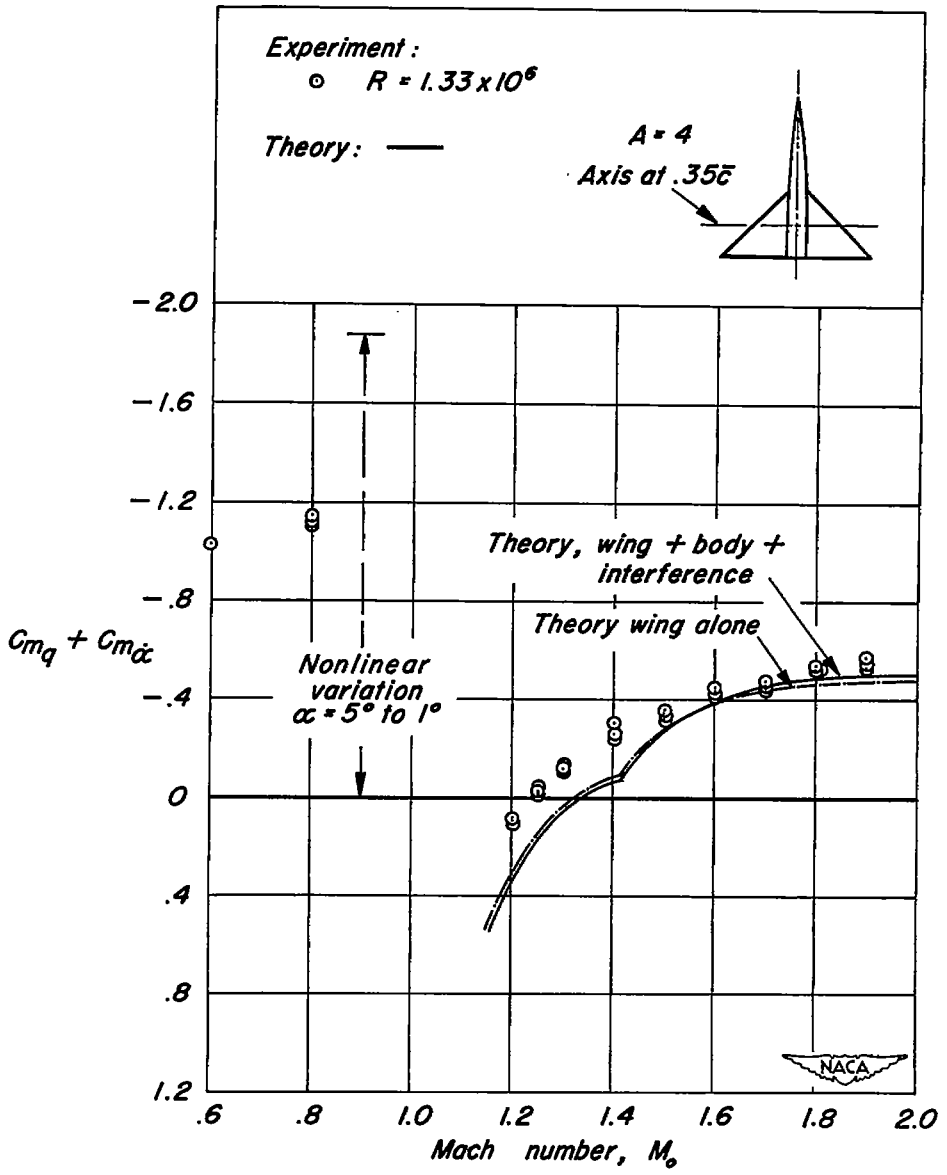

(b) Axis at 0.35$\bar{c}$.

Figure 11.—Continued.

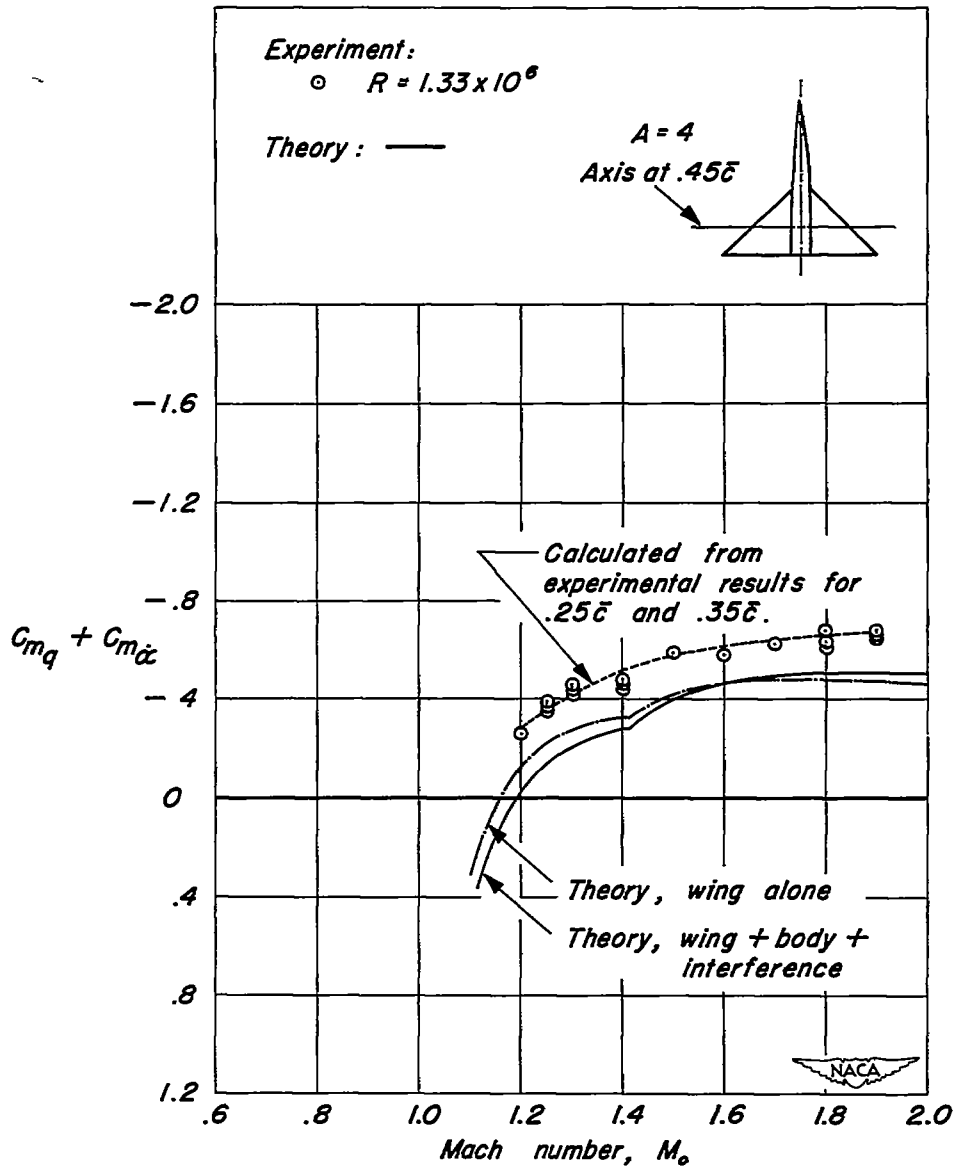

(c) Axis at 0.45c̄.

Figure 11.— Concluded.

[redacted]

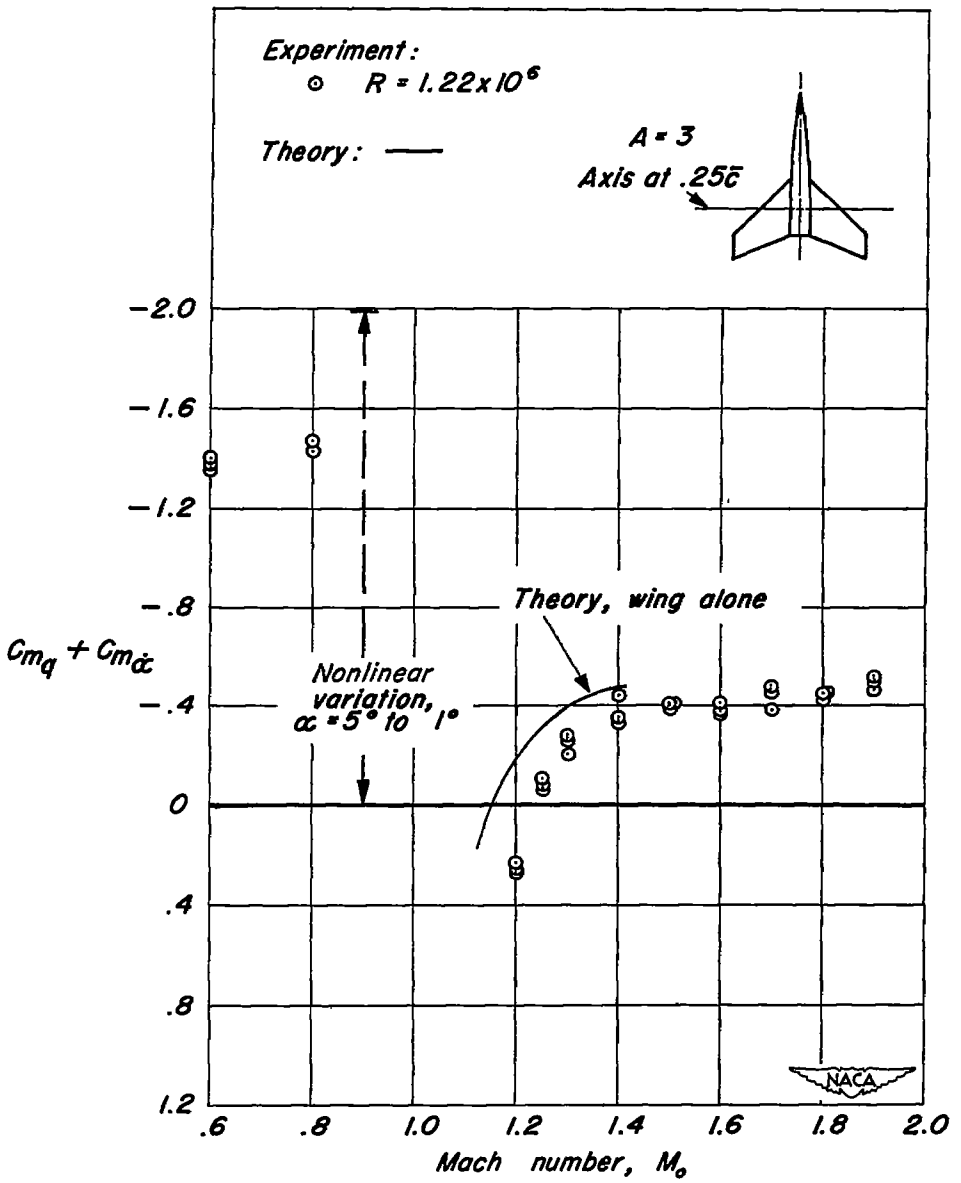

(a) Axis at 0.25c̄.

Figure 12.— Experimental damping-in-pitch coefficients for the wing-body combination having a swept wing of aspect ratio 3.

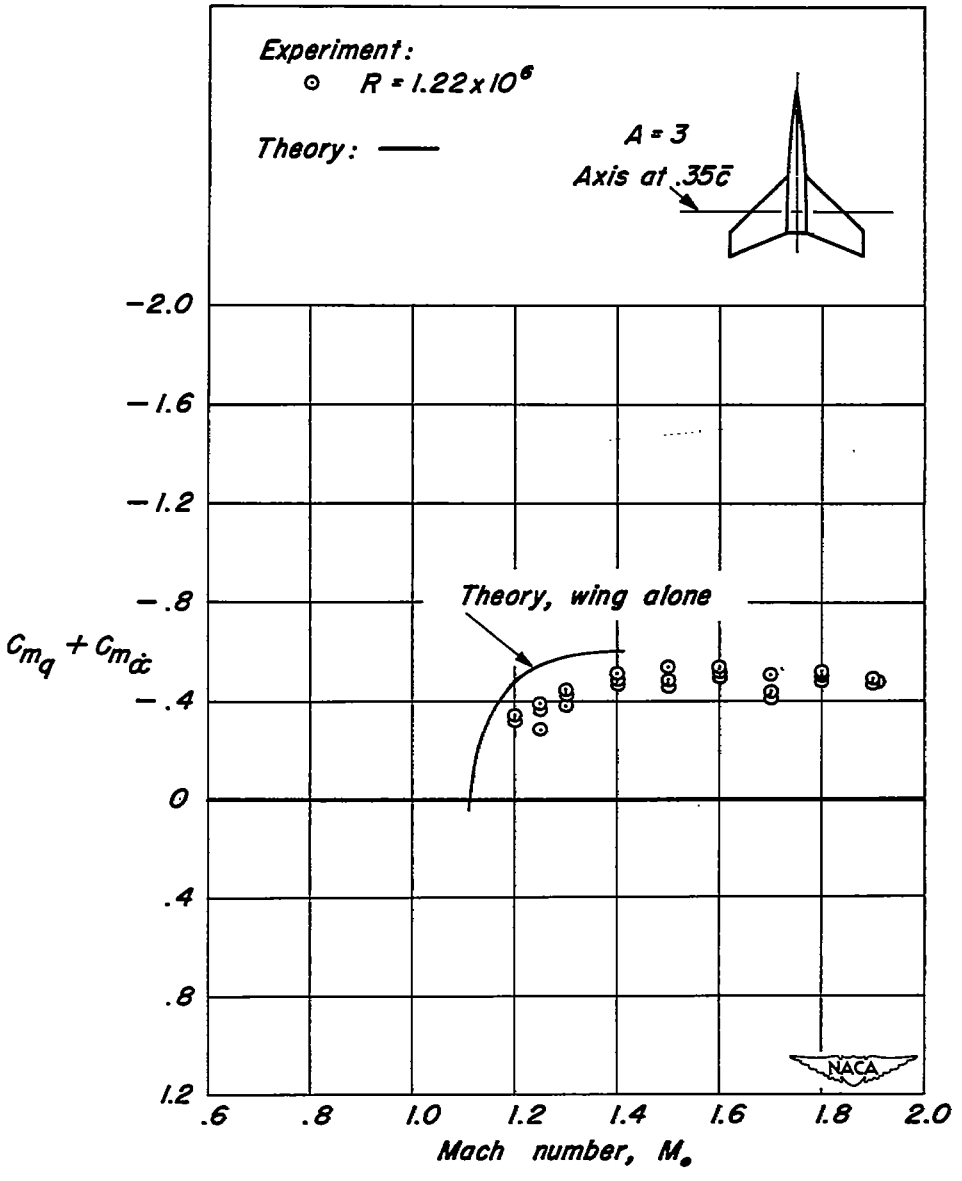

(b) Axis at 0.35c̄.

Figure 12.— Concluded.

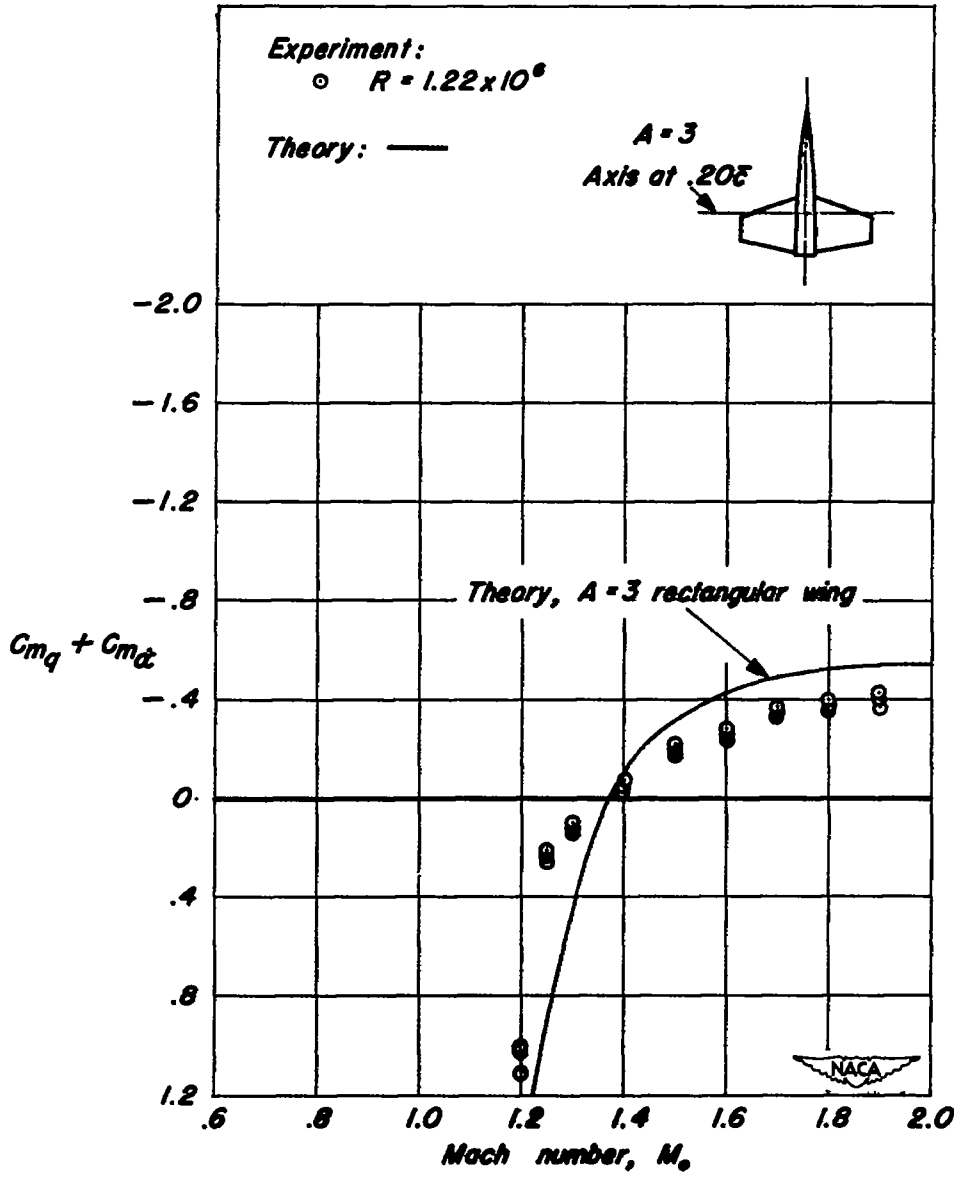

(a) Axis at 0.20c̄.

Figure 13.— Experimental damping-in-pitch coefficients for the wing-body combination having an unswept wing of aspect ratio 3.

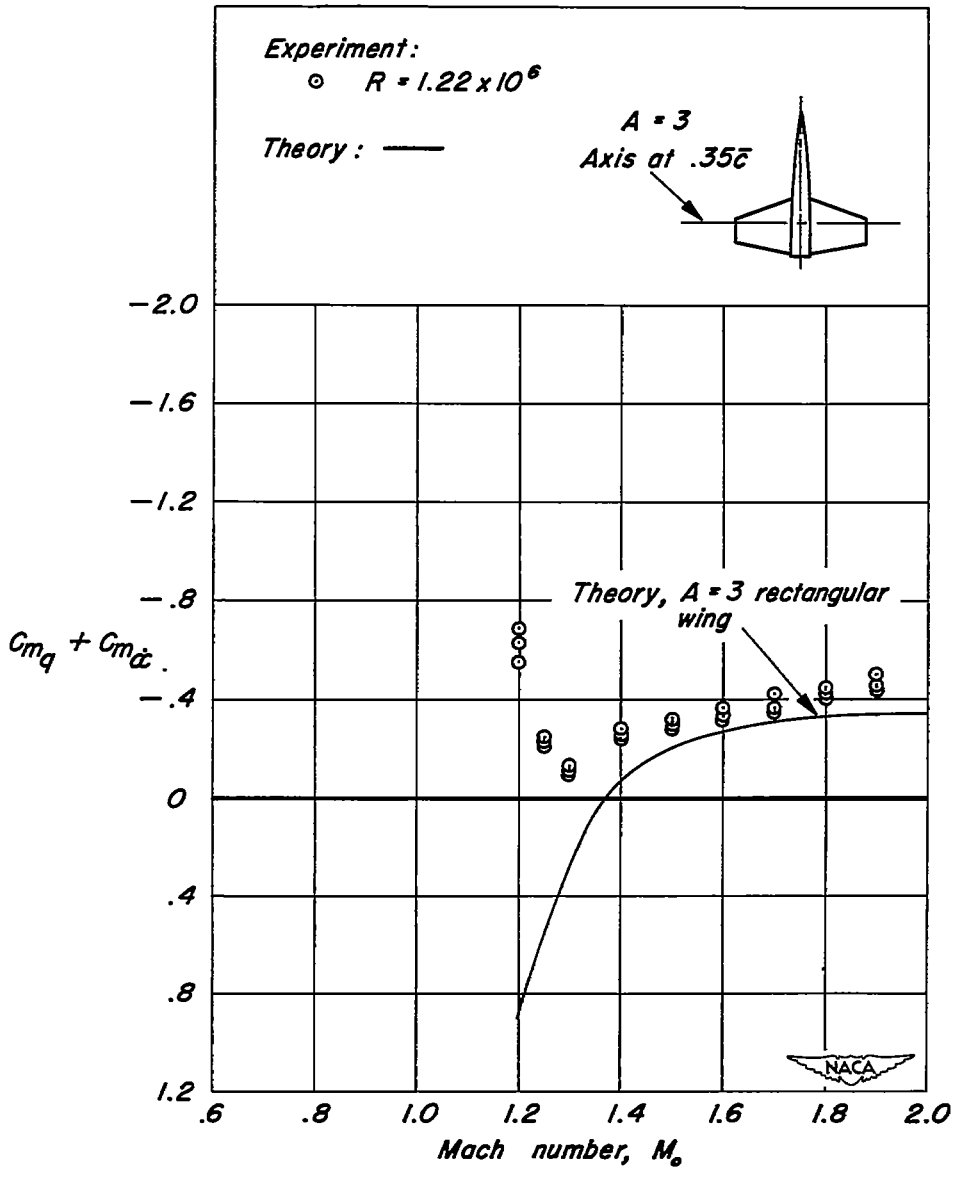

(b) Axis at 0.35$\bar{c}$.

Figure 13.— Continued.

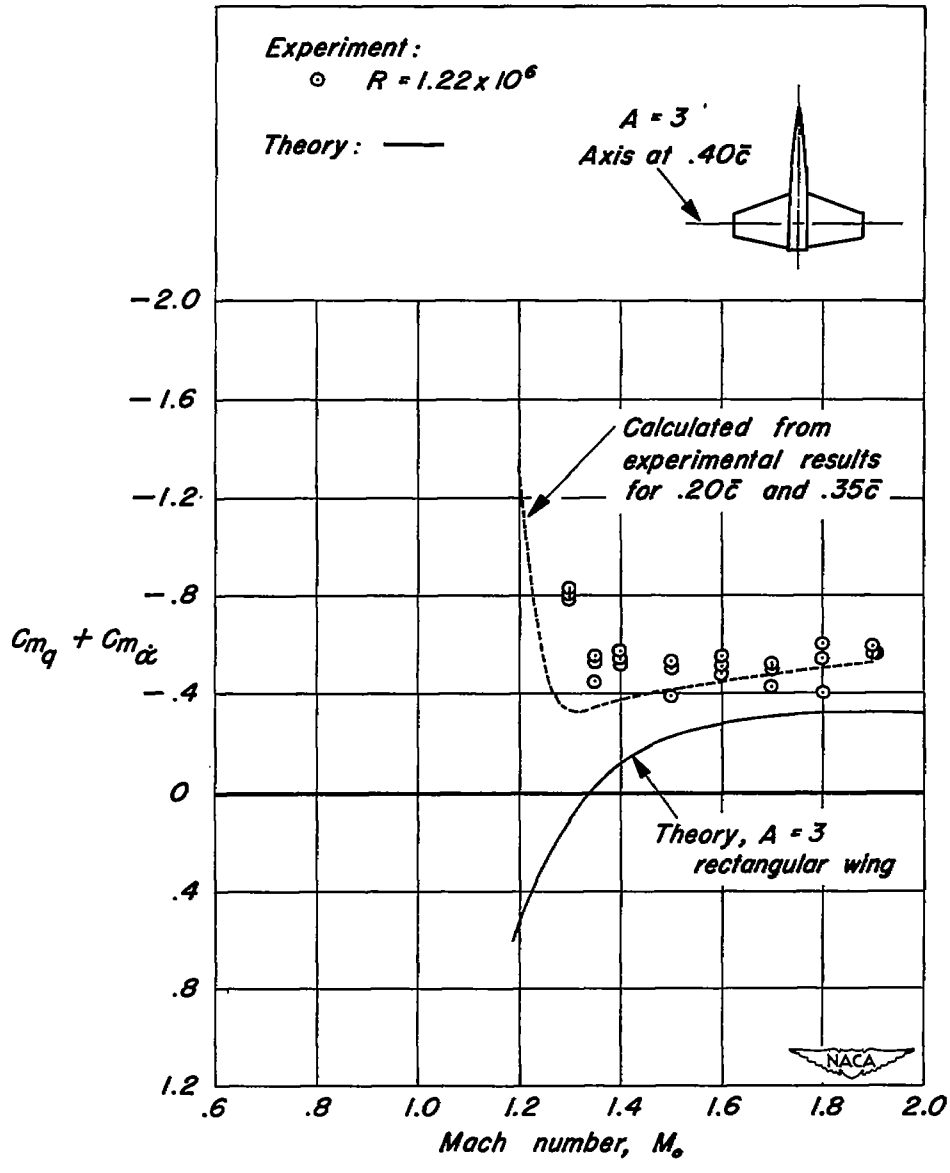

(c) Axis at 0.40c̄.

Figure 13.— Concluded.

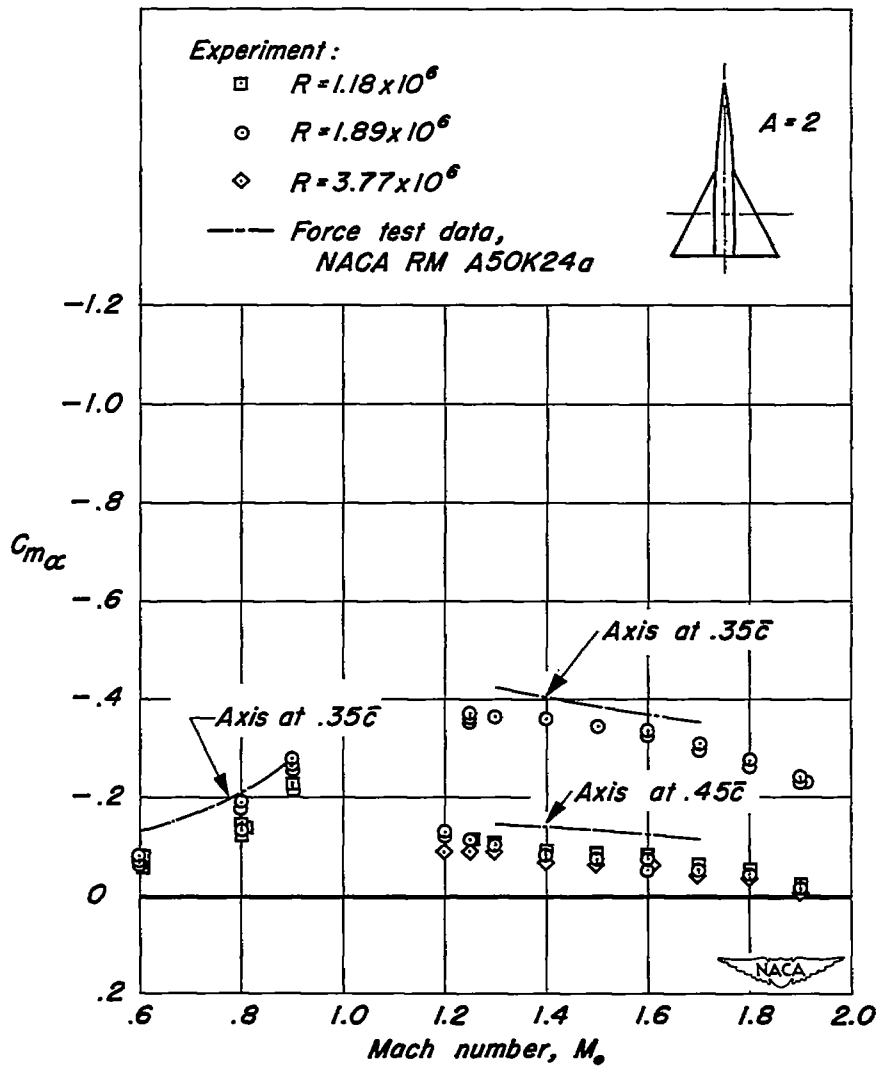

Figure 14.— Experimental pitching-moment-curve slopes for the wing-body combination having a triangular wing of aspect ratio 2. Axes of rotation at 0.35$\bar{c}$ and 0.45$\bar{c}$.

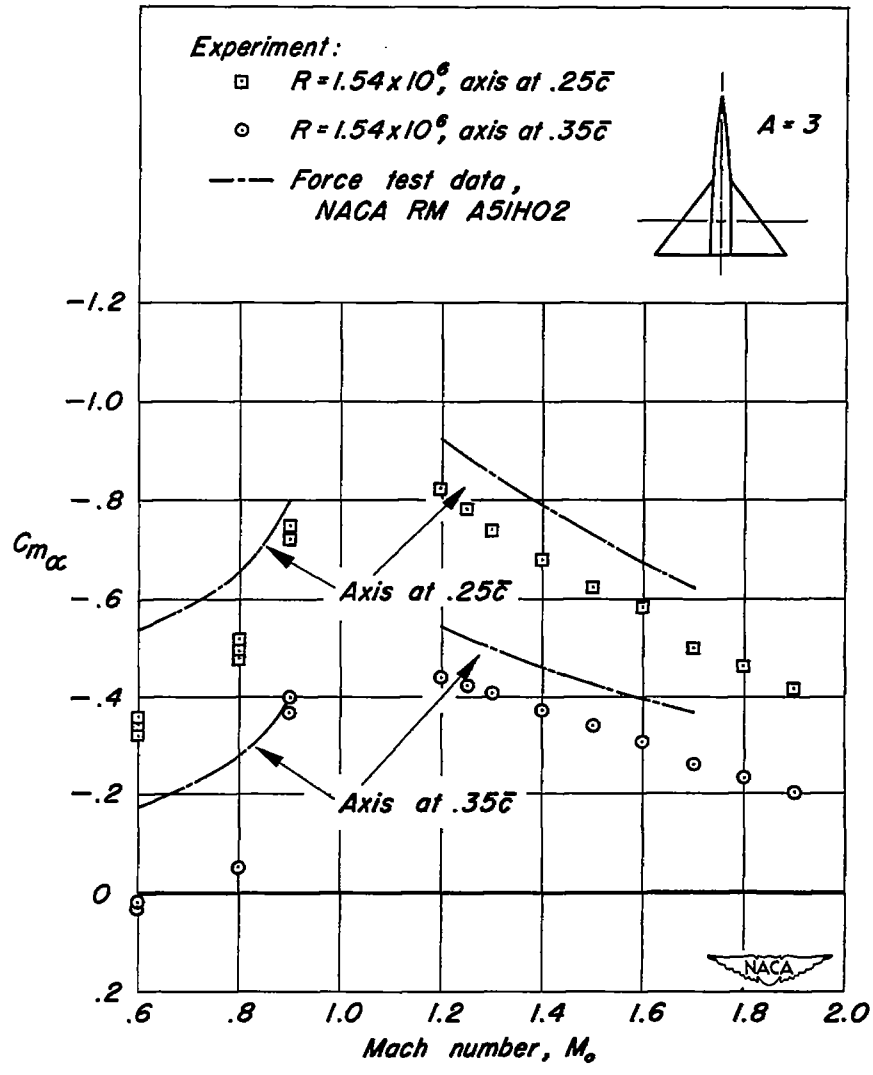

Figure 15.— Experimental pitching-moment -curve slopes for the wing-body combination having a triangular wing of aspect ratio 3. Axes of rotation at 0.25c̄ and 0.35c̄.

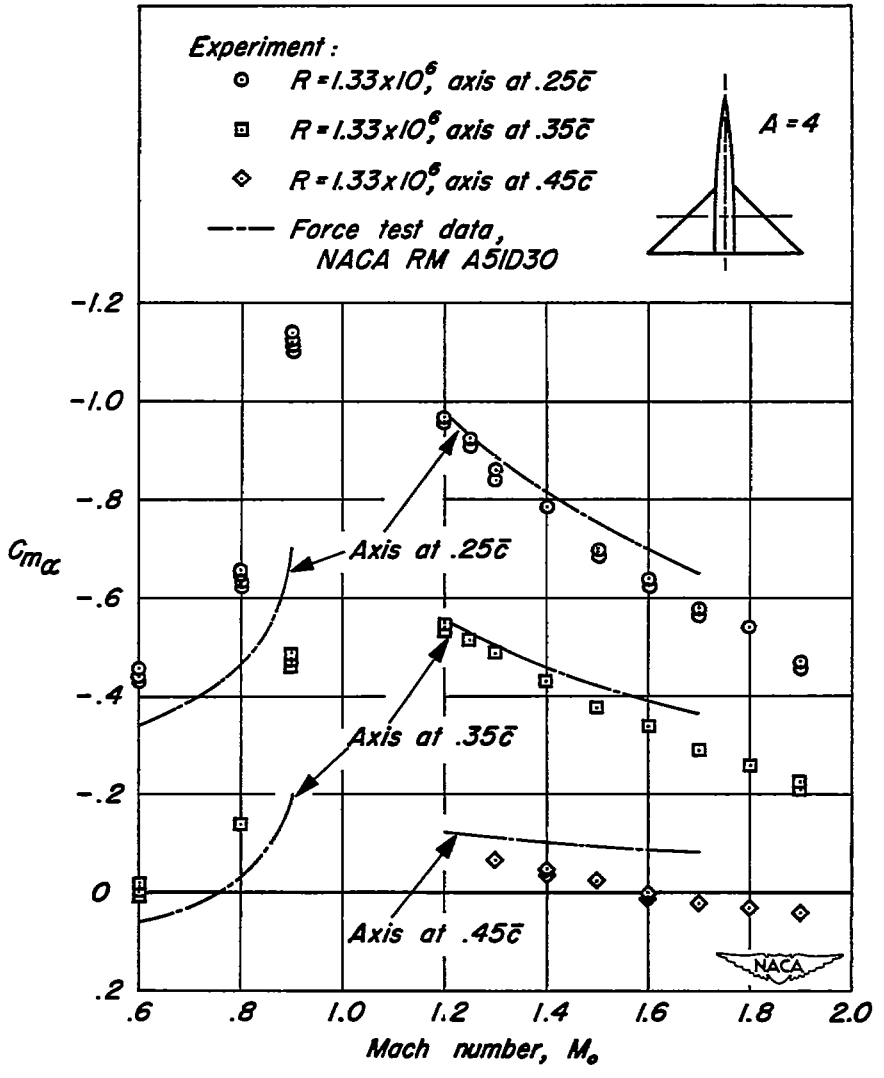

Figure 16.—Experimental pitching-moment -curve slopes for the wing-body combination having a triangular wing of aspect ratio 4. Axes of rotation at 0.25c̄, 0.35c̄, and 0.45c̄.

[redacted]

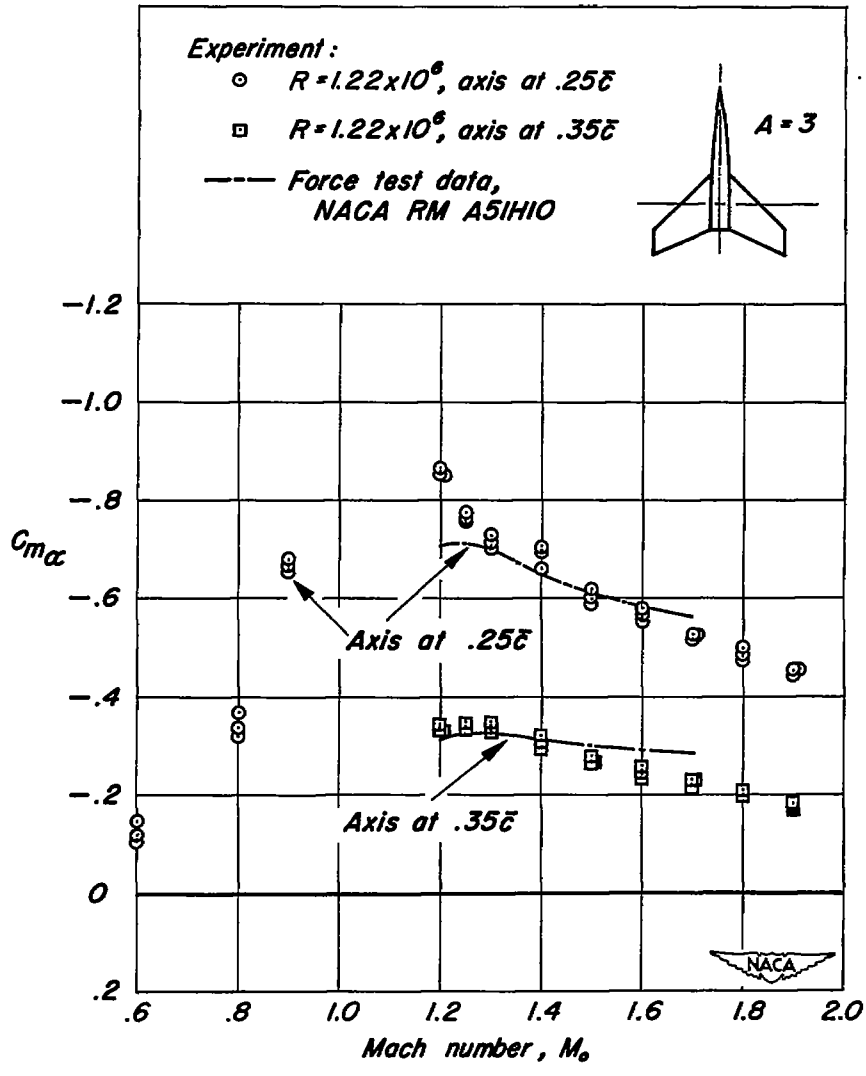

Figure 17.— Experimental pitching-moment-curve slopes for the wing-body combination having a swept wing of aspect ratio 3. Axes of rotation at 0.25c̄ and 0.35c̄.

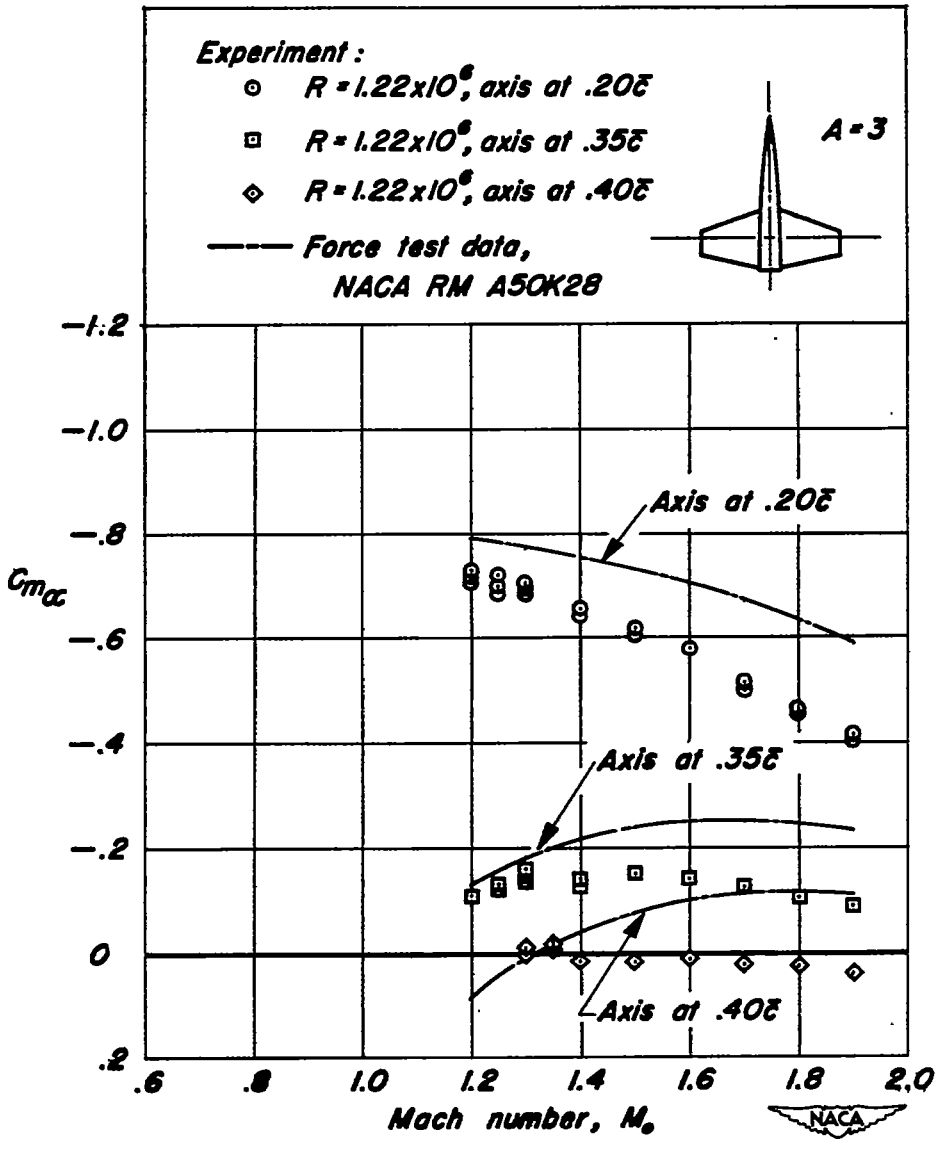

Figure 18.— Experimental pitching-moment -curve slopes for the wing-body combination having an unswept wing of aspect ratio 3. Axes of rotation at 0.20c̄, 0.35c̄, and 0.40c̄.

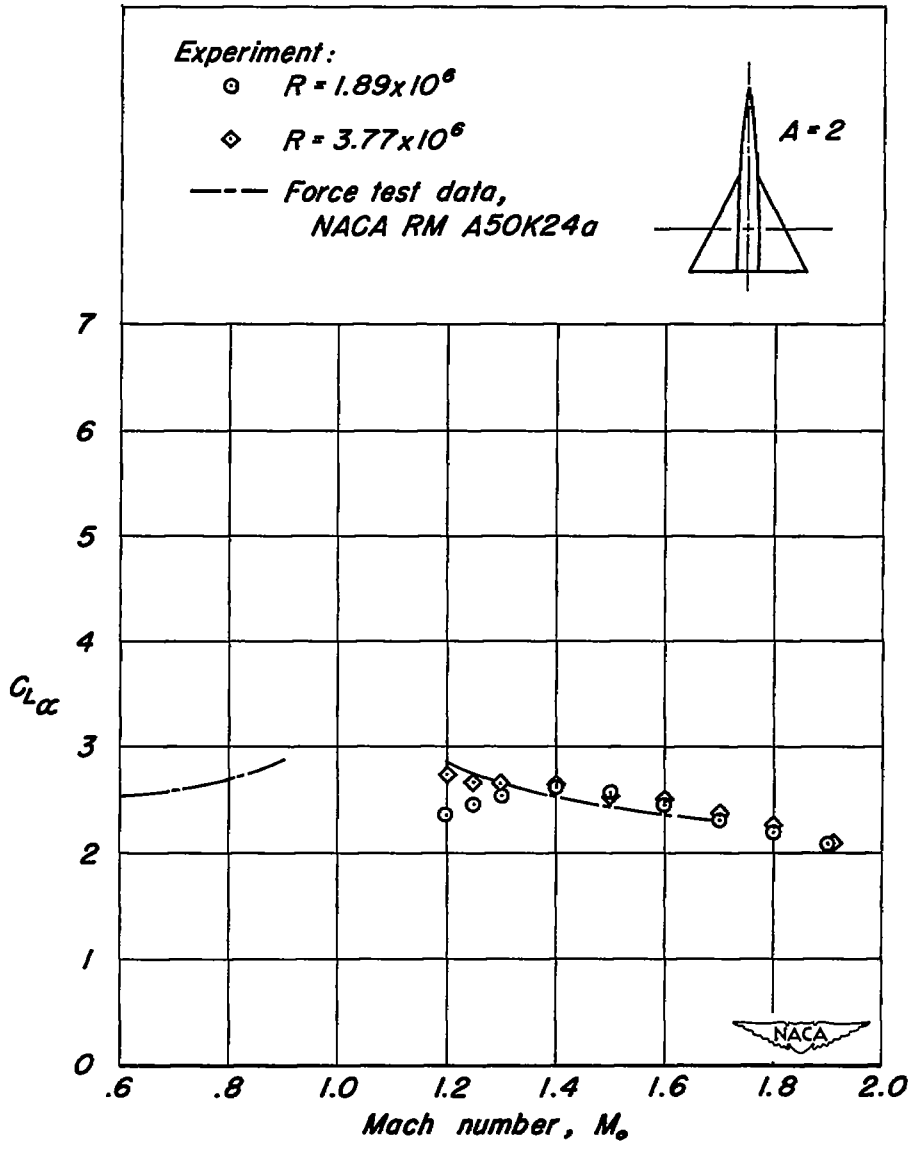

Figure 19.— Experimental lift-curve slopes for the wing-body combination having a triangular wing of aspect ratio 2.

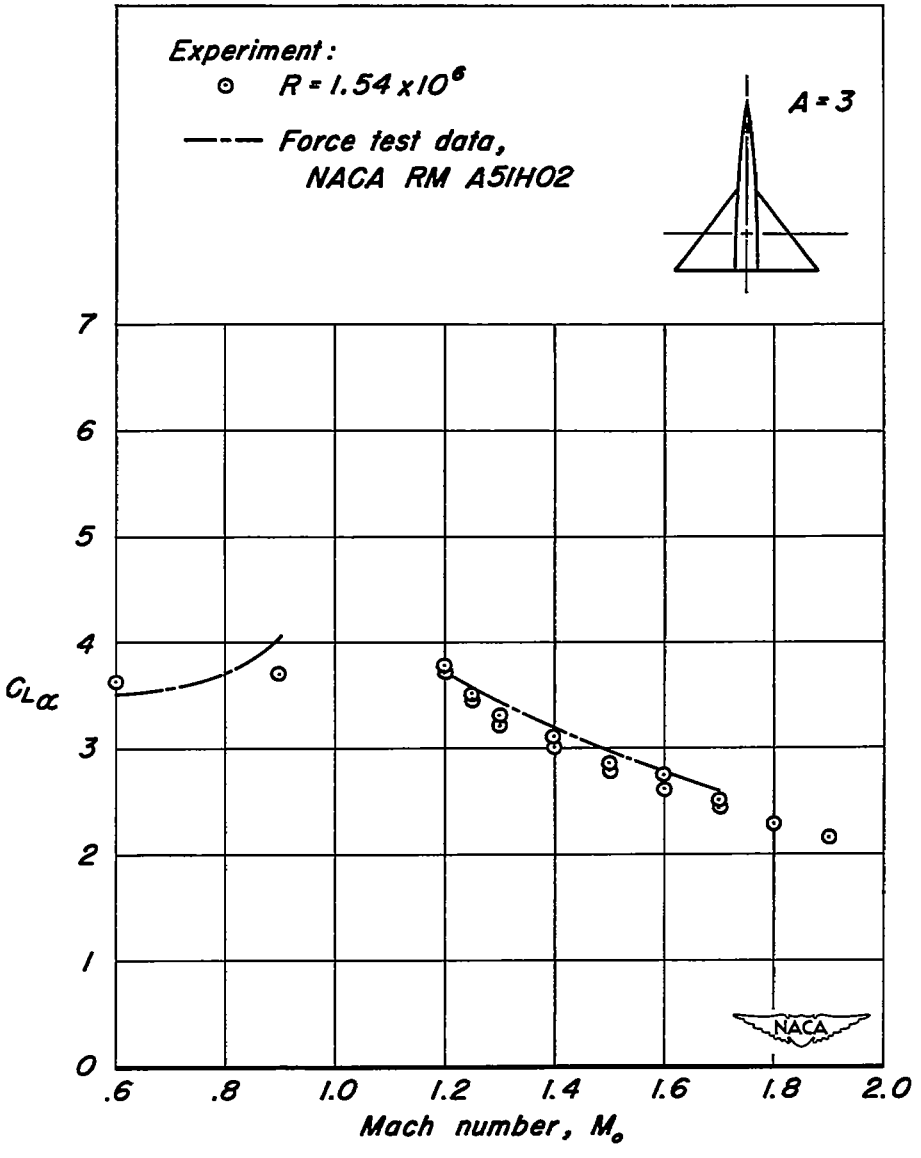

Figure 20.—Experimental lift-curve slopes for the wing-body combination having a triangular wing of aspect ratio 3.

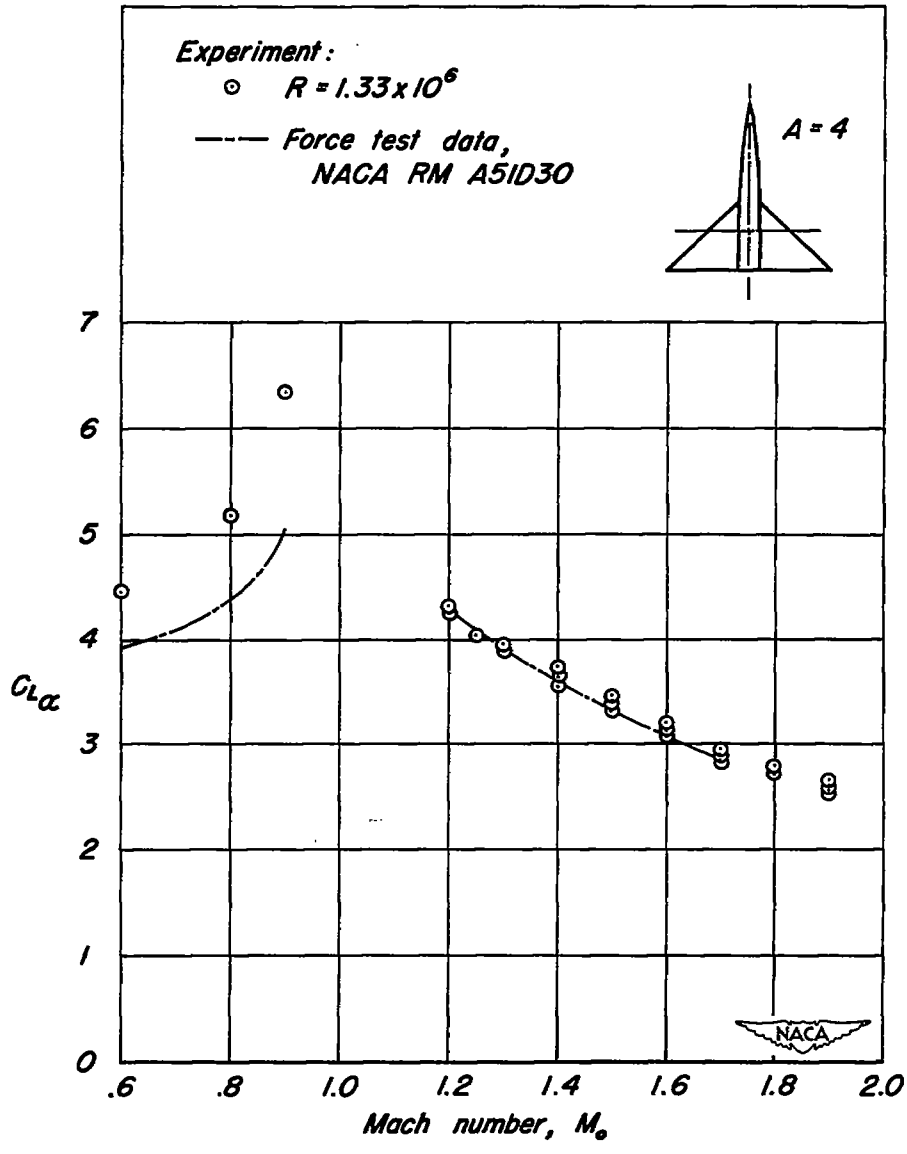

Figure 21.—Experimental lift-curve slopes for the wing-body combination having a triangular wing of aspect ratio 4.

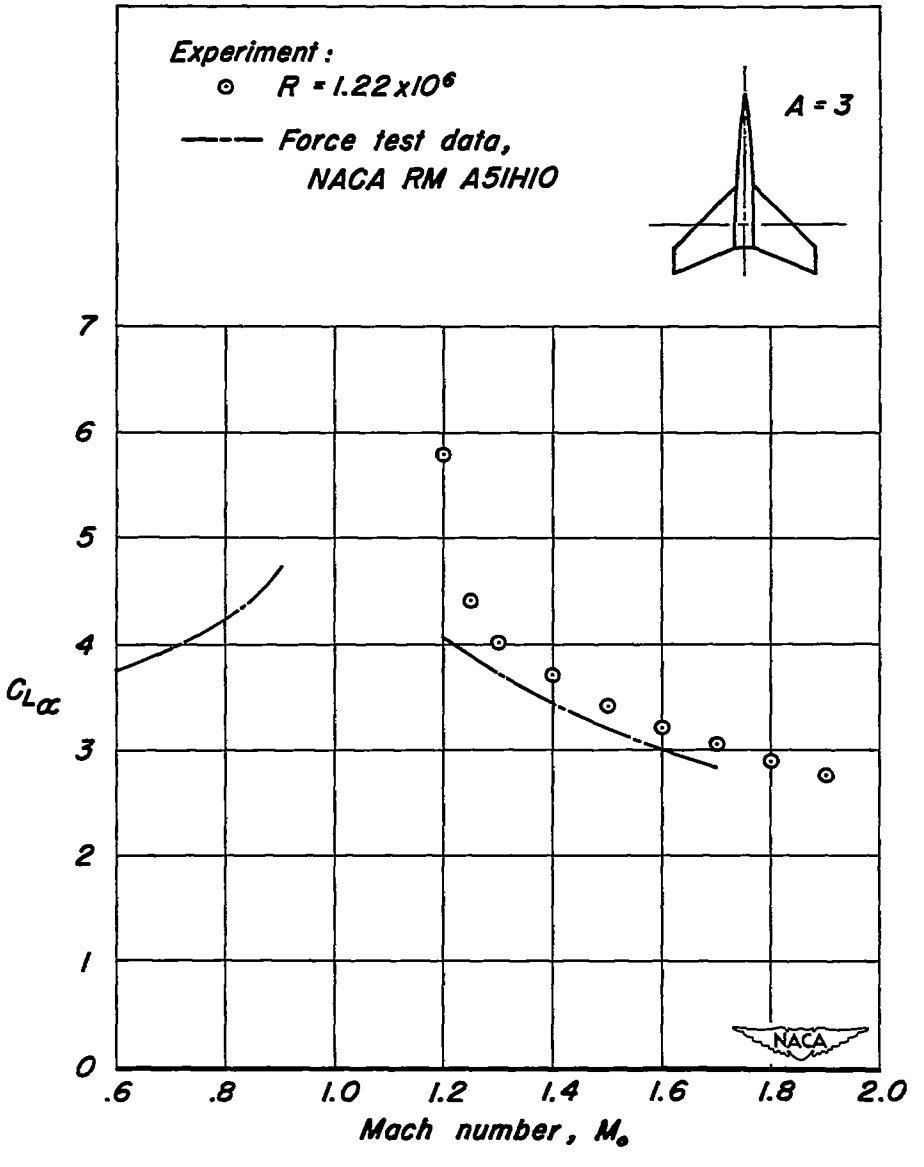

Figure 22.—Experimental lift-curve slopes for the wing-body combination having a swept wing of aspect ratio 3.

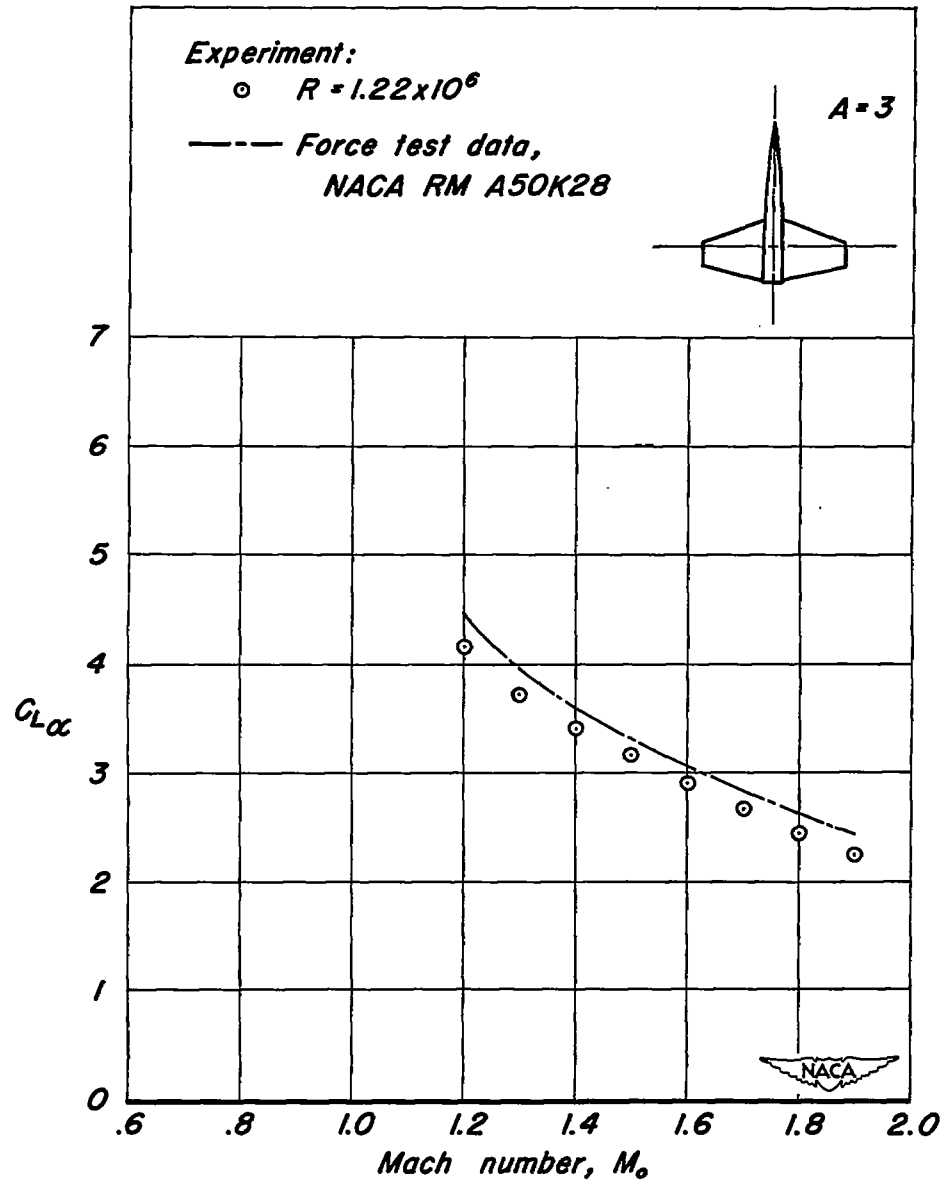

Figure 23.– Experimental lift-curve slopes for the wing-body combination having an unswept wing of aspect ratio 3.

[redacted]

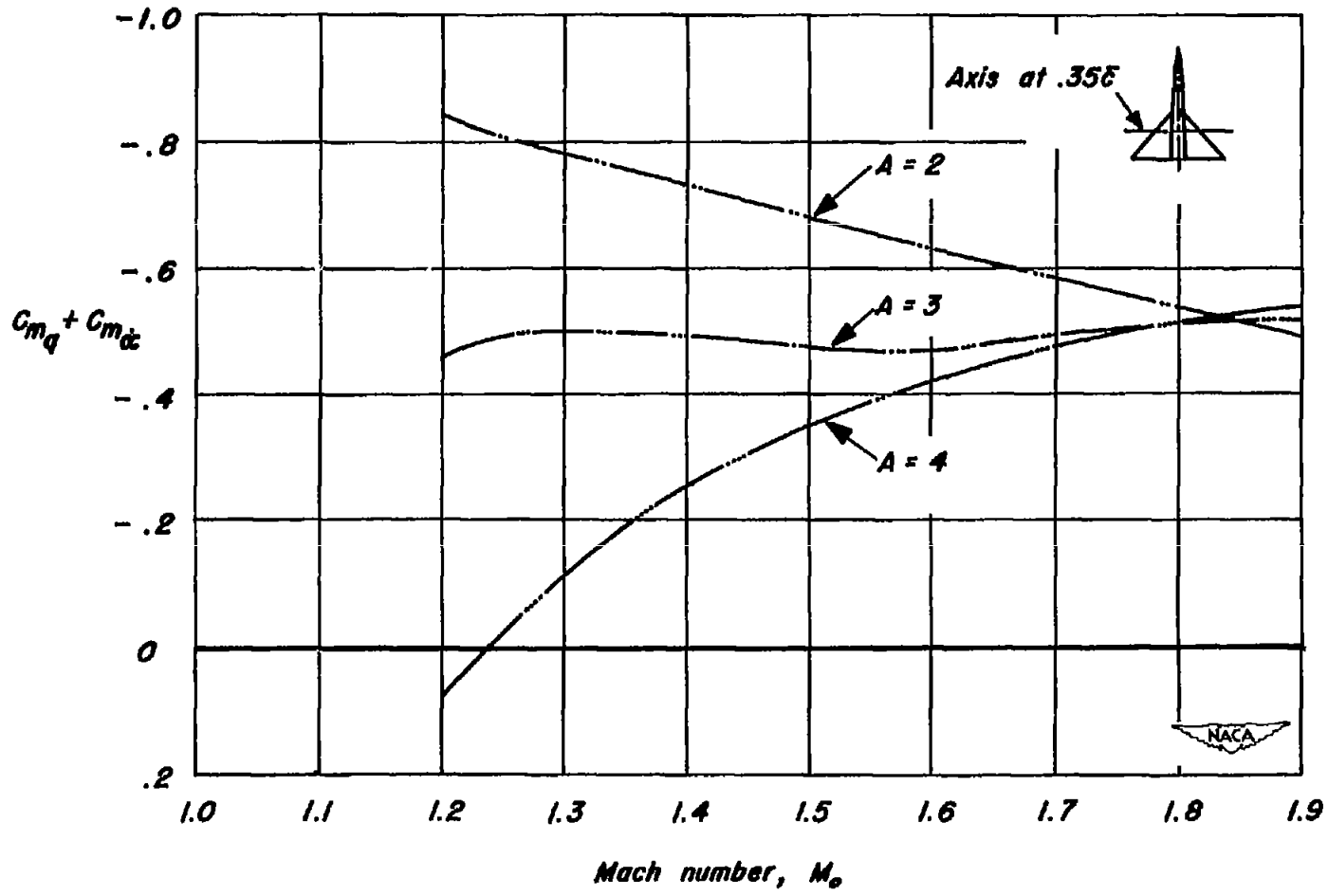

Figure 24.—Comparison of experimental damping-in-pitch coefficients for three wing-body combinations having triangular wings of aspect ratios 2, 3, and 4. Axes at 0.35$\bar{c}$.

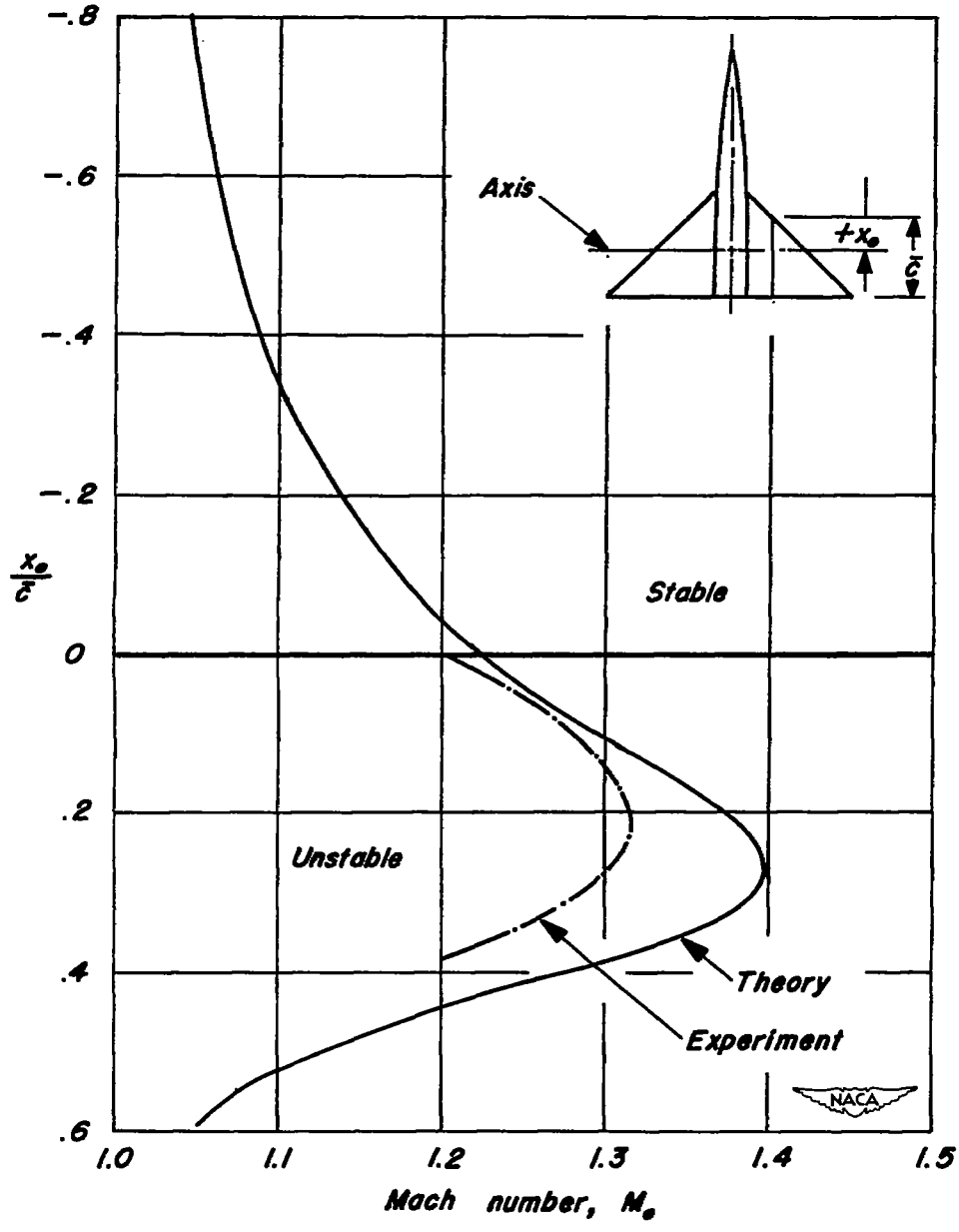

Figure 25.– Comparison of theoretical and experimental single-degree-of-freedom short-period pitching stability boundaries for a wing-body combination having a triangular wing of aspect ratio 4.

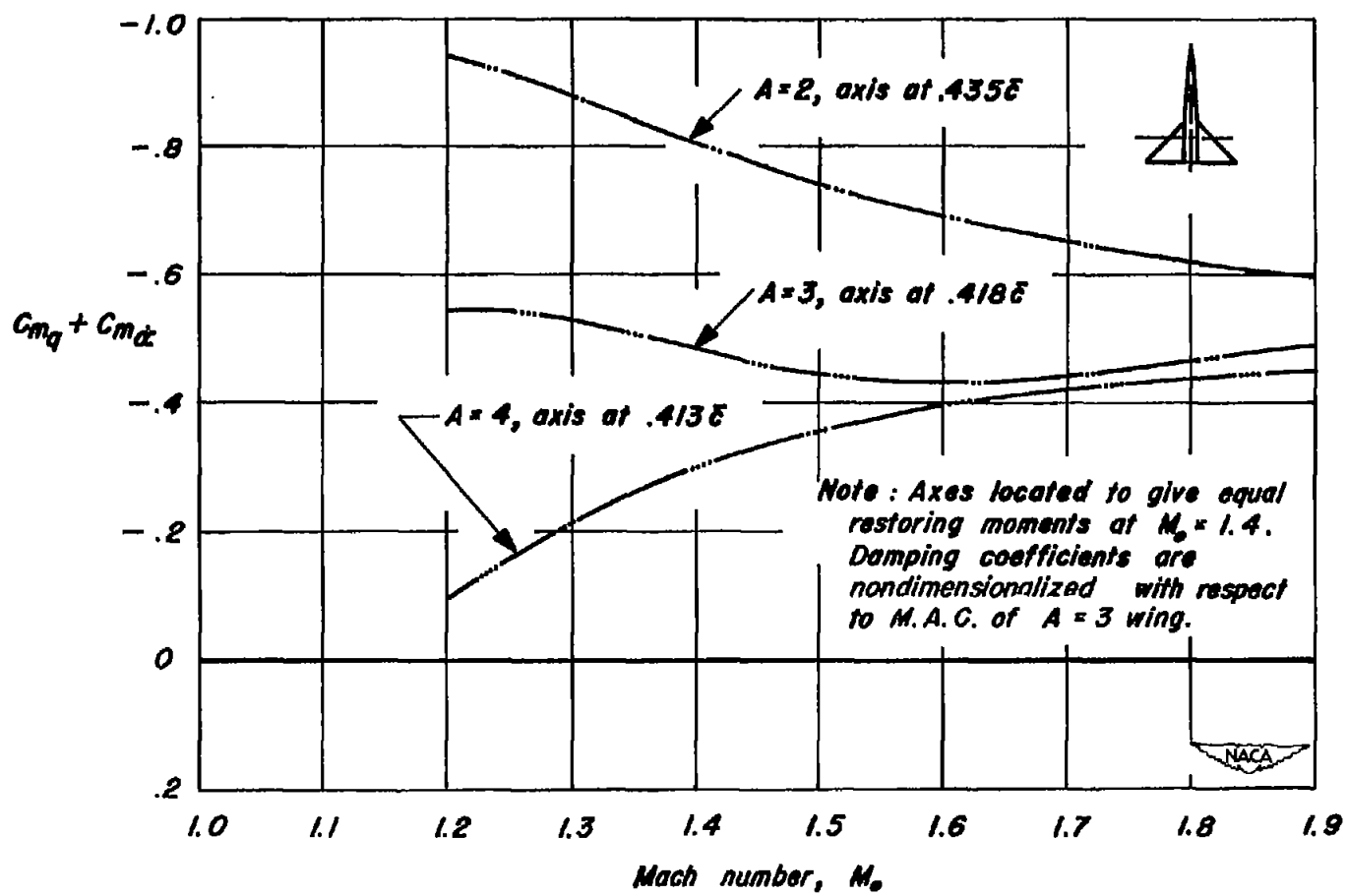

Figure 26.— Comparison of magnitudes of experimental rotary damping-moments for three wing-body combinations having triangular wings of aspect ratios 2, 3, and 4.

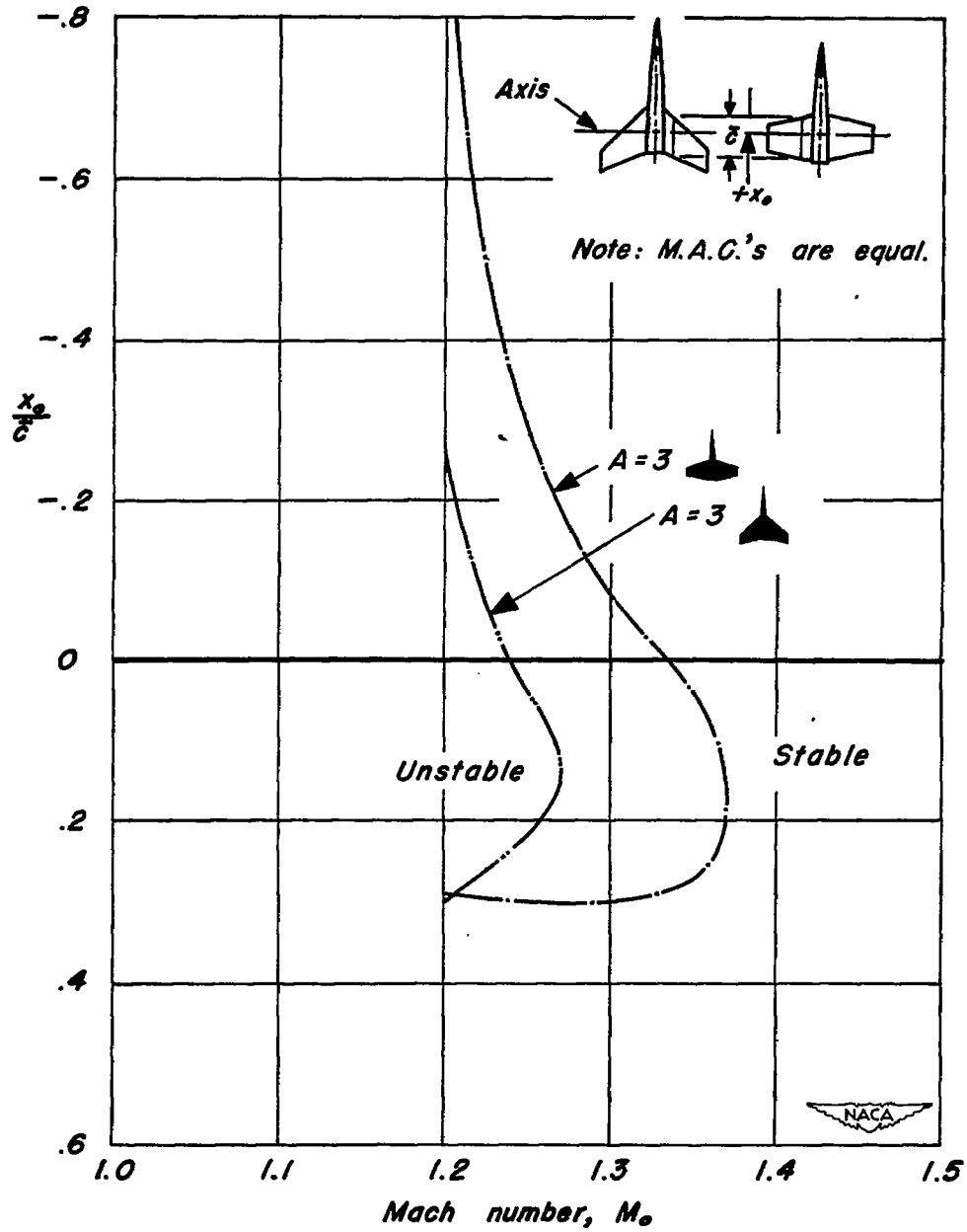

Figure 27.– Comparison of experimental single–degree–of–freedom short–period pitching stability boundaries for two wing–body combinations having swept and unswept wings of aspect ratio 3.

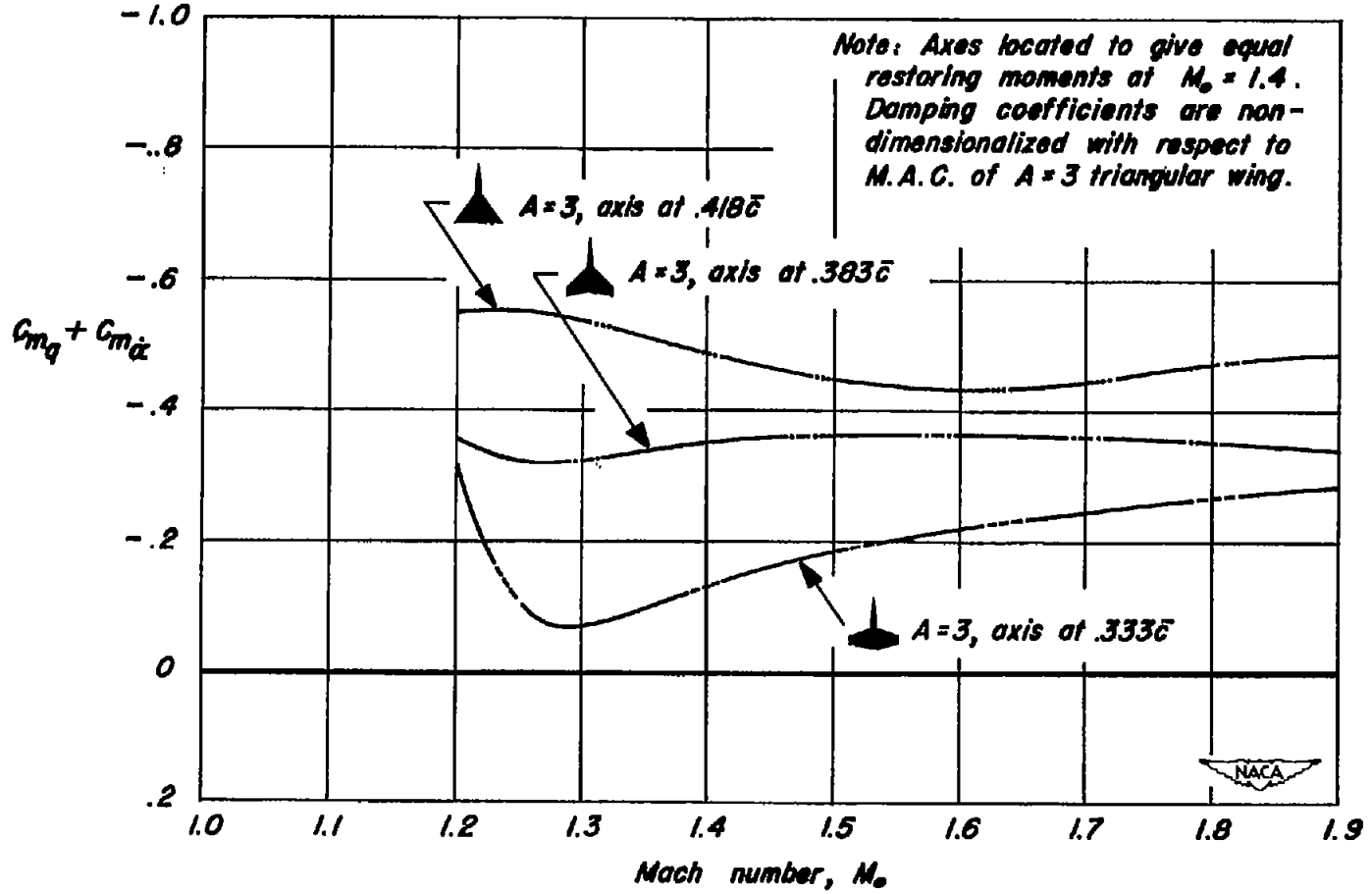

Figure 28.—Comparison of magnitudes of experimental rotary damping moments for three wing-body combinations having triangular, swept, and unswept wings of aspect ratio 3.

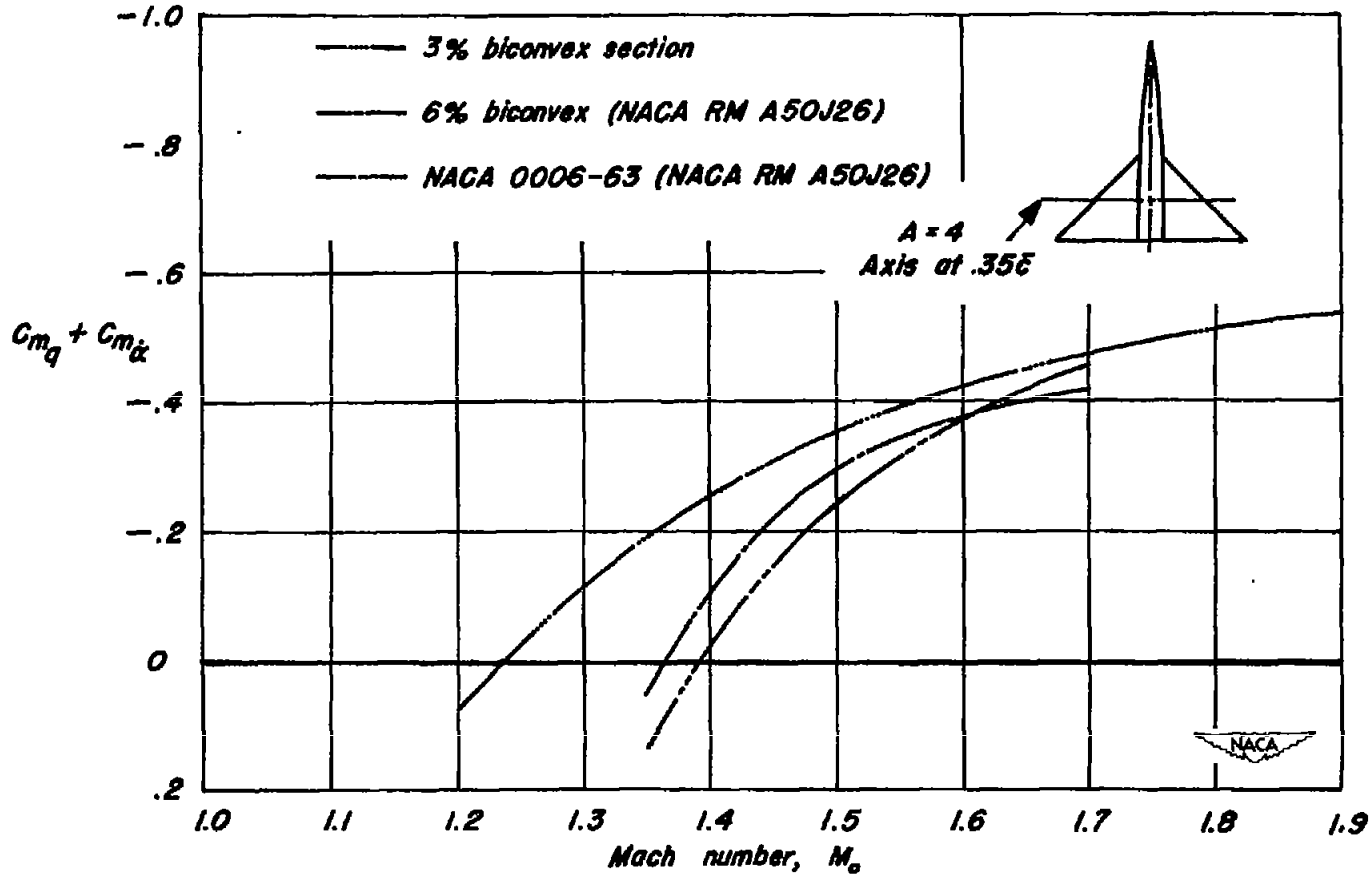

Figure 29.- Comparison of experimental damping-in-pitch coefficients for three wing - body combinations having triangular wings of aspect ratio 4 and thickness ratios of 3 and 6 percent.

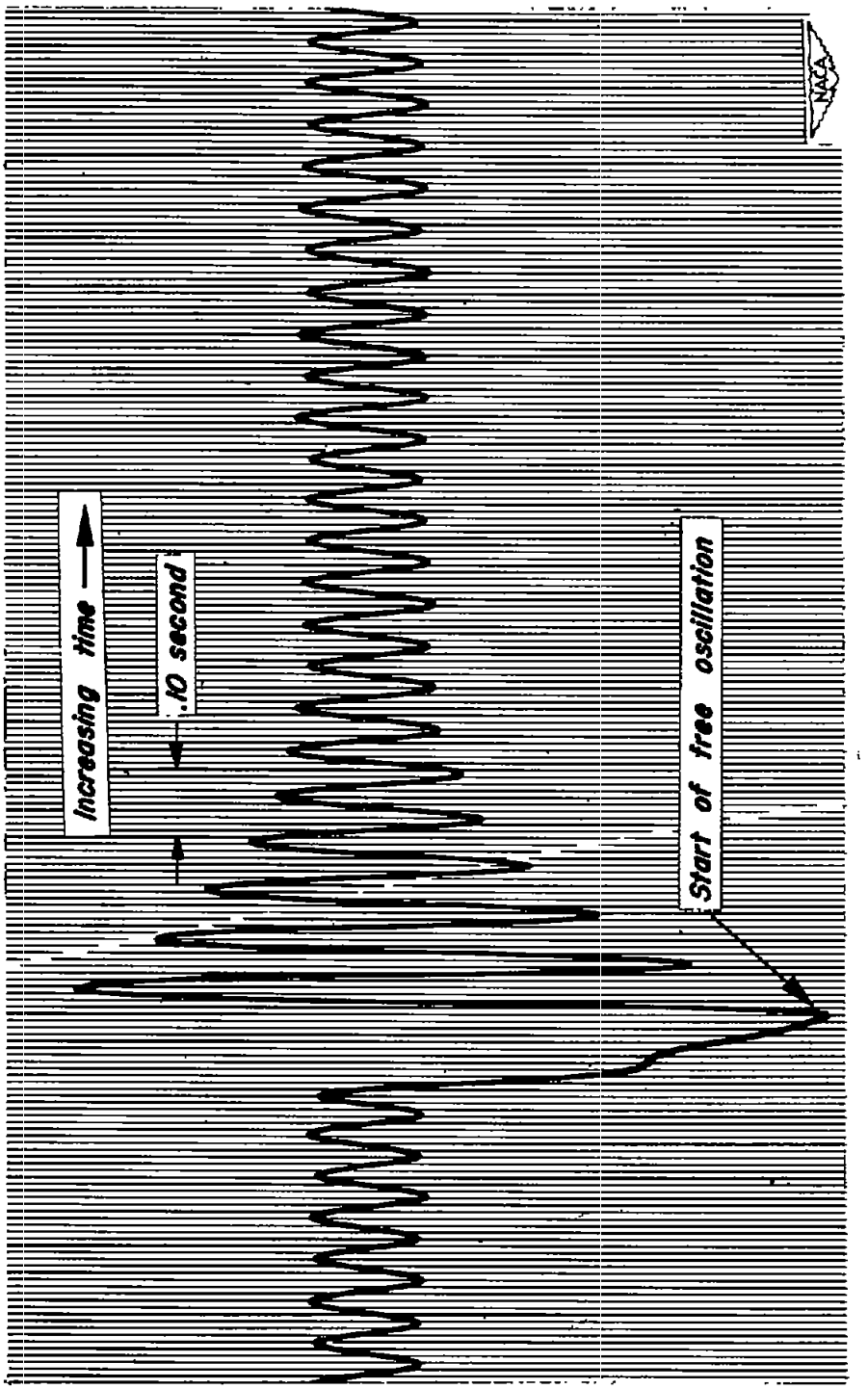

Figure 30. – Oscillograph record at Mach number 0.90 for the wing-body combination having a triangular wing of aspect ratio 3. Axis at 0.25c̄.

NACA-Langley - 4-8-53 - 325